PULSED NUCLEAR MAGNETIC RESONANCE IN METAL SINGLE CRYSTALS

by

Leslie Allan McLachlan

M.Sc.(Hons), University of New Zealand, 1961.

A THESIS SUBMITTED IN PARTIAL FULFILMENT OF

THE REQUIREMENTS FOR THE DEGREE OF

DOCTOR OF PHILOSOPHY

in the Department

of

Physics.

We accept this thesis as conforming to the required standard.

THE UNIVERSITY OF BRITISH COLUMBIA

November, 1965

In presenting this thesis in partial fulfilment of the requirements for an advanced degree at the University of British Columbia, I agree that the Library shall make it freely available for reference and study. I further agree that permission for extensive copying of this thesis for scholarly purposes may be granted by the Head of my Department or by his representatives. It is understood that copying or publication of this thesis for financial gain shall not be allowed without my written permission.

Department of Physics

The University of British Columbia
Vancouver 8, Canada

Date 9th Dec 1965

The University of British Columbia

FACULTY OF GRADUATE STUDIES

PROGRAMME OF THE

FINAL ORAL EXAMINATION

FOR THE DEGREE OF

DOCTOR OF PHILOSOPHY

of

LESLIE ALLAN McLACHLAN

B.Sc., University of New Zealand
1960
M.Sc.(Hons), University of New Zealand
1961

THURSDAY, DECEMBER 9th, 1965, AT 2:30 P.M.

IN ROOM 100, HENNINGS BUILDING

COMMITTEE IN CHARGE

Chairman: I. McT. Cowan

M. Bloom	E. Teghtsoonian
L. W. Reeves	B. G. Turrell
C. F. Schwertfeger	D. Ll. Williams

External Examiner: A. G. Redfield

I.B.M. Watson Laboratory, New York

Research Supervisor: D. Ll. Williams

PULSED NUCLEAR MAGNETIC RESONANCE IN A METAL SINGLE CRYSTAL

ABSTRACT

A pulsed nuclear magnetic resonance spectrometer using phase sensitive detection was constructed for use on metal single crystals. Its capabilities and limitations were established, both experimentally and theoretically.

The spin-lattice relaxation time was measured as a function of temperature in aluminium, niobium and vanadium single crystals. An unsuccessful attempt was made to measure the anisotropic spin-lattice relaxation time in an isotopically pure tin single crystal. The orientation dependence of the tin spin-spin relaxation time was measured and analysed in terms of the random fluctuation model of Anderson and Weiss. Values for both the pseudo-dipolar and psuedo-exchange constants were obtained.

Spin echoes were observed in the isotopically pure tin and were used to measure the spin-spin relaxation time. This was shorter than that measured from the free induction decay. The reason for this could not be determined.

GRADUATE STUDIES

Field of Study: Nuclear Magnetic Resonance

Quantum Theory of Solids	R. Barrie
Advanced Topics in Solid State Physics	D. Ll. Williams
Advanced Magnetism	M. Bloom
Low Temperature Physics	J. B. Brown
Statistical Mechanics	R. Barrie

Related Studies

Electronic Instrumentation	F. K. Bowers

PUBLICATIONS

L. A. McLachlan. "Thermoluminescent Emission Spectra of X-ray Irradiated Alkali Halides". J. Phys. Chem. Solids 23, 1344 (1962).

ABSTRACT

Spin-lattice relaxation times have been measured in metal single crystals with a pulsed nuclear magnetic resonance apparatus at both room and liquid nitrogen temperatures. The values obtained for aluminium and vanadium agreed well with the values given in the literature for powdered samples. The niobium value was slightly lower than the most reliable powder value, possibly because of impurities. Measurements were made on isotopically pure tin to see if any anisotropy could be detected in the spin-lattice relaxation time. No anisotropy could be detected, but the crystal orientation used was so unfavourable that an anisotropy of less than about 50% could not be detected.

The spin-spin relaxation time was measured in the isotopically pure tin for five different magnetic field orientations. These showed that exchange narrowing occurred. With a suitable choice of operating conditions, the apparatus measured the equivalent of the absorption mode in steady state nuclear magnetic resonance as a function of magnetic field orientation. This was combined with the spin-spin measurements to give the complete orientation dependence of the latter. These measurements gave a value of (2.1 ± 0.3)Kc/s. for the pseudo-exchange constant in tin. The pseudo-dipolar second moment was found to be twice the dipolar second moment.

Spin echoes were observed in the isotopically pure tin and were used to measure the spin-spin relaxation time. These gave values which were much shorter than those measured by free induction decays. The reason for this was not determined.

TABLE OF CONTENTS

CHAPTER PAGE

LIST OF TABLES

LIST OF ILLUSTRATIONS

ACKNOWLEDGEMENTS

It is a pleasure to thank Dr. D. Ll. Williams for his constant and painstaking help in all aspects of this work and especially for his encouragement when things looked black.

Dr. M. Bloom also made important contributions to this work, both directly through suggestions and an iconoclastic reading of this thesis and indirectly through all the nuclear magnetic resonance theory I have learnt from him. For all this I would like to thank him.

Of the other people who have contributed to this work, I would like to acknowledge an informative discussion with Dr. J.B.Brown on the acoustical aspects of this work and Mr. Riseborough for taking the X-rays. Dr. H.E. Schone is to be thanked for the loan of the isotopically pure single crystal.

The financial support from the University of British Columbia, the British Columbia Hydro Authority, and the National Research Council of Canada which made this work possible, is gratefully acknowledged.

Finally, I must acknowledge my indebtedness to Mr. and Mrs. R. F. Carswell and to Mr. and Mrs. P. K. Diggle for their innumerable kindnesses and also to my fellow students of the Lower Mall for two intellectually stimulating and socially chaotic years.

INTRODUCTION

Ever since the early days of nuclear magnetic resonance, experiments have been made on metals. These experiments were always made on finely ground powders suspended in an insulating oil. This is because of the rf skin effect which prevents rf fields penetrating more than a few microns in a metallic sample. Studies of spin-lattice relaxation, spin-spin relaxation, and the Knight shift were made on several metals and were even extended into the superconducting region. These gave considerable information on the spherically symmetric part of the conduction electron distribution. It was soon found that some lines were asymmetric and this was correctly interpreted as being due to an anisotropic Knight shift. By analysing the asymmetric line shape, the magnitude of the anisotropic Knight shift could be obtained with considerable accuracy.[1] Experimental work was also extended to alloys and to liquid metals. Later on the analysis of powder measurements was extended to cover the case of the presence of an anisotropic Knight shift and a quadrupole interaction. More recently spin echo experiments have been made on powders which directly give the pseudo-exchange strength.

Despite the considerable success of the powder method in measuring anisotropic properties, it seemed obvious to try and directly measure anisotropic properties in a metal single crystal. This was first done in this laboratory several years ago, using a sample constructed from thin single-crystal slabs

separated by insulating layers. The apparatus used a conventional marginal oscillator and phase sensitive detection with the sample cooled to liquid helium temperature to get an adequate S/N ratio. Under favourable circumstances this was as high as 50. In the first measurements, both the anisotropic Knight shift and line widths were measured. Since then experiments of this type have been made on several different metals, both in this laboratory and elsewhere. Some of these experiments detected details which were obscured by the averaging overall orientations which occurs in a powder measurement. Early on it was found that a coil fairly tightly wound on a cylindrical sample was just as good as the layered sample.

The aim of this work was to build a pulsed NMR apparatus for single crystals which could be used in conjunction with the steady state apparatus. Pulsed NMR measurements had never been made in single crystals before, so that this work was of an exploratory nature. In the early stages the apparatus worked at 700Kc/s. This low frequency was chosen with the intention of ultimately doing experiments on super-conductors. However, it soon became clear that the S/N was going to be too small at this frequency, so the apparatus was rebuilt to operate in the frequency range 6Mc/s. to 10Mc/s. The apparatus worked satisfactorily at these frequencies. For various experimental reasons, measurements could not be made at liquid helium temperatures and this restricted the experiments which could be done.

The anisotropy in T_2 had often been observed in steady state experiments. Anisotropy in T_1 had never been detected since steady state apparatus is quite unsuitable for T_1 measurements. Detection of any T_1 anisotropy was thus the main experiment to be attempted. There is no theoretical estimate of the magnitude of such an effect. All the theories developed so far have only been applied to a cubic lattice, or else make assumptions about the conduction electron distribution which may not be valid in a non-cubic lattice. It seems unlikely that an anisotropic T_1 would occur for a spherical electron distribution so that a search for T_1 anisotropy should be confined to metals with a non-cubic lattice and an anisotropic Knight shift.

Because of the exploratory nature of this work, most of the emphasis has been placed on the experimental aspects of the topic, rather than on the theoretical side. The fragmentary nature of the theory of NMR in metals was another incentive for concentrating on the experimental nature of the problem.

The rudimentary state of the theories of spin-lattice and spin-spin relaxation in metals is not surprising when its complexity is considered. The main feature of the electronic structure of metals have been known for about three decades. They are described in terms of either free electrons, or else by tightly bound electrons. Most of the mechanisms involved in NMR in metals can be qualitatively described in terms of these models. However, a quantitative description is impossible since many of the NMR properties are very dependent on details of the electron wave functions. A quantitative com - parison of theoretical and experimental results must thus

await the compution of much more accurate electron wave functions. Such a comparison would provide an extremely sensitive test of any computed wave function. However, it will be many years before such a comparison is possible for any but the simplest of metals.

In the first two chapters this basic theory of NMR in metals is discussed and the properties of all the important mechanisms involved are listed. The third chapter exhaustively covers the experimental details. Some of this overflows into the Appendices. The results are given in the fourth chapter and the thesis concluded with suggestions for future work.

Finally, a note on the units employed in this thesis. For the classical electromagnetic sections M.K.S. units are used, whilst c.g.s. units are used in all the quantum mechanical expressions. In the sections involving both electromagnetic and atomic considerations, the choice of units depends upon the ultimate use of the expressions in the section.

CHAPTER I

THE ELECTRONIC STRUCTURE OF METALS

'Accidental and Fortuitous Concurrence of Atoms.'

- Lord Palmerston.

The purpose of this chapter is to summarise the properties of the electronic structure of metals necessary for an understanding of their nuclear magnetic resonance. It is assumed that the reader is familiar with the concept of Brillouin zones and Fermi surfaces, as described in the standard texts (9, 36, 37). The first section describes the standard forms of electronic wave functions and their limitations. The final section concerns the effects of a static magnetic field upon the conduction electrons.

The electron energy levels can, in principle, be got by solving the Schroedinger equation of all the electrons and nuclei in the metal. This is an impossible task so a much simplified model is adopted. The nuclei form a periodic lattice and are surrounded by closed shells of tightly bound electrons whose only effect is assumed to be to partially shield the nuclear charge. There are also loosely bound conduction electrons shared to some extent by all the nuclei in the lattice. The Schroedinger equation for all these electrons must then be solved. To do this, the crucial assumption is made that the electrons interact so weakly that they

can move independently of each other. The wave functions and energy levels obtained are thus those for an independent electron.

1.1 The Wave Function of Conduction Electrons

The most important effect of the periodic lattice potential is to restrict the solutions of Schroedinger's equation to the form

$$\psi(\underset{\sim}{k},\underset{\sim}{r}) = U(\underset{\sim}{k},\underset{\sim}{r}) \exp(i\underset{\sim}{k}.\underset{\sim}{r}).$$

$U(\underset{\sim}{k},\underset{\sim}{r})$ is a function, depending on the wave vector $\underset{\sim}{k}$ of the electron, which has the periodicity of the lattice. These solutions are known as Bloch functions and are similar in form to the plane wave $\exp(i\underset{\sim}{k}.\underset{\sim}{r})$.

There are other restrictions on the form that the conduction electron wave function can take. The coulomb attraction is very strong close to the nucleus and so the conduction electron must have a compensatingly large kinetic energy to avoid being captured. It thus oscillates rapidly, rather in the manner of the wave function of a valence electron in a free atom. However, unlike the free atom, there is no experimental evidence in most metals for the electron having any orbital angular momentum. This " quenching " of the orbital angular momentum occurs because the electron moves in a potential field having the lattice symmetry, not spherical symmetry as in a free atom (36). This means that the wave function depends on the lattice symmetry, as well as on the

valence band from which it originated. Between the ions the electron moved in a more uniform potential and behaves rather like a free electron.

Even if many-body effects are ignored, the exact solution of Schroedinger's equation is impossible. The first problem is deciding on the correct form of the periodic potential. This in itself is a complex many-body problem and even if it were solved computational difficulties preclude an exact solution of Schroedinger's equation. It is thus necessary to assume various approximate forms for the wave function and then see how well they satisfy Schroedinger's equation.

Three of the simplest types of approximate wave functions will now be described.

(i) The Tight Binding Approximation.

This assumes that inside each ion the wave function is similar to the wave function of an electron in a free atom. A suitable set of atomic wave functions is then chosen for each ion in the lattice and then a linear combination of these taken to give a Bloch function for the whole lattice of the form

$$\psi(\underset{\sim}{r}) = \sum_{j} \sum_{c} \phi_c(\underset{\sim}{r} - \underset{\sim}{r}_j) \exp(i\underset{\sim}{k}.\underset{\sim}{r}_j).$$

ϕ_c is the c th core wave function on the j th atom in the metal. For this method to be satisfactory, it is necessary that the atomic wave functions on different atoms do not overlap much, so that each electron is predominantly in the near neighbourhood of its parent atom. It is particularly suitable

for describing the narrow d band in the transition metals.

There are more elaborate versions of this principle which give better results, but they all have severe computational difficulties.

(ii) The Nearly Free Electron Approximation

Exactly the opposite assumption to the tight binding case is made. It is that the electrons move in a periodic potential which is much less than their kinetic energy so that they can be described by plane waves and the periodic potential treated as a perturbation. This treatment leads directly to the concept of Brillouin zones. It also shows that electrons in a metal can be treated as a simple electron gas moving in a constant potential, provided the electron mass m is replaced by an effective mass m* which depends on the way the electron energy varies with wave number. Using this very simple model surprisingly accurate Fermi surfaces and energy bands can be calculated for quite a few metals (22).

Due to its simplicity and ability to easily describe the electronic structure of a metal, the nearly free electron model is the one most commonly used, even in cases where it is clearly not very suitable.

(iii) The Orthogonalised Plane Wave Method.

In nearly all metals the situation lies somewhere between the nearly free electron case and the tight binding approximation. Many ways have been devised for treating this intermediate situation, but only the O.P.W. method will be described

here. This is because it gives a reasonably accurate wave function and also shows the limitations of the free electron approximation.

The O.P.W. method is based on the requirement that the conduction electron wave function be orthogonal to all the filled core wave functions to satisfy the exclusion principle. To do this a linear combination of core wave functions is subtracted from a plane wave in such a way that the resulting conduction electron wave function is orthogonal to all the core wave functions. Then a linear combination of these wave functions is found which best satisfies Schroedinger's equation.

The electron wave function thus appears as a plane wave between the ions, but oscillates rapidly near an ion core. This is fairly close to how a real wave function must look. This wave function is conventionally described by separating it into a sum of s,p,d,--- contributions, these having spatial symmetry properties similar to those of the corresponding atomic wave functions. The s electron wave function corresponds to a plane wave.

It is now clear why the nearly free electron approximation works as well as it does. The electron is nearly free between the ions, but close to an ion gains enough kinetic energy to approximately cancel the attractive coulomb potential. Thus the effective potential of an ion is quite small and is typically less than the kinetic energy of the electron

so that conditions are similar to those of the nearly free electron model. This is why nearly free electrons are a reasonably good approximation as far as band structure calculations are concerned. However, the O.P.W. method also shows that the true wave function usually also contains p,d,--- contributions which may be very important in calculating some other properties.

Another reason why the nearly free electron model works is that an electron feels not only the coulomb potential of a given ion, but that of all the other electrons and ions in the lattice as well. The latter screen the ion potential so that it is negligible beyond about a lattice spacing (37). This considerably reduces the effect of the ion potential on a fast moving electron.

All the calculations rely on the assumption that the conduction electrons interact weakly. This, at first, seems a poor assumption since the average electron separation is about a lattice spacing, giving an average coulomb repulsion energy of several ev. However, the screening effect of the electrons and ions converts the long range coulomb potential into a short range screened potential. This reduces the cross-section for electron-electron collisions to such an extent that electron-lattice imperfection scattering is far more likely (37). There is also a repulsive force between electrons with parallel spins due to the exclusion principle, but it does not drastically modify the screening effect.

These effects are often discussed in terms of quasi-particles (38). For a dilute electron gas the quasi-particles are identical with the real particles. In the dense electron gas in a metal, the quasi-particles behave like electrons with an effective mass m^* which is larger than the " bare " mass of a free electron.

So far the spin-orbit interaction has been neglected. This is the coupling of the electron spin and orbital angular momentum through relativistic magnetic effects which increase rapidly in strength with increasing atomic number. It can have several effects on the conduction electrons. Ordinarily the energy levels are doubly degenerate because of the electron spin. The spin-orbit interaction can lift some of this degeneracy and this slightly alters the Fermi surface structure (22). It can also reinstate some of the orbital angular momentum quenched by the lattice potential.

1.2 The Magnetic Susceptibility of Conduction Band Electrons.

The effect of a magnetic field on the conduction band electrons will now be considered. This is actually a problem involving difficult questions of gauge invariance and the validity of perturbation methods. These conceptual difficulties will be ignored in the following discussion which is based on the work of Kubo and Obata (39).

The free energy F of a highly degenerate Fermi gas is

$$F = NE_F - kT.Tr[g(\mathcal{H})]$$

where $g(\mathcal{H}) = \ln\{1+\exp[\beta(E_F-\mathcal{H})]\}$ and $\beta=(kT)^{-1}$.

The magnetic susceptibility χ is given by the thermodynamic relation

$$\chi = \lim_{H\to 0}\left(\frac{\partial^2 F}{\partial H^2}\right)_{T=\text{constant}}$$

Consider a single electron in a metal influenced by a static external magnetic field $\underset{\sim}{H}$ derived from a vector potential $\underset{\sim}{A}$. The Hamiltonian is assumed to be

$$\mathcal{H} = \frac{1}{2m}(i\hbar\nabla - \frac{e}{c}\underset{\sim}{A}) + V(\underset{\sim}{r}) + \frac{e\hbar}{mc}\underset{\sim}{H}\cdot\underset{\sim}{S} + \Lambda.$$

$V(\underset{\sim}{r})$ is the periodic electrostatic lattice potential, S is the electron spin, $\frac{e\hbar}{mc}\underset{\sim}{H}\cdot\underset{\sim}{S}$ is the Zeeman energy, and Λ is the spin-orbit coupling operator.

If, for the moment, the spin-orbit interaction is ignored and the symmetric gauge $\underset{\sim}{A}=\frac{1}{2}(\underset{\sim}{H}\times\underset{\sim}{r})$ chosen, the Hamiltonian can be divided into two parts

$$\mathcal{H} = \mathcal{H}_0 + \mathcal{H}_1$$

where

$$\mathcal{H}_0 = -\frac{\hbar^2}{2m}\nabla^2 + V(\underset{\sim}{r}) + \frac{e^2}{2mc^2}A^2$$

$$\mathcal{H}_1 = \mu\underset{\sim}{H}\cdot(\underset{\sim}{L} + 2\underset{\sim}{S}).$$

$\underset{\sim}{L}$ is the electron orbital angular momentum operator and has the lattice periodically, while μ is the Bohr magneton.

The wave functions to be used in evaluating $\mathcal{H}$ are Bloch functions. Since $\mathcal{H}$, $\mathcal{H}_0$, and $\mathcal{H}_1$ are periodic in the lattice potential, these give a representation which is diagonal in the wave vector $\underset{\sim}{k}$(9). If spin-orbit coupling effects are small the electron spin up and spin down states can be considered separately. The wave function corres-

ponding to the energy $E_n(\underset{\sim}{k})$ is thus $|n,k\rangle$. It is important to note that because of Brillouin zones, excited states, and the applied magnetic field several different energies can correspond to the same value of $\underset{\sim}{k}$.

If it is assumed that $\mathcal{H}_0 \gg \mathcal{H}_1$, $\mathrm{Tr}\left[g(\mathcal{H})\right]$ can be expanded in powers of $\mathcal{H}_1$ by means of McLaurin's theorem and standard perturbation theory to give

$$\mathrm{Tr}\left[g(\mathcal{H})\right] = \mathrm{Tr}\left[g(\mathcal{H}_0)\right] + \sum_a f(E_a)\langle a|\mathcal{H}_1|a\rangle + \tfrac{1}{2}\sum_a \sum_{c \neq a} \frac{f(E_a)-f(E_c)}{E_a - E_c}\left|\langle a|\mathcal{H}_1|a\rangle\right|^2 \ldots$$

$$+ \; - \; - \; - \; - \; -$$

where $f(\mathcal{H}) = g'(\mathcal{H}) = \left[1+\exp\{\beta(E_F - \mathcal{H})\}\right]^{-1}$ is the Fermi function. The summation is overall possible energy values for all possible values of $\underset{\sim}{k}$.

After considerable mathematical labour $\mathrm{Tr}\left[g(\mathcal{H}_0)\right]$ can be shown to give the diamagnetic susceptibility of the conduction band electrons (9). For nearly free electrons this is the Landau diamagnetism (9), (36). This arises from the electron moving in a circular orbit around the applied magnetic field.

The second term requires a permanent magnetic moment to be present and so only occurs for ferromagnetic metals, a case which will not be considered here.

The last term gives the paramagnetic susceptibility. To evaluate this summation over all possible energy values is changed to an integration over k space and a summation over all the values of $E_n(\underset{\sim}{k})$ which correspond to each value of $\underset{\sim}{k}$. Substituting in the thermodynamic relation for χ gives

$$= \frac{\mu^2}{(2\pi)^3} \sum_{n} \sum_{m \neq n} \int \frac{f(E_n) - f(E_m)}{E_n(\underset{\sim}{k}) - E_m(\underset{\sim}{k})} \langle n\underset{\sim}{k} | \underset{\sim}{L} + 2\underset{\sim}{S} | m\underset{\sim}{k} \rangle \langle m\underset{\sim}{k} | \underset{\sim}{L} + 2\underset{\sim}{S} | n\underset{\sim}{k} \rangle \, d\underset{\sim}{k}.$$

χ consists of three contributions.

(i) The Pauli spin paramagnetism.

$$\chi_p = \frac{\mu^2}{(2\pi)^3} \sum_{n} \sum_{m} \int \frac{f(E_n) - f(E_m)}{E_n(\underset{\sim}{k}) - E_m(\underset{\sim}{k})} \langle n\underset{\sim}{k} | 2\underset{\sim}{S} | m\underset{\sim}{k} \rangle \langle m\underset{\sim}{k} | 2\underset{\sim}{S} | n\underset{\sim}{k} \rangle \, d\underset{\sim}{k}.$$

To get this expression into a more familiar form, the assumption is made that the Fermi surface is spherical and that the electrons are nearly free.

$$\therefore \chi_p = \frac{\mu^2}{(2\pi)^3} \sum_{n,m} \int_0^\infty \frac{f(E+\mu H) - f(E-\mu H)}{(E+\mu H) - (E-\mu H)} \sqrt{2m^* E} \, dE = \frac{4\pi m^* \mu^2}{h^2} \left(\frac{3N}{\pi}\right)^{\frac{1}{3}}.$$

This term arises from a surplus of electrons with their magnetic moments parallel to $\underset{\sim}{H}$.

(ii) Spin-orbit paramagnetism.

$$\chi_{so} = \frac{\mu^2}{(2\pi)^3} \sum_{n,m} \int \frac{f(E_n) - f(E_m)}{E_n - E_m} \Big[\langle n\underset{\sim}{k} | \underset{\sim}{L} | m\underset{\sim}{k} \rangle \langle m\underset{\sim}{k} | 2\underset{\sim}{S} | n\underset{\sim}{k} \rangle + \langle n\underset{\sim}{k} | 2\underset{\sim}{S} | m\underset{\sim}{k} \rangle \langle m\underset{\sim}{k} | \underset{\sim}{L} | n\underset{\sim}{k} \rangle \Big] d\underset{\sim}{k}.$$

The effect of spin-orbit coupling is to lift slightly the quenching of the orbital angular momentum by mixing in other states of appropriate angular momentum and symmetry. The orbital angular momentum is approximately $\frac{\lambda}{\Delta}$, where λ is the spin-orbit coupling constant and Δ is the mean energy between the state being considered and the states being mixed in (36). The arrangement of energy levels within the conduction band is so complex that Δ is almost impossible to calculate, but is of the order of the bandwidth, a few ev. λ is about a tenth of

an ev. or less (22). If the orbital matrix elements are now evaluated by using the tight binding approximation, it is seen that the remainder of the expression closely resembles that for χ_p.

$$\therefore \chi_{so} \simeq \frac{\lambda}{\Delta} \chi_p .$$

Since $\frac{\lambda}{\Delta} \ll 1$ it is not an important term.

(iii) Van Vleck paramagnetism.

$$\chi_v = \frac{\mu^2}{(2\pi)^3} \sum_{n,m} \int \frac{f(E_n) - f(E_m)}{E_n - E_m} \langle n\underset{\sim}{k} | \underset{\sim}{L} | m\underset{\sim}{k} \rangle \langle m\underset{\sim}{k} | \underset{\sim}{L} | n\underset{\sim}{k} \rangle \, d\underset{\sim}{k}.$$

This is a second order effect arising through the orbital angular momentum operator mixing unoccupied excited states into an occupied ground state with quenched orbital angular momentum. It is the same as the Van Vleck temperature independent induced orbital paramagnetism found in some solids (36). If a tight binding approximation is used $\underset{\sim}{L}$ only has matrix elements between states with the same value of $\underset{\sim}{k}$ which differ in the value of their magnetic quantum number m . Thus there are only contributions from matrix elements between levels in the same partially filled band. Most metals have mainly s electrons in their conduction band and so χ_v is negligible. However transition metals have a partially filled d band which can give rise to a significant value of χ_v .

Figure 1.1 shows the typical structure of the d band and the types of transitions that give rise to χ_v.

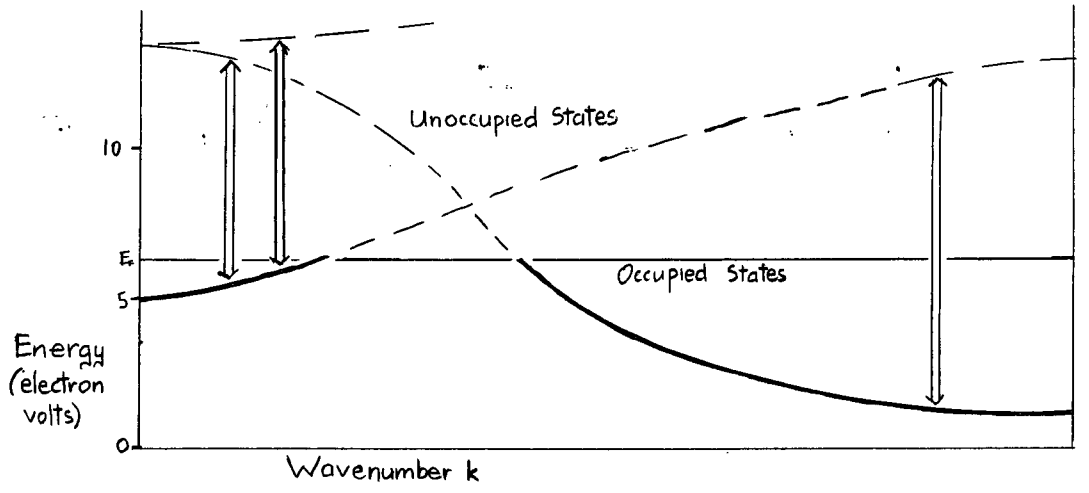

Fig. 1.1 Energy versus Wavenumber for the d Band in a Typical Transition Metal

$$\chi_v \simeq \frac{M^2}{(2\pi)^3 \mathcal{E}}$$

where $\mathcal{E}$ is the energy separation between the ground and excited states, suitable averaged over k space.

There are also two other contributions to the susceptibility; the core electron diamagnetism, and the Langevin paramagnetism of the orbital angular momentum caused by spin-orbit coupling. These are always very small terms.

The bulk susceptibility is due to at least six terms. These usually only have a secondary effect on the magnetic field at the nucleus, which may be much different from that expected from the value of χ. This is since the bulk susceptibility depends on the electron distribution throughout the whole solid, whilst the magnetic field at the nucleus depends predominantly upon the currents and magnetic moments in its very near vicinity.

The magnetic field shifts at the nucleus are usually mainly due to indirect effects occurring through the magnetic field polarising the conduction electrons (Pauli spin paramagnetism). These then couple with the nucleus through various mechanisms to produce a field shift much larger than that directly due to the Pauli spin paramagnetism. The Van Vleck paramagnetism, and the Landau diamagnetism are the only direct terms which can sometimes be of importance in determining the magnetic field at the nucleus.

CHAPTER II

NUCLEAR MAGNETIC RESONANCE IN METALS

'My mind is in a state of philosophical doubt as to magnetism.'

- Coleridge.

It is the purpose of this chapter to describe the properties of the NMR of metals which differ from those of other solids. In accordance with this aim, the elementary aspects of pulsed and steady state NMR will not be given, these being comprehensively discussed in Chapter III of Abragam's book (1). The various reasons why the magnetic field at a nucleus differs from that of the applied magnetic field are given. The spin temperature concept is introduced and its importance in the return to equilibrium shown. There are two decays involved in the return to equilibrium, the spin-lattice relaxation governing energy transfer to the lattice and spin-spin relaxation, which is concerned with internal equilibrium of the spin system. Spin-lattice relaxation and the magnetic field shift are often related. Both of these effects are principally due to the conduction electrons, which can also affect the spin-spin relaxation. Many metals have a quadrupole interaction which alters the energy levels in the system. The last section shows how this modifies the pulsed NMR in single crystals.

2.1 The Magnetic Field at The Nucleus

The resonant frequency of a nucleus in a metal differs

from its value in an insulator. The fractional change in the magnetic field at the nucleus which causes this is known as the Knight shift. It is the sum of various contributions whose relative importance varies in different metals.

Two of these contributions arise from the magnetic coupling of the nuclear dipole moment $\underset{\sim}{\mu}_n$ to the electron dipole moment $\underset{\sim}{\mu}_e$ and to the current produced by its motion. This interaction can be treated non-relativistically, provided care is taken to avoid divergences, to give as the Hamiltonian (1).

$$\mathcal{H}_1 = \underset{\sim}{\mu}_n \cdot \underset{\sim}{\mathcal{H}}$$

where $\mathcal{H} = \frac{8\pi}{3} \underset{\sim}{\mu}_e(\underset{\sim}{r}) + r^{-3}\left[\underset{\sim}{\mu}_e - 3\underset{\sim}{r}(\underset{\sim}{\mu}_e \cdot \underset{\sim}{r})r^{-2}\right] - 2\beta \underset{\sim}{L} r^{-3}$.

$\underset{\sim}{r}$ is the separation between the nucleus and the electron. The operator $\mathcal{H}$ can be regarded as the magnetic field produced by the electron at the nucleus. The last term can be ignored since the electron orbital angular momentum $\underset{\sim}{L}$ is quenched. The other two terms each give rise to a contribution to the Knight shift.

(i) The "Contact" term.

This is the dominant term in most metals and is extensively discussed in the literature (1, 16, 40). The Hamiltonian is

$$\mathcal{H} = \frac{8\pi}{3} \underset{\sim}{\mu}_n \cdot \sum_i \underset{\sim}{\mu}_e^{(i)} \delta(r).$$

The most important features of this interaction are its dependence on the spin orientations and its Dirac δ function form. This means that there is no interaction unless the electron wave function has a finite value at the nucleus. p,d,... electrons make no contribution to this interaction since they

all vanish at the nucleus. The coupling is only to the isotropic s electrons and is given by

$$\frac{8\pi}{3}\mu_{ez}\mu_{nz}\sum_i |\psi_i(0)|^2.$$

$|\psi(0)|^2$ is the s electron density at the nucleus, while the z axis is along the applied magnetic field H_0. The conduction electrons are not localised so the nucleus is equally influenced by all of them. The summation thus becomes an ensemble average, using Fermi-Dirac statistics, over all the conduction electrons. H_0 has polarised the conduction electrons (Pauli spin paramagnetism), so this averaging gives a magnetic field ΔH_0 at the nucleus. The resulting Knight shift is

$$K_c = \frac{\Delta H_0}{H_0} = \frac{8\pi}{3}\left\langle |\psi(0)|^2 \right\rangle_{E_F} \chi_p.$$

$\left\langle |\psi(0)|^2 \right\rangle_{E_F}$ is the averaged value of $|\psi(0)|^2$ over all electrons with the Fermi energy E_F, while χ_p is the nearly free electron Pauli paramagnetism. A more accurate equation results if the electron-electron interactions are approximately taken into account by using a many-body theoretical, or an experimental, value of χ_p.

K_c ranges from about 0.1% to about 3%, increasing steadily with increasing atomic number. Although K_c can be measured very accurately, it usually does not give much information about $|\psi(0)|^2$ because in most metals χ_p is not accurately known. This is unfortunate since $|\psi(0)|^2$ is a parameter with considerable theoretical interest. K_c is

temperature and magnetic field independent in most metals, except for small effects due to lattice expansion.

(ii) The Anisotropic Knight Shift.

The Hamiltonian for this interaction is

$$\mathcal{H} = \underset{\sim}{\mu}_n \cdot \sum_i r_i^{-3} \left[\underset{\sim}{\mu}_e^i - 3\underset{\sim}{r}_i (\underset{\sim}{\mu}_e^i \cdot \underset{\sim}{r}_i) r_i^{-2} \right] .$$

This couples the nucleus to all the non-s electrons through their dipole-dipole interactions. For an axially symmetric crystal, a calculation similar to that for the contact term gives (16)

$$K_{an} = q' (3\cos^2\Theta - 1)\chi_p ,$$

where $q' = \left\langle \int \Phi^* \left[(3\cos^2\alpha - 1) r^{-3} \right] \Phi \, d^3x \right\rangle_{E_F}$.

Θ is the angle between H_0 and the crystal axis of symmetry, α the angle between H_0 and $\underset{\sim}{r}$, and Φ is the total non-s electron wave function. q' is a measure of the spatial anisotropy of the Fermi surface electron's charge distribution. A positive q' means that the non-s electron density is largest along the symmetry axis, a negative q' that it is largest in a plane perpendicular to the symmetry axis. A group theoretical treatment shows that q' is zero for a cubic lattice, irrespective of the electron states (41).

K_{an} can easily be measured in both powders and single crystals, but gives little useful information, apart from the sign of q'. It varies in magnitude from zero to about 0.2% and tends to increase with increasing atomic number. Bi^{209} is an anomalous case in which $K_{an} \gg K_c$.

(iii) Core Polarisation Knight Shift.

The filled electron shells have so far been ignored, apart from their electronic screening effect and their negligible diamagnetism. However, they can sometimes give the most important contribution to the Knight shift by means of the Heisenberg exchange interaction

$$\mathcal{H}_E = \int \psi^*_{\text{conduction}} \left(\frac{e^2}{r}\right) \psi_{\text{core}} \, d^3x.$$

This interaction is zero for conduction and core electrons with antiparallel spins and is repulsive if they have parallel spins (22). A conduction electron thus pushes an s core electron with a parallel spin inwards, increasing $|\psi(0)|^2$ for this spin orientation.

If a magnetic field H_o is applied, there is a population difference between conduction electrons with spins parallel and antiparallel to H_o . In a simple case this causes an increase in $|\psi(0)|^2$ from the electrons parallel to H_o proportional to H_o . This is equivalent to a small additional magnetic field at the nucleus; the core polarisation Knight shift. In all but the simplest metals the exchange interaction makes necessary a renormalisation of the wave functions and this allows the core polarisation to be either positive or negative (42).

The importance of this interaction has only recently been recognized and as yet there is little knowledge of its magnitude, but it is probably present to a significant extent in all

metals (42). In Pt^{195} it is the dominant term, giving a Knight shift of -3.5% (16). This is one of the two known negative Knight shifts and is the largest Knight shift found so far.

(iv) Van Vleck Orbital Knight Shift.

The orbital currents causing the Van Vleck paramagnetism can be split into two parts. Firstly, there is a long range demagnetising factor which is small enough to be neglected. Secondly there is the short range effect of the orbital currents which gives a Knight shift (43)

$$K_v = 2\Omega \langle r^{-3} \rangle \chi_v.$$

Ω is the atomic volume and $\langle r^{-3} \rangle$ is the value of r^{-3} averaged over all the occupied conduction band wave functions.

For transition metals this term can be very important. It cannot be measured accurately, nor can $\langle r^{-3} \rangle$ or χ_v be separately determined, so little information is gained from this term.

The spin-orbit interaction removes some of the orbital quenching. The effects of this are uncertain since only very simple calculations can be done and there are no experimental measurements in metals of spin-orbit effects alone. It is known that it enhances the anisotropic Knight shift (41) and gives a contribution to the isotropic Knight shift in any lattice with inversion symmetry (43). It also presumably causes the electron g factor to become anisotropic, as in crystal field theory (44). If λ is the spin-orbit coupling

constant and Δ is the average separation between electron states, then λ/Δ is approximately the fraction of unquenched orbital angular momentum (44). It is generally assumed that the effects of spin-orbit coupling are negligible if λ is very much less than the conduction band width. This seems to be the case for most metals.

There are various other diamagnetic and paramagnetic terms, but these are usually negligible. Paramagnetic, or ferromagnetic, impurities are the only other important cause of line shifts. With metals of five nines purity, or better, there should be no effects from this source.

The Knight shift thus seems to be predominantly due to four interactions. Of these the contact term is important in nearly all metals while core polarisation probably occurs to some extent in all metals, but is dominant in only a few transition metals. The Van Vleck term is probably only important in some transition metals, while the anisotropic Knight shift only occurs for non-cubic lattices.

2.2 The Spin Temperature

The Hamiltonian for a system of N identical nuclei is

$$\mathcal{H} = \mathcal{H}_z + \mathcal{H}_d,$$

where

$$\mathcal{H}_z = -\underset{\sim}{H_0} \cdot \sum_i \underset{\sim}{\mu_i},$$

$$\mathcal{H}_d = \tfrac{1}{2} \sum_{j \neq k} r_{jk}^{-3} \underset{\sim}{\mu_j} \left[\underset{\sim}{\mu_k} - 3\underset{\sim}{r}_{jk} \left(\underset{\sim}{\mu_k} \cdot \underset{\sim}{r}_{jk} \right) r_{jk}^{-2} \right].$$

Only the case where the Zeeman term $\mathcal{H}_z \gg \mathcal{H}_d$ will be considered here.

The applied magnetic field H_o splits the ground state energy level of a nucleus with spin I into 2I+1 equally spaced energy levels separated by μH_o . If the spin system is in thermal equilibrium with the lattice then the populations p_m, p_{m-1} of the m th and (m-1)th levels are given by the Boltzmann distribution

$$\frac{P_{m-1}}{P_m} = \exp(-\frac{\mu H_o}{kT}),$$

where T is equal to the lattice temperature T_L.

Under certain circumstances the spin system can still be described in this way by a spin temperature T_S, which can be different from the lattice temperature (40). If such a system is perturbed, the T_S relaxes towards T_L at a rate given by (1)

$$\frac{d}{dt}(T_S^{-1}) = -\frac{1}{T_1}(\frac{1}{T_S} - \frac{1}{T_L}).$$

Since $M_z = CH_o/T$ (Curie's law), this becomes

$$\frac{dM_z}{dt} = -\frac{1}{T_1}(M_z - M_o).$$

$$\therefore M_z \propto 1-\exp(-\frac{t}{T_1}).$$

T_1 is the spin-lattice relation time and is a measure of the rate at which energy is transferred from the spin system to the lattice energy reservoir.

The Hamiltonian $\mathcal{H}_d$ for the magnetic dipole-dipole interaction between the nuclei can be written as

$$\mathcal{H}_d = \gamma_j \gamma_k \hbar^2 r_{jk}^{-3} \sum_{j \neq k} (A+B+C+D+E+F),$$

where $B=-\frac{1}{4}(I_j^+ I_k^- + I_j^- I_k^+)(1-3\cos^2\theta)$.

The other terms are unimportant in the following discussion which is based on that of Slichter (40).

The term B plays a decisive role in the establishment of a spin temperature. It couples two neighbouring nuclei, flipping one spin up in energy and the other one down. If $\gamma_j = \gamma_k$ the mutual spin flip conserves the Zeeman energy of the system, yet alters the population distribution of the levels. Because of these properties, it can be shown that if the spin system is disturbed, the mutual spin flips restore the spin system to a Boltzmann distribution.

This decay of a perturbed spin system towards internal equilibrium manifests itself externally as a decay of the components M_x and M_y, of $\underset{\sim}{M}=\sum_i \underset{\sim}{\mu}_i$ which are perpendicular to H_0, towards zero. This decay of M_x and M_y is characterised by the spin-spin relaxation time T_2. Thus after a perturbation has been applied to the spin system, it undergoes internal reorganization for a time of about T_2, until a quasi-equilibrium state describable by a spin temperature has been reached. The spin temperature then exponentially relaxes, with a time constant T_1, towards the lattice temperature. This situation requires the spins to be much more tightly coupled to each other than they are to the lattice, i.e. $T_1 \gg T_2$. Most metals satisfy this condition.

If the energy levels are not equally spaced, the mutual spin flips no longer conserve Zeeman energy and so have negligible probability of occurring. Thus after a disturbance no

internal relaxation towards a spin temperature can occur, but instead each level independently transfers its energy to the lattice. The spin-lattice relaxation is then no longer described by a single exponential. This situation will be returned to later.

2.3 Spin-Lattice Relaxation

In a metal the strongest coupling of the nuclei to the lattice is via the conduction electrons. A conduction electron can be regarded as being inelastically scattered by means of a collision with a single nucleus. In the process it changes the nuclear spin from I_m to I_{m-1} and undergoes compensating changes in its own angular momentum and kinetic energy, as required by the conservation laws. This is only an approximation since an electron wave packet extends over several nuclei, so it can be scattered from an initial to a final state by simultaneous collision with more than one nucleus (40). This is a rare occurrance if $\mathcal{H}_z \gg \mathcal{H}_d$ (45). A subsequent inelastic collision between the electron and an ion transfers the excess energy to the lattice. Since the electron must be able to change its kinetic energy by small amounts, only the electrons near the Fermi surface can take part in the relaxation.

(i) Contact Relaxation.

Relaxation is caused by the nucleus scattering s electrons. The scattering interaction is thus the contact

term $\mu_n \mu_e \delta(\underset{\sim}{r})$. A perturbation calculation then gives T_1 at a temperature T as (40)

$$(T_1 T)^{-1} = \frac{64}{9} \pi^3 k \gamma_e^2 \gamma_n^2 \langle |\psi(0)|^2 \rangle^2 Z_s^2 (E_F).$$

γ_e, γ_n are the electronic and nuclear gyromagnetic ratios respectively, and $Z_s(E_F)$ is the average s electron density of states at the Fermi surface.

The most important feature of this expression is that $T_1 T$ is a constant. This has been experimentally verified for several metals over a wide temperature range, the small deviations observed being due to the effects of thermal expansion of the lattice.

$T_1 T$ is related to the Knight shift due to the contact term by

$$T_1 T K_c^2 = (\pi k \gamma_e^2 \gamma_n^2 \hbar^3)^{-1} \left[\frac{\chi_p}{Z_s(E_F)}\right]^2$$

If the nearly free electron model is assumed, this expression simplifies to the "Korringa relation"

$$T_1 T K_c^2 = \frac{\hbar}{4\pi k} \left(\frac{\gamma_e}{\gamma_n}\right)^2.$$

A more accurate expression which allows for interactions between the conduction electrons is

$$T_1 T K_c^2 = \frac{\hbar}{4\pi k} \left(\frac{\gamma_e}{\gamma_n}\right)^2 \left(\frac{\chi_p}{\chi_p^0}\right).$$

χ_p^0 is the free electron value, while χ_p can be either an experimental value, or a calculated value using quasi-particle theory. This expression differs from the corres-

ponding one in Abragam (1) or Slichter (40), since recent theoretical work shows that it is the free electron density of states that is involved in spin-lattice relaxation, not the quasi-particle density of states (46).

The Korringa relation, or its more accurate version, is commonly used to estimate unknown values of $T_1 T$ from the known Knight shift, or else the value of T_1 derived from the Korringa relation can be compared with the experimental value. A large discrepancy between the two values indicates that other interactions besides the contact interaction are important in the metal.

(ii) Dipolar Relaxation.

The interaction between the nuclear and electronic dipole moments provides the scattering mechanism. This gives (47)

$$(T_1 T)^{-1} = 4\pi (\gamma_e \gamma_n)^4 \hbar^3 Z^2 (E_F) \langle r^{-3} \rangle^2 C.$$

C is a term whose value depends on the lattice and electronic structure. It has a value of about unity and no anisotropy for a cubic lattice. $\langle r^{-3} \rangle$ is averaged over all the conduction band electrons. Z is here density of states of all the non-s electrons.

Unlike the anisotropic Knight shift, T_1 can be non-zero in a cubic lattice. There is no Korringa-like relation between T_1 and K_c for this interaction.

(iii) Orbital Relaxation.

The scattering is caused by the interaction between the dipole magnetic field generated by orbital motion of the conduction electron and the nuclear magnetic dipole. Unlike the previous two scattering processes, there is no reorientation of the electron spin; the nuclear spin change being compensated for by an equal change in orbital angular momentum. $T_1 T$ is given by the same expression as the dipolar relaxation, except that C has different values (47).

Dipolar and orbital relaxation have only been calculated for a cubic lattice, for which no anisotropy is predicted. Theory has not yet shown whether there should be a significant anisotropic T_1 in non-cubic lattices.

(iv) Core Polarisation Relaxation.

A non-s electron polarises the core electrons when it is scattered by them. The transient polarisation acts on the nucleus through the contact term to give nuclear relaxation. In the collision the electron suffers a spin flip to conserve angular momentum. The relaxation time calculation is difficult and has only been done for transition metals with a cubic lattice (27). For this case, $T_1 T$ has a form similar to that of the contact relaxation. It also satisfies the Korringa-like relation

$$T_1 T K_{core}^2 = \frac{\hbar}{4\pi k} \left(\frac{\gamma_e}{\gamma_n}\right)^2 F.$$

F is a factor of about unity which depends on the degeneracy of the conduction band.

These relaxation mechanisms via the conduction electrons are the most important ones. Contact relaxation is the dominant mechanism in most metals, but core or orbital relaxation can dominate in some transition metals. Dipolar relaxation is never important. These relaxation mechanisms are stronger than those in most other types of solids; $T_1 T$ typically being about one sec-deg.

There are probably no significant interference terms between the various relaxation mechanisms so they can, in principle, be unambiguously separated (27). In practice this is very difficult and requires an extensive series of measurements of T_1, the Knight shift, and the magnetic susceptibility over a wide temperature range and the use of several not very reliable theoretical parameters. The result of this type of analysis shows which is the dominant mechanism, but is quantitatively unreliable.

Various relaxation mechanisms which directly couple the nucleus to the lattice vibrations through magnetic dipole, or electric quadrupole, interactions also occur (1). These are all unimportant in metals. Impurities can sometimes cause noticeable relaxation. Paramagnetic, or ferromagnetic, ions have a large magnetic field near them which strongly couples neighbouring nuclei to the lattice vibrations, thus forming quite an efficient relaxation mechanism (1). In very impure samples at low temperatures, this paramagnetic relaxation could be important. Impuri-

ties also disturb the lattice symmetry and this results in a large long range electric field gradient near the impurity (22). If the nucleus has an electric quadrupole moment it can couple to this and hence to the lattice through the vibrating impurity atom. This mechanism is probably not very strong since deliberate introduction of impurities into aluminium left T_1 unaffected by an impurity concentration of 0.2% (48).

2.4 Spin-Spin Relaxation

It is well known that after the application of a rf pulse the transverse magnetisation has a decreasing amplitude which is the Fourier transform of the line shape (1). The spin-spin relaxation time T_2 governs the decay of the transverse magnetisation. T_2 can thus be related to the properties of the line shape and in particular to the second moment. The second moment is one of the few properties of the line shape which can often be calculated exactly. For this reason, the following discussion will concern line widths and second moments, rather than T_2 directly.

In metals there are three main contributions to the line width.

(i) The Dipolar Line Width.

This is due to the nuclear magnetic dipole-dipole interaction. For this interaction the second, and higher, moments can be calculated for a given lattice structure (1). From these the line shape can, in principle, be got. The

line shape should be approximately gaussian with a width of a few gauss. This corresponds to $T_2 \sim 100 \mu s$.

(ii) Pseudo-Exchange (Ruderman-Kittel) Coupling.

In this interaction two adjacent nuclei couple by means of the conduction electrons. A conduction electron is scattered from a nucleus by the contact term $\underset{\sim}{I}_i \cdot \underset{\sim}{S} \delta(\underset{\sim}{r})$ to an excited state. The spin orientation of the excited state depends on that of the nucleus. If the electron is then scattered off a second nuclear spin $\underset{\sim}{I}_j$, the nucleus feels the spin of the excited state and hence senses the orientation of the first nucleus. An elaborate second order perturbation theory calculation, using the nearly free electron model and a spherical Fermi surface, gives the pseudo-exchange Hamiltonian as (4)

$$\mathcal{H}_{ex} = J_{ij} \, \underset{\sim}{I}_i \cdot \underset{\sim}{I}_j .$$

The constant J_{ij} is given by

$$J_{ij} (\underset{\sim}{r}_{ij}) = \frac{\hbar^2}{9\pi} \gamma_e^2 \gamma_i \gamma_j \hbar m^* \langle |\psi(0)|^4 \rangle_{E_F} \; r_{ij}^{-4} \left[2k_F r_{ij} \cos(2k_F r_{ij}) - \sin(2k_F r_{ij}) \right] .$$

The important features in this expression are its oscillatory nature and its dependence on $m^* \langle |\psi(0)|^4 \rangle_{E_F}$. The latter also occur in the expression for the isotropic Knight shift in a different combination. $\langle |\psi(0)|^2 \rangle_{E_F}$ can thus be obtained by comparing measurements of these quantities.

The simplifications in the theories reduce the significance of the value obtained. The effect of the oscillatory

part has not been worked out for ordinary metals and it is usually ignored; J being assumed proportional to the asymptotic form r^{-3}.

The effect of this interaction depends upon the structure of the metal. If there is only a single isotope present, the pseudo-exchange interaction narrows the line. However, if there are several isotopes, or a quadrupolar interaction, so that there are two or more lines, the interaction broadens the lines.

(iii) Pseudo-Dipolar Broadening

This is a similar type of interaction to the pseudo-exchange interaction, except that excitation of the electron is through the interaction of the nuclear and electronic magnetic moments. The de-excitation occurs through the contact interaction. A similar calculation to that of the pseudo-exchange contribution gives the pseudo-dipolar Hamiltonian as (50)

$$\mathcal{H}_{pd} = B_{ij}\, \underset{\sim}{I}_i \cdot \left[\underset{\sim}{I}_j - 3\underset{\sim}{r}_{ij} (\underset{\sim}{I}_j \cdot \underset{\sim}{r}_{ij}) r_{ij}^{-2} \right] r_{ij}^{-3} .$$

B_{ij} is a complicated expression which involves an integration over the non-s electrons at the Fermi surface and so is related to the anisotropic Knight shift. It also contains the same oscillatory term that J does.

If a spherical Fermi surface is assumed, group theory shows that $\mathcal{H}_{pd}$ must have the dipolar form (50). It can also be shown that higher order contributions to the interaction do

not alter this form. However, if the spherical assumption is not made there is no group theoretical proof that $\mathcal{H}_{fd}$ must be dipolar (1).

Because it is of the dipolar form it must always broaden the line. Both of these interactions increase rapidly in strength with increasing atomic weight. Below an atomic weight of about 80 the interactions are undetectable, but for very high atomic numbers they can increase the second moment by over an order of magnitude. This corresponds to decreasing T_2 to below 10μs. Usually both interactions are simultaneously present; their relative magnitudes depending upon the fractions of s and non-s electrons present.

The only other line broadening mechanisms of importance are T_1 broadening and quadrupolar effects in a strained or impure crystal. Because of the uncertainty principle, T_1 broadens the line by an energy $\sim \hbar/T_1$. If $T_1 \sim T_2$ this significantly broadens the line. Quadrupolar effects slightly smear the resonant frequency and this appears as a broadening of the line.

2.5 The Quadrupolar Interaction

Many nuclei are non-spherical and so have an electric quadrupole moment Q. The quadrupole moment interacts with the electric field gradients present in a non-cubic lattice to give a series of energy levels. Consider a metal with an axially symmetric lattice, so that it produces an axial electric field gradient $V_{zz} = \frac{\partial^2 V_{zz}}{\partial z^2}$. If a magnetic field H_o is

applied at an angle θ to the crystal symmetry axis, the Hamiltonian for a single nucleus becomes (40)

$$\mathcal{H} = \mathcal{H}_z + \mathcal{H}_Q ,$$

where

$$\mathcal{H}_z = -\gamma\hbar H_0 I_{z'} ,$$

$$\mathcal{H}_Q = \frac{eQV_{zz}}{4I(2I-1)}\left[3I_{z'}\cos^2\theta + 3I_{x'}\sin^2\theta + \tfrac{3}{2}(I_{z'}I_{x'} + I_{x'}I_{z'})\sin 2\theta - I^2\right].$$

When $\mathcal{H}_z \sim \mathcal{H}_Q$ the energies and wave functions of the Hamiltonian have to be found by numerical computation (51). Perturbation theory can be used outside this region. The low field case ($\mathcal{H}_Q \gg \mathcal{H}_z$) will not be considered here.

If $\mathcal{H}_z \gg \mathcal{H}_Q$ the axis of quantisation is along the magnetic field so a perturbation theory calculation gives the resonant frequencies as (1)

$$\nu_m = \nu_L + \tfrac{1}{2}\nu_Q(m-\tfrac{1}{2})(3\cos^2\theta - 1) + \text{higher terms},$$

where the quadrupole frequency $\nu_Q = \frac{3eQV_{zz}}{2I(2I-1)}$.

ν_L is the Larmor frequency, while ν_m is the frequency of the transition from the m-1 to the mth energy level.

There are several features to note about the quadrupole interaction. The most important is that unless $I \geqslant 1$ it vanishes. The other feature is that the 2I+1 Zeeman energy levels are no longer equally spaced. The result of this is that the resonance line is split into 2I separate lines. If only the first order term is considered, the frequency of the central $m-1 = -\frac{1}{2} \rightleftharpoons m = \frac{1}{2}$ transition remains the same as ν_L. The

other 2I-1 satellite lines are symmetrically displaced from the central line. Furthermore, if the magnetic field is rotated until $\theta=\cos^{-1}(\frac{1}{3})$, the 2I lines coalesce into a single line. If higher order terms are considered, then the frequency of the central line is shifted and it is also no longer possible for the 2I lines to exactly coalesce.

The electric field gradient V_{zz} is derived from all the electrons and ions in the metal. The closed electron shells are spherically symmetric and so do not directly contribute to V_{zz}, even though they are the nearest charges to the nucleus. The potential at a nuclear site due to all the other ions in the lattice can be calculated with considerable accuracy. However, this is not the potential gradient actually felt by the nucleus. The field from the other ions slightly distorts the closed shells. Because they are so close to the nucleus their distortion magnifies the effect of the external field by a factor $1+\gamma_\infty$ (40). γ_∞ is the Sternheimer antishielding factor and is usually at least ten. Unfortunately, it cannot be accurately calculated. There is also a contribution from the non-spherical electron distribution of

$$V'_{zz} = e\left\langle \int \Phi^* [(3\cos^2\alpha - 1) r^{-3}] \Phi \, d^3x \right\rangle .$$

This is related to the term q' in the expression for the anisotropic Knight shift. They are not usually identical since q' is averaged over the Fermi surface electrons and V'_{zz} is averaged over all the conduction electrons. If the conduction band has a complex structure, it is not even necessary

for them to have the same sign. The meagre evidence available suggests that most of the electric field gradient is due to the conduction electrons (49).

2.6 The Line Width With A Quadrupole Interaction

It is assumed that the quadrupole interaction is large enough to clearly separate the 2I lines. If just the dipolar interaction is considered, there is little change in the line width (1, 52). The presence of a pseudo-exchange interaction causes a considerable change in the line width. When any of the lines overlap this interaction causes a narrowing of the lines. However, when they do not overlap many of the mutual spin flips no longer conserve Zeeman energy and so are suppressed. The effect of this is to allow the interaction to broaden the line (56). The pseudo-dipolar interaction also broadens the line. The line width in metals with an atomic weight above 80 and with a quadrupole interaction is thus always greater than the dipolar width.

2.7 Pulsed NMR With a Quadrupole Interaction

In the system to be discussed $\mathcal{H}_z \gg \mathcal{H}_Q \gg \mathcal{H}_d$. There will thus be 2I separate lines in the spectrum. Because of the inequality in energy level spacing, the only mutual spin flips which are energetically allowed are those which do not change the energy level populations. Thus if the system is perturbed it is no longer possible to establish a spin temperature for the whole system. This changes some of the NMR properties.

Initially assume that there is no coupling between separate energy levels. Thus a pulse applied at the resonant frequency of one line does not affect the other levels so that they can be disregarded. This assumes that the pulse contains only one frequency, a situation unattainable in practice. The condition for a 90° pulse for the $m \rightleftharpoons m+1$ line becomes (1)

$$\gamma H_1 \tau = \tfrac{1}{2}\pi\left[(I-m)(I+m+1)\right]^{-\frac{1}{2}},$$

where τ is the rf pulse width. Since only two levels are involved, the precessing magnetic moment is much smaller than when a spin temperature allows all $2I+1$ levels to be involved in the transitions. The system can be assumed to have a fictitious spin of $\frac{1}{2}$ (1), rather than its true spin of I, so that the fractional reduction in magnetisation is $3/4I(I+1)$. After application of an rf pulse, the two level sub-system can be described by a spin temperature which relaxes towards the lattice temperature. The relaxation need not be a simple exponential decay. Pulsed NMR in a system of this type thus requires shorter pulses, but gives a weaker signal, than in a normal Zeeman system.

If there is coupling between the lines, the situation can be very complicated. However, the basic features of such a system can be understood from studying the simpler case of two different systems, each describable by a spin temperature, coupled together. Energy conserving spin flips are by far the strongest coupling mechanism. However, some other terms in the dipolar Hamiltonian give a much weaker coupling.

Mutual spin flips which do not conserve Zeeman energy can also occur if phonons, or some other source, can supply the energy difference. This is usually a weak coupling mechanism because of the scarcity of phonons with the required energy.

Let both systems be perturbed and then set up the rate equations for the population changes of all the levels. When combined with the principle of detailed balance, this gives the rate equations for the spin temperatures as (40, 53)

$$\frac{d}{dt}(\theta_1^{-1}) = -T_{11}^{-1}(\theta_1^{-1} - \theta_0^{-1}) - A\theta_1^2(\theta_1^{-1} - \theta_2^{-1}),$$

$$\frac{d}{dt}(\theta_2^{-1}) = -T_{22}^{-1}(\theta_2^{-1} - \theta_0^{-1}) + A\theta_2^2(\theta_1^{-1} - \theta_2^{-1}).$$

θ_1 and θ_2 are the spin temperatures, and T_{11} and T_{22} the spin-lattice relaxation times in systems 1 and 2 respectively. In both equations, the first term on the right is the spin-lattice relaxation towards the lattice temperature θ_0, while the last term involves an energy transfer (cross relaxation) to the other system at a rate depending on the temperature difference between them. The time constant governing this cross relaxation can be found by putting $T_{11} = T_{22} = \infty$ and combining the two equations to give

$$\frac{d}{dt}(\theta_1^{-1} - \theta_2^{-1}) = -A(\theta_1^2 + \theta_2^2)(\theta_1^{-1} - \theta_2^{-1}).$$

The cross relaxation time T_{12} is thus given by

$$T_{12} = A(\theta_1^2 + \theta_2^2).$$

When T_{11} , $T_{22} \gg T_{12}$, the system first cross relaxes to a common spin temperature, which then relaxes towards the lattice temperature. Its behaviour can thus be described by two independent exponential decays. If $T_{12} \gg T_{11}$, T_{22} the systems decay almost independently toward the lattice temperature at rates described by T_{11} and T_{22} respectively. For the intermediate case where $T_{12} \sim T_{11}$, T_{22} a simple description of the system is no longer possible; its decay depending on the three time constants and also on the way it is perturbed.

Although some details of the energy levels and couplings are different, a quadrupole split Zeeman system also shows cross relaxation effects. An experimental investigation of such a system showed that a cross relaxation theory based upon the idea of mutual spin flips when the lines overlapped was only moderately successful in describing the system (54). When the lines overlapped extensively cross relaxation between the levels occurred in a time less than 60ms., but when they were widely separated the cross relaxation time constant was 47 seconds, not much less than T_1 . If the lines only partially overlapped the cross relaxation time was intermediate between these values, as expected theoretically. However, there was often an extended period in the middle of the cross relaxation when energy transfer ceased. A more serious discrepancy is that if a satellite line is perturbed by a very short rf pulse the equilibrium distribution after cross relaxation is not a Boltzmann distribution. Perturbing the central lines gives a

Boltzmann distribution after cross relaxation has occurred, in agreement with the theory.

Recent theoretical and experimental work (55) suggests that the failure of the rate equation approach to cross relaxation is due to neglect of the dipole-dipole system. The nuclear magnetic system actually consists of sub-systems described by the Zeeman terms and by the dipole-dipole terms of the Hamiltonian. Each of these sub-systems has its own energy and spin temperature and can be weakly coupled to other sub-systems. Cross relaxation involves energy transfer from Zeeman to dipole-dipole sub-systems, as well as energy transfer between Zeeman sub-systems. It is believed that a careful consideration of these energy exchanges can explain the discrepancies in the cross relaxation experiments.

CHAPTER III

THE EXPERIMENTAL METHOD

'A Mighty Maze! But Not Without a Plan.'

- Pope:

The pulsed NMR spectrometer is to be discussed here is designed specifically to measure the anisotropy of T_1 in metallic single crystals, but it does have sufficient versatility to measure T_1 and T_2 in metallic powders, or non-metallic substances, with only trivial modifications.

In a standard pulsed NMR system, the nuclear spin system, initially aligned along H_o, is tipped by a huge uniform rf pulse applied at right angles to H_o. At the end of the rf pulse all the nuclei are aligned at the same angle to H_o. The recovery of the spin system is then studied by amplifying the short lived free induction signal induced in a coil wound round the sample. Abragam (1) gives a general description of the principles involved, while Clark (2) lucidly describes the compromises and experimental details involved in the design and construction of a pulsed NMR apparatus.

The writer's apparatus is based on Clark's apparatus, both in principle, and in some electronic circuitry. However, the use of metallic single crystals samples causes some differences in design philosophy, and also in the circuitry.

In a non-metallic sample, or a very finely divided metallic powder, the rf field completely penetrates the sample, but it can only penetrate a very short distance into a metallic sample. This is because of the well-known skin effect (3). The skin effect has two main experimental consequences.

(i) A signal is only obtained from nuclei within a distance of about the skin depth δ of the surface. These are usually only about 1% of the total number of nuclei in the sample, so that the signals are much weaker than in a normal NMR experiment. They are so weak that they are always obscured by noise when displayed on an oscilloscope, so that a boxcar integrator, a device for improving the S/N ratio of repetitive signals, must always be used.

(ii) The rf field $2H_1$ varies rapidly in both size and phase with increasing distance from the surface of the sample. Thus at the end of the rf pulse, the nuclei are not all aligned at the same angles to H_0, so that conventional pulse trains such as a $\frac{\pi}{2}-\pi$ pulse sequence cannot be used.

Because of these facts a rather laborious special method of measuring T_1 had to be developed.

3.1 General Description of the Apparatus

The main features of the apparatus are:

(i) ability to operate at any frequency between about 5 and 10 Mc/s without extensive retuning

(ii) a rf magnetic field H_1 of 25 gauss

(iii) a recovery time of 15μs

(iv) phase sensitive detection

(v) boxcar integration

(vi) a coil system designed specifically for metal samples.

Two signals are taken from the master Colpitts oscillator. One is used as a reference phase and is passed through a phase shifter into the amplifier. The other signal passes into the gated power amplifier. This is gated by positive pulses from a timing unit, and delivers rf pulses of about 1.8 KV. peak to peak to the transmitter coil. The induced signal from the coaxial pickup coil is amplified in a tuned pre-amplifier with a bandwidth of about 0.5 Mc/s and then passed into an Arenberg WA600D amplifier. In the amplifier the signal and the much larger reference signal, are linearly added to give a phase sensitive system. This improves the S/N ratio slightly, but its main advantage is that it removes the nonlinearity in the Arenberg amplifier which is caused by the small signal characteristics of the rectifier diodes. The signal plus reference is then rectified and passed, after amplification, into a boxcar integrator. The boxcar integrator improves the S/N ratio by a factor ranging from about 10 to 100. The output from the boxcar is then recorded on a Varian Model G-11A chart recorder (Fig. 3.1).

The timing unit can also send synchronised pulses to the recorder event marker, so that timing pips at intervals of 100 μs to one second can be recorded on the chart along

with the signals.

The timing unit can also supply a quench pulse to the preamplifier which helps reduce the recovery time. It does this by lowering the Q of the pickup coil whilst the rf pulse is on, and then raising it soon after the pulse has ceased.

The timing unit also provides a two pulse sequence of arbitrary widths, separation and repetition rate for gating the power amplifier. It also provides a boxcar gating pulse, and event marker pulses which are synchronised with the basic rf pulse sequence. As well as this it contains a sawtooth generator which can be used for linearly sweeping the main magnetic field, for linearly varying the separation between two pulses, or linearly varying the separation between a rf pulse and the boxcar gating pulse.

The dewer system was designed and built to operate at helium temperatures. However, no helium temperature measurements have been made and it was subsequently necessary to modify the apparatus in such a way that helium temperatures are now unattainable. Liquid nitrogen temperature measurements are still easily made.

3.2 The Timing System

The basic repetition rate of the pulse sequence is determined by a free running multivibrator which triggers a Tektronix 162 sawtooth generator. This repetition rate can be varied from $(8\text{ms.})^{-1}$ to $(9\text{ sec})^{-1}$. The pulse from the

Gate Out terminal of the generator is used to trigger the marker pulse, while the sawtooth output is fed into two Tektronix 163 pulse generators. One of the pulse generators is set to trigger at the beginning of the cycle, while the second one is set to trigger at some later time in the cycle. Thus the two pulses can be separated by any desired interval up to nine seconds. The width of each of these pulses can be independently varied from 5μs up to many milliseconds. The two pulses are then fed into a pulse mixer which also amplifies them to the 90 volts required to gate the power amplifier (Fig. 3.2).

The risetime and decay time of the gating pulses are less than 0.5μs. Observation on an oscilloscope shows that this causes half a cycle jitter in the rf pulse length. This jitter causes slight variations in the angle through which the nuclei are tipped and this shows up as extra noise. However, the S/N ratio with metal samples is so poor that the extra noise due to the pulse jitter is usually unobservable. Jitter due to variations in the triggering time of the pulse generators is usually also unobservable.

A pulse is also taken from the Pulse Out terminal of the second Tektronix 163 pulse generator and used for gating the boxcar. This is done by triggering a Tektronix 162 sawtooth generator whose output is fed into a Tektronix 161 pulse generator. This can trigger on any part of the sawtooth, so that its output pulses (fifty volts positive and

negative), which gate the boxcar, can occur any time after the beginning of the second rf pulse (Fig. 3.6).

This completes the description of the basic part of the timing unit. There are, however, several auxiliary parts of the timing unit, some of which are not often used.

In the Tektronix 161 and 163 pulse generators, a voltage comparator stage compares the instantaneous voltage of the input sawtooth with a voltage set by a potentiometer. When the decreasing sawtooth voltage equals the preset voltage, the pulse generator is triggered. If the preset voltage is now varied slowly and linearly, the time delay between the start of the sawtooth and the generator triggering will also vary linearly with time. The preset voltage is varied in this fashion by disconnecting the comparator grid from the potentiometer and instead feeding a slowly varying negative sawtooth voltage onto it (4). A Tektronix 161 and a 163 pulse generator were modified in this way; a two-way switch being used so that either the internal preset voltage or the external sawtooth voltage can be fed onto the comparator grid.

If the external sawtooth is applied to the modified 163 pulse generator gating the power amplifier, a two pulse sequence is obtained with linearly increasing separation between the pulses. This sequence enables the recovery of the magnetisation after a pulse to be directly recorded on a chart, from which T_1 can be quickly obtained.

Applying the external sawtooth to the modified 161 pulse generator gating the boxcar, sweeps the boxcar gate over the whole induction tail following a rf pulse. From the recording of the boxcar output T_2 can be found.

The comparison sawtooth is got from a phantastron which starts a sweep when manually triggered. Normally the sawtooth decreases from 140 volts to 20 volts, but a bias voltage can be applied so that the output voltage remains constant at any voltage between 140 volts and 100 volts, until the decreasing sawtooth reaches this voltage. The output voltage then follows the sawtooth voltage. This feature allows for the finite width of the rf pulses, a necessary feature when sweeping with some pulse sequences. The sawtooth duration can be varied from ten seconds to thirty minutes in seven steps. The sawtooth linearity deviation is less than 1% over 80% of the sweep, but then increases rapidly to about 10% at the end of the sweep. A series of measurements showed that the sawtooth length was reproducible to within 2% of its length. Neither of these imperfections affects the results since either a linear sweep is not necessary, or else calibrated timing pips are used.

The sawtooth generator is usually used for sweeping the magnetic field through the resonant value. To do this, an attenuated sawtooth voltage is taken from the sawtooth generator and fed into the magnet power supply.

To measure T_1 or T_2 it is necessary to measure time intervals such as those between rf pulses, or between one rf

pulse and the boxcar gating pulse, with an accuracy of 2% or better. Two alternative timing methods are available.

If the slow sawtooth is being applied to the 161, or the 163 generator, a pulse is taken from the Gate Out terminal of the relevant 162 sawtooth generator triggering it and fed into the Gate In terminal of the 162 sawtooth generator used as a marker pulse generator. This is set to run at some convenient repetition rate, such as 1Kc/s. When the pulse is applied to the Gate In terminal, the generator gives out pulses at, say, one millisecond intervals until the gating pulse ceases. This train of pulses, which is synchronised to the rf pulses, is then fed into a coincidence unit. A pulse from the boxcar gate, or the second rf gate pulse, is also fed into the coincidence unit and when these two pulses coincide, a current pulse actuates the event marker pen on the recorder. Thus the boxcar output and a series of timing pips are recorded on the same chart.

Alternatively a double beam oscilloscope can be used with the train of marker pips displayed on one channel and the rf pulse sequence displayed on the other channel. The separation between rf pulses can then be manually adjusted to coincide with the desired timing pip.

The pulse generator was calibrated with a C.M.C. 707BN frequency counter. It was found to be accurate to within 1.5% on all ranges and repetition rates after a warm-up period of several hours. The coincidence unit requires the pulses

to overlap 0.6μs before it triggers. However, the minimum separation between marker pulses is 100μs, so that this is a negligible systematic error. If a double beam oscilloscope is used the timing error due to aligning the two pulses visually is still less than 1%. This is since the screen is 10cm. wide and the full width of the screen is always used. As the lines are less than 1mm. wide, it is easy to make them coincide to within less than 1% of the screen width. It thus is safe to assume an error less than 2% in all timing measurements. The S/N ratio is nearly always less than fifty, so that the error in the timing measurements is sufficiently small.

The pulse mixer also provides a two volt positive pulse which is used for triggering the oscilloscope and a minus twenty volt quenching pulse of variable width for the pre-amplifier quenching circuit.

3.3 The Gated Power Amplifier

The Colpitts oscillator can be tuned from about 5 to 11 Mc/s. and has a long term frequency drift of one part in 5×10^4 per hour. This is adequate stability for most measurements on broad metal lines.

The output from the oscillator passes through a cathode follower to a gating circuit designed by Blume (5) for negligible rf leakage when the gate is off. It is very satisfactory in this respect, but when the gate is switched on by a ninety volt positive pulse from the pulse mixer, it loads the cathode

follower sufficiently to decrease its output by about 20%. In Blume's circuit, the phase reference signal is also taken from the same cathode follower. In this case, the drop in output upsets the phase reference signal for about 50μs after the gate is switched off. To cure this trouble, a separate cathode follower was added for the phase reference signal channel.

After the grating circuit there are three class C amplifier stages. These give high power amplification, good carrier suppression, and short rise and fall times with reasonably high Q circuits in the first two stages. The final stage is an 829B which is operated with 1500 volts on the plate and a screen voltage which can be varied from 450 to 600 volts. Under these operating conditions, the maximum power output is about 2KW. As in Clark's transmitter (2), variable damping of the transmitter coil is provided by biased diodes placed across it. With large applied rf voltages one of the diodes is always open circuited so that negligible damping occurs. However, when the rf pulse decays to about one volt, both diodes conduct and shunt the coil with an impedance of about 600Ω. Rise times and fall times are typically about 1μs, while pulses up to 600μs long can be generated before sagging in the rf output voltage becomes excessive. The piezoelectric properties of ceramic condensers did not cause ringing in the output circuit, provided they were used well below their maximum rated voltage. This is contrary to the experience of Clark (2).

3.4 The Preamplifier

This is a tuned voltage amplifier slightly modified from one designed by Clark (2). It has a gain of 16 and a bandwidth of about 0.5Mc/s. The main difference is that crossed silicon diodes limit the grid swing of the input stage to ± 1 volt, even for applied voltages of several hundred volts. They also heavy damped the pickup coil for large applied rf voltages, but have negligible effect when only the very small signal voltage is present. Instead of crossed diodes, Clark used a quenching circuit in which a quenching pulse derived from the pulse mixer and amplifier circuit switched a low impedance loud across the pickup coil during the rf pulse, and for a variable time afterwards.

However, in the present apparatus the input rf pulses are so large that crossed silicon diodes were initially added to protect the quenching circuit. It was then found that when the quenching circuit was switched off, a small transient occurred which swamped the very weak induced signal. This transient was due to the storage capacitance of the switching diode in the quenching circuit and could not be eliminated. Thus the quenching circuit had to be disconnected for all measurements on single crystals and the crossed diodes alone used for damping the coil. If powdered samples are used the much larger signal available completely obliterates the transient so that the quenching circuit can be used.

The equivalent series noise resistance of the preamplifier is about 250Ω so that for liquid nitrogen temperatures and above, the thermal noise from the resonant pickup coil is the dominant noise source. The preamplifier amplification is such that its noise output is much larger than the thermal noise generated in the input stage of the Arenberg amplifier.

3.5 The Main Amplifier

This is an Arenberg WA600D which has been modified to improve its recovery time. Originally the amplifier had a frequency response from 2 to 65 Mc/s. Auxillary tuning coils enabled the frequency response to be altered to a passband about 10Mc/s wide centred on any frequency within this range. However, there was an annoying overshoot present for about 20μs after the rf pulse. To eliminate this, the low frequency response was increased to 3.5Mc/s and the screen bypass condensers reduced in value. Later on the input stage was rebuilt along lines suggested by the manufacturer. These improvements reduced the overshoot to less than 5μs in duration.

The low frequency response of the video section was decreased from 20 to 2c/s to avoid noticeable baseline droop. This section also introduced considerable 60c/s pickup from the filaments into the output, so that the filaments were converted to run on regulated D.C. current.

The recovery time of the whole system is nearly 10μs from the end of the transmitter gating pulse. This is

probably about twice as long as the minimum practical limit, but significant reduction in the recovery time would require an exorbitant amount of time and labour.

Although neither the preamplifier nor the main amplifier has an automatic gain control, little trouble is experienced with long term drifts in gain. This is always less than 1% per hour, provided the amplifiers have been allowed to warm up for several hours. However, there are short term fluctuations in gain of about 10%, with a period of about ten minutes' duration which cause some trouble. G.A. DeWit has noticed similar fluctuations in gain in another Arenberg used in this laboratory (private communication to the writer).

The linearity of the Arenberg is poor; the linear region extending from about 2 to 12 volts at the output. To improve the linearity for small signals the reference voltage from the oscillator is added to the signal at the sixth stage of the amplifier through a high pass filter and a resistive network. A phase shifter and attenutor (2) are inserted in the reference channel between the oscillator and the amplifier. The amplitude of the reference voltage is much larger than the signal and is adjusted so that it is near the centre of the linear region. It thus performs the double function of making the amplifier linear for small signals and providing phase sensitive detection. This simple method of phase sensitive detection improves the S/N by a factor of $\sqrt{2}$ (1), but can

introduce considerable distortion if the reference signal is not much larger than the signal (Appendix I). In these experiments, the reference signal is at least ten times the signal, so that the distortion is always less than 5%. This is tolerable as it is less than the error caused by noise.

3.6 The Boxcar Integrator

This is an electronic device for improving the S/N ratio of a repetitive signal. It basically consists of an electronic switch which is switched on by a gating pulse occurring at a set time after an applied rf pulse, followed by a RC circuit which averages the voltages obtained during successive sampling intervals.

The boxcar was built to the design of Blume (4). The only major modification is the addition of a voltage amplifier stage at the input.

The boxcar circuit is linear within 2% for voltages up to ± 20 volts, but the voltage amplifier at the input is only linear for input voltages of about ± 8 volts. This voltage swing is adequate for the present experiments and can easily be increased if necessary.

The measured long term drift in the base line corresponds to a drift of 0.05 volts per hour at the input. This slow drift is hardly noticeable, even in experiments taking many hours.

In the ideal boxcar circuit (Fig. 3.3) the switch S is closed for a short time τ_s at the repetition rate T^{-1} of the

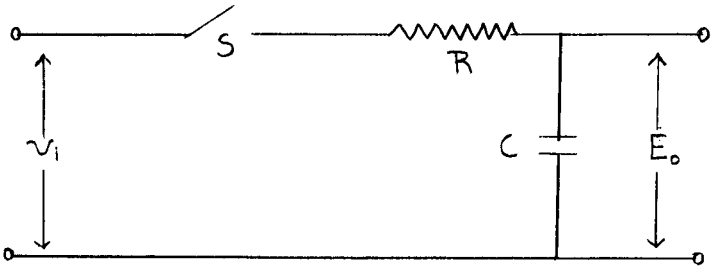

Fig. 3.3 Equivalent Circuit of the Boxcar Integrator

rf pulses. The time constant $RC \gg \tau_s$, so that the circuit acts as an integrator.

If the r.m.s. input noise voltage is $\overline{v_i}$ and the output noise voltage is $\overline{E}_o$ then (6)

$$\overline{E}_o = \left(\frac{\tau_c}{RC}\right)^{\frac{1}{2}} \overline{v_i} \ ,$$

where τ_c is the noise correlation time. For a thermal noise source $\overline{v_i} \propto \sqrt{B}$ and $\tau_c \propto B^{-1}$ so that $\overline{E}_o$ is independent of the bandwidth of any amplifier ahead of the boxcar integrator. This equation has been derived under the assumption that $\tau_s \gg \tau_c$, a condition which is easily satisfied experimentally.

If v_i is the input signal, then the boxcar response is the same as a low pass RC filter with a time constant $\tau' = RCT/\tau_c$ (6). Unless care is taken in the choice of τ' considerable distortion of the signal can occur.

An experimental test of these equations was made by using an amplifier as a thermal noise source with a frequency spectrum from about 2c/s to several megacycles. This was fed

into the boxcar integrator and the output measured on a chart recorder, while various parameters were systematically varied. The measurements were crude, but verified that the noise output is independent of the bandwidth and that the S/N$\propto$ RC, except for very large values of RC when the S/N became less than predicted. The equations for the boxcar voltages ignore the effect of the recorder time constant, which is about one second for the Varian recorder. This time constant performs a further integration of the noise for small values of T, so that the S/N ratio is increased. Experimentally $\overline{E}_o = \left(\frac{\tau_c}{RC}\right)^{\frac{1}{2}} \overline{v_i}$ for $T \gtrsim 70$ms., but decreases steadily for $T \lesssim 70$ms., being a factor of six smaller for T=1ms.

3.7 Power Supplies and Noise Suppression

The 1500 volts for the power amplifier is supplied by a simple unregulated power supply, which also gives 450, 525 or 600 volts for the screen regulated by voltage regulating tubes. The large output impedance of these supplies is overcome by the use of large storage condensers. A 200ma. regulated supply gives the 350 volts used in an earlier stage of the power amplifier.

Apart from the Arenberg which has its own regulated supply, the rest of the apparatus is powered by two Tektronix 160A regulated power supplies.

The 6.3 volt D.C. filament current comes from a simple transisterised regulated power supply (7) fed by a Heathkit battery eliminator.

Various combinations of battery eliminator and/or 6 volt accumulator had been tried earlier on but gave much poorer regulation than the transisterised supply.

The 110 volts A.C. for the whole apparatus is stabilised by a General Radio Type 1570/A automatic line voltage regulator.

Rf leakage from the oscillator to the amplifier is often a major source of trouble in a coherent NMR system. However this is easily eliminated by a careful filtering of all power leads connected to either the amplifiers or the oscillator, and by completely enclosing the oscillator in a copper can. Care was also taken with the interstage filtering in the amplifiers to eliminate any chance of regeneration occurring. In all of the rf filtering extensive use is made of Phillips ferrite beads along with 0.01μf ceramic bypass condensers.

In a perfect apparatus the only noise source is the thermal noise of the resonant pickup coil. This was sometimes so with the present apparatus, but often noise from external sources was much larger than the thermal noise. The most common external noise source is faulty fluorescent lights in the laboratory, followed by noise from heavy electrical machinery in other parts of the building. Both of these sources give rf pulses synchronised to the mains frequency. It is not certain whether these pulses travel along the power mains, or are detected by the tuned pickup coil wrapped around the sample.

Because of the small magnet gap not enough space is available to enclose the coils in an earthed metal shield, so the apparatus is susceptible to extraneous induced voltages. An attempt was made to place an earthed shield around the outside of the nitrogen dewar, but the resulting hum loop increased the noise level, so the pickup coil has been left unshielded. The whole earthing system of the apparatus had to be arranged so that there were no earthing loops increasing the noise level. This was mainly an empirical process that verged on black magic.

3.8 The Magnets and Magnetic Field Measurements

The apparatus was originally built for use with a Varian V/4007 6" electromagnet with a two-inch gap. This gives a field of up to 7KG. which is homogeneous to within a gauss over the volume of the sample. Part way through the experiments, the apparatus was shifted and used with a Varian V4012/313 12" electromagnet with a 2.25-inch gap and a field strength of up to 11.2KG. This magnet has a homogeneity of about 0.1 gauss over the sample volume. Both magnets were rotatable through over 180°.

The magnetic fields of both magnets were often swept through the resonance values by applying a sawtooth voltage of 8 volts to the External Sweep terminals of their respective magnet power supplies. This varies the field by about 100 gauss as an approximately linear function of time.

A simple marginal oscillator was built for any magnetic field measurements needed. It was used to calibrate the 6"

electromagnet, but with the 12" electromagnet a field calibration previously done by S.N. Sharma had sufficient accuracy for finding resonances, so that the marginal oscillator was never used with it.

3.9 The Low Temperature System

Originally it was intended to make measurements at very low temperatures so a conventional glass dewar liquid helium system was built. The dewars were built for the six magnet so the inner dewar has an internal diameter of only one inch, which severely restricts the coil dimensions.

When the apparatus was shifted to the 12" electromagnets the dewar head already there was unsuitable for pulsed NMR, so that the dewar system from the 6" magnet had to be used with the 12" magnet. As the dewar head did not match the helium return system already there, no liquid helium temperature measurements were possible without extensive rebuilding of the low temperature part of the apparatus. This rebuilding was not done for reasons to be given later.

All the measurements have either been made at room temperature, or at liquid nitrogen temperature. For liquid nitrogen measurements, the outer dewar is filled with liquid nitrogen, while air is used as an exchange gas in the inner dewar. If the inner dewar alone is filled with liquid nitrogen, its bubbling causes vibrations which decrease the S/N by two.

3.10 The Coil System for a Metallic Single Crystal

The most important part of the apparatus is the coil system. It is also the hardest part to design so that the coils used, and the reasons for using them, will be discussed in considerable detail in the following section.

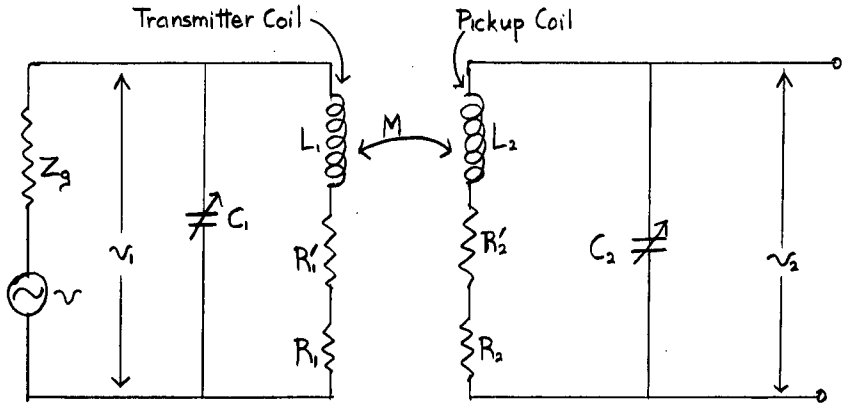

Fig. 3.4 Equivalent Circuit of the Coil System

The equivalent circuit of the coil system is given by Fig. 3.4. Z_g is the large signal output impedance of the final stage of the power amplifier, while L_1 is the inductance of the transmitter coil. R_1 is the equivalent damping resistance of this coil and is comparatively low when the rf pulse is on, but it is much higher when it is off. R_1' is the resistive component of the impedance coupled back from the pickup coil by the mutual inductance M. L_2, R_2 and R_1' are the corresponding parameters for the pickup coil. R_2 is larger during an rf pulse than when it is off. Clark (2) fully discusses all the requirements for the coils. Briefly they are that the transmitter coil must have the maximum number of ampere-turns

possible and a fairly low Q, while the pickup coil should have the largest number of turns and the highest Q possible.

The mutual inductance should be as small as possible since it causes the following undesirable effects to occur.

(i) The resonant coil pickup coil extracts a significant fraction of the power supplied to the transmitter coil. This reduces H_1 by the same fraction.

It is assumed that both resonant circuits are not very tightly coupled and that the transmitter coil is matched to the output impedance of the amplifier i.e. $Z_g = \omega L_1 Q_1$, where $Q_1 = \frac{\omega L_1}{R_1}$. Straightforward circuit analysis then quite accurately gives the power dissipated in the transmitter coil as

$$P = \frac{V^2(R_1' + R_1)}{Z_g(R_1' + 2R_1)} .$$

If the current passing through L_1 is i_1, then the power P absorbed by the resonant pickup coil is

$$P' = i_1^2 R_1'$$
$$= \frac{V^2}{Q_1^2(R_1' + 2R_1)} .$$

Thus the fraction of power absorbed by the pickup coil is

$$\frac{P'}{P} = \frac{R_1 R_1'}{(R_1' + 2R_1)(R_1' + R_1)}$$

by using $Z_g = Q_1 \omega L_1$. This has a maximum value of 0.17 when $R_1' = \sqrt{2}\, R$. For the present apparatus $L_1 = 1.2\mu h$ and $Q_1 \simeq 10$ so at 9Mc/s. $R_1 \simeq 7\Omega$. $L_2 \simeq 3\mu h$ and $Q_2 \simeq 5$ when the rf pulse is on, so that $R_2 \simeq 35\Omega$. $R_1' = \frac{\omega^2 M}{R_2}$ where $M = k\sqrt{L_1 L_2}$, with $0 < k \leqslant 1$, so it

is impossible to satisfy the condition for maximum power absorption. Representative values of the fraction of power absorbed are 5% for k=0.4 and 2% for k=0.1.

(ii) The transmitter coil damps the pickup coil.

$$Q = \frac{\omega L_2}{R_2 + R_2'}$$

where $R_2' = \frac{\omega M}{R_1}$. When the rf pulse is off $R_2 \simeq 6\Omega$ and $R_1 \simeq 15\Omega$. Thus $Q_2 \simeq 30$ for k=0, $Q_2 = 27$ for k=0.1 and $Q_2 = 20$ for k=0.4.

(iii) If the coils are very tightly coupled the two circuits cannot be tuned independently of each other. This becomes noticeable for $k \gtrsim 0.5$.

(iv) The rf pulse can induce a very large voltage which can damage the input stage of the preamplifier, or cause recovery time problems after the pulse is over.

The induced voltage across the pickup coil is given approximately by

$$V_2 = V_1 k \sqrt{\frac{L_2}{L_1}} Q$$

$$\frac{V_2}{V_1} = 8\ k.$$

Representative values of $\frac{V_2}{V_1}$ are 0.8 for k=0.1 and 0.25 for k=0.03.

From the above considerations it is clear that k should be less than 0.1 and preferably below 0.05. In the coil system finally adopted, k can be as low as 0.03.

The most unusual part of the apparatus is the sample coil with the metal cylindrical sample inside it. The fol-

lowing simple theory describes the behaviour of the sample coil with sufficient accuracy for most experimental purposes.

Assume that a coil of radius R_2 and length l_2 with n_2 turns/unit length is spaced from a metal cylinder whose radius is R_1, electrical conductivity is σ, and skin depth is δ at a frequency f. It is assumed that the metal cylinder is longer than the coil.

If the metal core is absent, then the magnetic field strength inside an infinite solenoid is (3)

$$H = nI$$

where I is the current in the coil. This is assumed to be uniform over the whole cross sectional area of the coil, so that the induced back emf is

$$\begin{aligned} v &= -\frac{\partial \phi}{\partial t} \\ &= -n l A \mu \frac{\partial H}{\partial t} \end{aligned}$$

where $A = \pi R_2^2$. If $I = I_0 \exp(i\omega t)$ then $Z = \frac{v}{I} = i\omega \mu n^2 A l = i\omega L_2$, where $L_2 = n_2^2 \mu A l_2$. This is the infinite solenoid formula for an air cored coil and is accurate to within ten percent provided $l > 2R_2$.

If the metal core is now inserted, the skin effect prevents magnetic flux penetrating more than about a distance δ into the metal so the effective cross sectional area of the coil is much less. Thus if it is assumed that H is still uniform outside the metal core, $\frac{\partial \phi}{\partial t}$ becomes approximately

$i n_2^2 \mu L_2 \omega \pi \left[R_2^2 - (R_1 - \delta)^2\right]$. Usually $R_2 - R_1 \gg \delta$, so that the inductance with a metal core becomes

$$L_2 = \pi \mu n_2^2 l_2 (R_2^2 - R_1^2).$$

The conditions for the validity of this equation are $R_2 - R_1 \gg \delta$ and $l_2 \gg 2(R_2 - R_1)$. The latter condition is more easily satisfied than the corresponding condition for an air cored coil.

Experimental measurements show that this formula is accurate to within 20%. The error is probably due to the non-uniform flux distribution which actually occurs.

To calculate the Q of the coil, consider what happens when a current $j = j_0 \exp(i\omega t)$ is passed through the coil. It generates a magnetic field $H = n_2 j$ parallel to the surface of the metal cylinder. The magnetic field generates an eddy current which circulates close to the surface in the opposite direction to the applied current. As far as power losses are concerned, the eddy current can be considered as a uniform current density equal to the actual current density at the surface of the metal and confined to a layer $2^{-\frac{1}{2}}\delta$ thick at the surface of the metal (3). Thus the eddy current circulates in a loop $2\pi R_1$ long, l_2 wide, and $2^{-\frac{1}{2}}\delta$ thick, so that the total resistance of the eddy current path is

$$\frac{2\sqrt{2}\,\pi R_1}{\sigma \delta l_2}.$$

The r.m.s. value of the eddy current is

$$I_r = 2^{-\frac{1}{2}} l_2 H$$

Thus the power P disapated in the sample is

$$P = \frac{2\sqrt{2}\pi R_1}{\sigma\delta l_2}\left(\frac{l_2 H}{\sqrt{2}}\right)^2$$

$$= \frac{\sqrt{2}\pi R_1 l_2 H^2}{\sigma\delta}.$$

If the r.m.s. value of j is j_r, then $H = 2^{\frac{1}{2}} n_2 j_r$.

$$\therefore P = \frac{2\sqrt{2}\pi R_2 l_2 n_2^2}{\sigma\delta} j_r^2$$

$$= j_r^2 R_s,$$

where $$R_s = \frac{2\sqrt{2}\pi R_2 l_2 n_2^2}{\sigma\delta}.$$

R_s is the effective resistance of the coil due to the metal core so that

$$Q = \frac{\omega L_2}{R_s}$$

$$= \frac{\omega\mu\sigma\delta R_1}{2\sqrt{2}}\left[\left(\frac{R_2}{R_1}\right)^2 - 1 + \frac{2\delta}{R_1}\right].$$

The actual Q of the resonant circuit is reduced by the rf resistance R_w of the wire in the coil and the external part of the circuit to

$$Q = \frac{\omega L_2}{R_s + R_w}$$

$$= \frac{Q_s Q_w}{Q_s + Q_w},$$

where $Q_s = \omega L/R_s$ and $Q_w = \omega L/R_w$. Thus it is easy to include the wire resistance in the design of an actual coil system.

The induced signal is proportional to a number of factors which depend upon the ratio R_1/R_2 of the sample to coil radius. These factors will now be given and the optimum ratio of R_1/R_2 calculated from them.

The maximum flux change generated by the sample is $\dot{\theta} = -\mu \frac{\partial}{\partial t} \int_{sample} \underset{\sim}{M} \cdot d\underset{\sim}{a}$. If the coil is not tightly wound on the sample magnetic flux leakage occurs, so that the flux θ' intercepted by the pickup coil is less than θ. This flux leakage is taken care of by defining an efficiency factor η as

$$\eta = \frac{\frac{\partial \theta'}{\partial t}}{\frac{\partial \theta}{\partial t}} = \frac{\theta'}{\theta} .$$

This depends only on the coil and sample geometry and can, in principle, be calculated for any coil configuration. In practice such calculations are unwieldy. For a short coil wound on a sample much longer than its diameter, a calculation gives η as

$$\eta = 1 - k\left[\left(\frac{R_2}{R_1}\right)^2 - 1\right]$$

where $k = \frac{R_1^2}{2(R_1^2 + L^2)}$ and L is the sample length. Most of the coil configurations approximated these conditions.

The induced voltage is also proportional to the number of turns n_2 in the pickup coil. At a fixed frequency, the inductance $L_2 = \pi n_2^2 \mu l (R_2^2 - R_1^2)$ is a constant.

$$\therefore n_2 \propto (R_2^2 - R_1^2)^{-\frac{1}{2}} .$$

It is also proportional to the cross sectional area $A = 2\pi R_1 \delta$ of the perturbed magnetic moments.

If v is the output voltage from the resonant pickup coil then

$$V \propto Q \eta n A$$

$$\propto \frac{(x^2-1)^{\frac{1}{2}} [1 - kR_1^2 (x^2-1)]}{Q_w + K(x^2-1)}$$

where $x=R_2/R_1$ and $K=\frac{\omega\mu\sigma\delta R_1}{2\sqrt{2}}$.

This has a maximum value when $R_2 \simeq R_1 (1+\frac{Q\omega}{K})^{\frac{1}{2}}$. With typical values of Q and K, R_1/R_2 lies in the region of 0.7 to 0.8. In the coils actually built R_1/R_2 varied from about 0.6 to 0.9.

It should be noted that slicing the sample into thin slabs may not increase the induced voltage. This is because increasing the surface area not only increases the number of nuclei excited, but also increases the path lengths of the circulating currents and this causes a compensating drop in Q. Thus if the Q of the resonant circuit is determined by the sample, slicing it will have little effect. However, if the wire resistance is dominant, slicing increases the signal until the stage is reached where the sample losses become as large as the wire losses. The full benefits of slicing are not obtained unless the slabs are about δ thick, when the eddy current losses become considerably reduced. Manufacture and alignment of metal slabs less than 10^{-2}cm. thick is such a formidable technical problem that no experiments along these lines have been attempted.

The most difficult part of building the apparatus was finding a suitable coil configuration. Clark (2) lists the relative merits of three different configurations. Two of these were examined both theoretically and experimentally, and one only theoretically, before they were all rejected.

The easiest system to reject was the combined transmitter-receiver coil, as simple calculations showed there was

no change of finding a satisfactory compromise between the conflicting requirements for the transmitter and receiver coils. Also the Q damping circuits on the transmitter and receiver could not be used.

A rf bridge (8) was tried and quickly rejected. It reduced the rf field considerably, did not balance very well with a metal cored coil, still used a combined transmitter-receiver coil, and did not allow the use of Q damping circuits.

Crossed coils were studied more carefully, both experimentally and theoretically. They have the advantages that conflicting transmitter and receiver coil requirements can simultaneously be met. The coupling coefficient k is very small, while Q damping circuits can also be used. Acoustic oscillations are also hard to excite when using crossed coils. They have the major disadvantage that measurements of orientation dependent NMR properties are very difficult. This is since only the component of H_1 perpendicular to H_0 tips the nuclear magnetic moment, while with this configuration H_0 can make any angle between 0° and 90° with H_1 as it is rotated with respect to the sample. To eliminate this problem, the whole sample and coil assembly could be rotated with respect to H_0; a difficult mechanical and electrical problem, especially at liquid helium temperatures. An easier solution, which was tried, was to add another transmitter coil which gave a rf field orthogonal to both H_0 and the rf field from the first transmitter coil. Switching the transmitter output to the

appropriate coil can always give a fairly large rf field perpendular to H_0. The cylindrical sample shape and the limited space available meant the long rectangular transmitter coils had to be used. This system easily gave $k < 0.5$, even without an electrostatic shield, but could not give $H_1 > 10$ gauss with the power available from the transmitter. H_1 was also non-uniform over the surface of the metal, decreasing to zero on some parts of the surface, so that not all the surface nuclei were perturbed. For these reasons, the crossed coil system was abandoned.

This left a coaxial coil system with the sample coil inside a transmitter coil of inductance L_3, n_3 turns, radius R_3, and length l_3 as the only usable configuration.

The coupling constant of this configuration is easily derived.

$$L_3 = \pi \mu l_3 n_3^2 (R_3^2 - R_1^2)$$

so if v_3 is the rf voltage applied across the transmitter coil then

$$\begin{aligned} H &= n_3 i_3 \\ &= \frac{v_3 n_3}{\omega L_3} = \frac{v_3}{\pi \omega \mu l_3 n_3 (R_3^2 - R_1^2)} \\ &= \frac{\partial \phi}{\partial t} = \frac{v_3 (R_2^2 - R_1^2)}{(R_3^2 - R_1^2)} \cdot \frac{n_2 l_2}{n_3 l_3} \end{aligned}$$

But for a rf transformer, $\frac{v_2}{v_3} = k \frac{n_2 l_2}{n_3 l_3}$

$$\therefore k = \frac{(R_2^2 - R_1^2)}{(R_3^2 - R_1^2)} .$$

With the coil configuration initially used this for-

mula gives $k \sim 0.3$. Even though this value was known to be too large, the configuration was tried out and showed most of the defects predicted for it.

In order to reduce k, a bucking coil is added in series with the pickup coil in such a way that the voltage induced in it opposes the voltage induced in the pickup coil. The bucking coil has to be located where it cannot pick up the large signal from the sample. The mutual coupling between the bucking coil and the pickup coil should also be as small as possible.

Various positions and types of bucking coil windings were tried and eventually a single coil wound on the same coil former as the transmitter coil and just above it was chosen. The directions of the windings, and the positions of all the wires were carefully arranged so that any capacitive coupling opposed the inductive coupling. It was impossible to get a perfect cancellation, even after extensive experimentation, because of the capacitive coupling and the inductive coupling between the bucking and pickup coils. A Faraday shield significantly reduced the capacitive coupling.

Another complication was the distortion of the magnetic field caused by the presence of the metal sample. The eddy currents exclude flux from the interior of the sample and increase the magnitude of H_1 at the sample surface. This means that the bucking coil requires more turns than expected on the basis of assuming a uniform flux intensity over the cross section of the transmitter coil; an assumption which gave good

results for a powdered sample. The magnitude of the increase in H_1 varied from sample to sample, but was typically about 30% and was never more than 50%.

Since the inductance of the pickup coil plus that of the bucking coil should equal the maximum possible inductance for a pickup coil, the use of a bucking coil reduces the number of turns in the pickup coil and hence reduces the size of the induced signal. This reduction and the number of turns required in the pickup coil, could in principle be calculated from the above restriction on the inductances, plus the requirement that the total areas of the bucking and pickup coils cut by the magnetic flux are equal to each other. However, the bucking coil has a length much less than its radius so that no simple formula for its inductance exists. The magnetic flux distributions is also uneven. It is thus impractical to do any calculations involving the bucking coil. The number of turns in the bucking coil thus had to be found experimentally.

The coil configuration is reasonably satisfactory in practice. It typically has $k \simeq 0.05$, while reducing the signal by about 30% of its maximum possible value. If considerable trouble is taken in empirically finding the optimum number of turns for the coils, k can be reduced to about 0.02. This was done for the first two samples but then, for reasons of convenience and mechanical stability, one bucking coil was used for all the subsequent samples. This caused little deterioration in the performance of the system.

In the configuration finally adopted there are two coaxial cylindrical coil formers. These are made of Teflon which has a high electrical resistance and the ability to withstand repeated cycling to low temperatures without cracking. The outer one has a diameter of 2 cm. and has the transmitter and bucking coils wound on it. The transmitter coil has 11 turns and an inductance of 1.2μh and with 1.8 KV peak to peak across it, gives an H_1 of about 20 gauss. The bucking coil has 4 turns and an inductance of 0.9μh. Both coils were wound in grooves cut in the former and then imbedded in epoxy resin to give as much mechanical rigidity as possible. The diameter of the inner cylinder depends on the metal sample being used. The sample fits snugly inside the cylinder and the pickup coil is wound on the outside. None of the samples have the same dimensions, so that a different pickup coil has to be wound for each sample. The coil is coated with G.C. Electronics Polystyrene Q Dope No. 37-2 to prevent mechanical vibration. The coil system is very easily assembled and mounted on the end of a stainless steel tube, which also acts as the outer conductor of a coaxial cable leading to the preamplifier.

3.11 Acoustic Oscillations

Often in pulsed NMR apparatus a troublesome damped oscillation appears after the rf pulse. This oscillation is caused by the mechanical force generated by the interaction between H_o and the large circulating current in the transmitter coil causing some part of the transmitter coil, or sample,

to vibrate at an ultrasonic frequency. The acoustic oscillations persist after the rf pulse has finished and somehow induce a voltage in the pickup coil which obliterates the induced nuclear signal (2).

Acoustic oscillations were not often noticed when the 6" magnet was used. However, with the 12" magnet acoustic oscillations became a severe problem because of the increased magnetic field and also because the lower part of the coaxial cable and the wire leading to the transmitter coil were not in the magnetic field. Both the transmitter lead and the inner wire of the coaxial cable were originally very thin to reduce heat leakage during helium runs. However, they both vibrated badly and had to be replaced by heavy 24 A.W.G. wires. The bottom end of the coaxial cable was also filled with polystyrene glue. These measures eliminated acoustic oscillations from these wires, but introduced such a large heat leakage that helium runs were rendered impossible.

In all cases acoustic oscillations only occurred when the sample was present, so that they must come from the sample itself. Two experimental observations were made on rhenium which suggest the cause of these oscillations. The first of these is that the amplitude of the acoustic oscillations is proportional to H_o^2 (Fig.3.5). This is not very restrictive since most possible mechanisms have this H_o^2 dependence. The second is that the oscillatory frequency is about 70Kc/s for a sample 3.15cm. long. Thus if the sample is assumed to be

$\frac{1}{2}\lambda$ long, the longitudinal velocity of sound in rhenium is about 4400 metres/sec. This is a typical longitudinal velocity of sound for a metal, but it is too high for a transverse velocity (10). It was also noticed that the longer samples had a lower acoustical oscillation frequency. The frequency also increased on going to liquid nitrogen temperature. Thus the oscillations are probably due to an acoustical longitudinal standing wave being set up in the sample. This suggests that the following sequence of events occurs.

The rf pulse generates a circulating eddy current of about 50 amps. in the sample which interacts with the large static magnetic field. This produces oscillatory driving forces parallel to the cylindrical axis of the sample which set up an acoustical standing wave. There is such a large acoustic mismatch at each end that there is nearly perfect reflection of the sound wave, so that the standing wave persists long after the rf pulse is turned off.

This standing wave causes a variation $\Delta\rho$ in the density ρ of the sample. If N_e is the number of free electrons/unit volume, then the standing wave produces a variation $\Delta N_e = N_e \frac{\Delta\rho}{\rho}$ in their number. The electronic magnetic susceptibility $\chi_e \propto N_e \gamma_e^2$, where γ_e is the electron gyromagnetic ratio, so that $\Delta\chi_e/\chi_e = \Delta N_e/N_e = \Delta\rho/\rho$. The pickup coil is wound around the centre of the sample and has a voltage of $v_e \propto \omega_e \Delta\chi_e \delta_e = \omega_e \chi_e \frac{\Delta\rho}{\rho}$ induced in it. δ_e is the skin depth at the frequency ω_e of the acoustic oscillations.

The nuclear susceptibility $\chi_a \propto N_a \gamma_a^2$, so that

$$\frac{\chi_e}{\chi_a} \simeq \left(\frac{\gamma_e}{\gamma_a}\right)^2 \frac{N_e}{N_a}$$
$$\simeq \left(\frac{\gamma_e}{\gamma_a}\right)^2$$

since $N_a \simeq N_e$ for a metal.

$$\therefore \frac{\Delta\chi_e}{\chi_a} \simeq 4\times10^6 \frac{\Delta\rho}{\rho}.$$

The induced voltage from the nuclear spins is $v_a \propto \omega_a \chi_a \delta_a$, so that the ratio of the two voltages is

$$\frac{v_e}{v_a} \simeq \frac{\omega_e \chi_e \Delta\rho}{\omega_e \chi_a \rho} \cdot \frac{\delta_e}{\delta_a}$$
$$\simeq 4\times10^6 \sqrt{\frac{\omega_e}{\omega_a}} \frac{\Delta\rho}{\rho}.$$

In a typical case $\omega_a \simeq 100\omega_e$ so that

$$\frac{v_e}{v_a} \simeq 4\times10^5 \frac{\Delta\rho}{\rho}.$$

With this mechanism it only requires $\frac{\Delta\rho}{\rho} \gg 5\times10^{-6}$, a quite reasonable inequality (11), for the acoustic oscillations to dominate the nuclear signal.

With the coaxial coil system it is impossible to stop the standing wave being generated in the sample, so that the only method of eliminating the oscillations is to very quickly damp them. Frictional damping within the metal is very small so that the main acoustical energy loss is by transmission through the ends of the sample, with frictional losses at the sides of the cylinder playing some part. Thus the only way to damp the oscillations is by increasing the acoustic losses through the ends and sides.

If the densities and velocities in two infinite media are ρ_1 , ρ_2 and c_1 , c_2 respectively, the reflection coefficient

R at the interface is (11)

$$R = \frac{\rho_1 c_1 - \rho_2 c_2}{\rho_1 c_1 + \rho_2 c_2} \quad .$$

The media are not actually infinite, but instead the situation is closer to that of a piston radiating into an infinite medium. For this case the acoustic impedance Z_2 is of the form (11)

$$Z \doteq \tfrac{1}{2} \rho_2 c_2 \pi^2 (R_1/l)^2 \text{ for } 4\pi R_1 \ll 1,$$

$$\doteq c_2 \rho_2 \text{ for } \pi R_1 \gg 1.$$

These equations have used the substitution $\lambda = 2l$.

The easiest way of damping the acoustic oscillations is thus using a sample with a large ratio of R_1/l immersed in a medium with a density and velocity of sound much closer to those of a metal than air has.

These ideas were experimentally tested by immersing a rhenium sample in glycerine so that the reflection coefficient was reduced from 1 to 0.9. The duration of the acoustic oscillations decreased by 30% and their initial amplitude decreased by 20%. The damping also increased with an increase in the ratio R_1/l. Rhenium ($R_1/l=0.05$) and bismuth ($R_1/l=0.09$) had large acoustic oscillations, whilst in indium ($R_1/l=0.35$) the oscillations were just noticeable. The reduction in oscillations with both increasing R_1/l and decreasing reflection coefficient is much larger than the simple theory predicts and suggests that surface frictional losses play a significant part in the damping.

Unfortunately, glycerine has a very low thermal conduc-

tivity and so the rf pulses can heat the sample to temperatures well above that of the dewar system. For this reason glycerine was not often used to dampen acoustic oscillations. Instead the sample was embedded in a porcelain cement[1] which was a good acoustical match. The cement is water soluble, so that dismantling the sample mounting is easy. Part of the sample was always left exposed so as to provide a good thermal contact. The cement reduced acoustic oscillations to a tolerable level in nearly all the samples it was used with.

3.12 Calculation of the Signal to Noise Ratio

Since no measurements were made below 78 K. it is assumed that the normal skin effect theory is applicable.

The voltage induced in the pickup coil by the precessing nuclei is (Appendix III)

$$v = \pi \eta \mu n \omega M_0 R_1 \int_0^\infty \exp(-\tfrac{z}{\sqrt{2}\delta}) \sin(\gamma \tau B_1 e^{-\frac{z}{\sqrt{2}\delta}}) \cos^2(\tfrac{z}{\sqrt{2}\delta}) dz.$$

This integral has been evaluated and has a maximum value of about $0.7\,\delta$ when $\gamma B_1 \tau \simeq \frac{3}{4}\pi$ radians. The maximum induced voltage is thus

$$v = 0.7 \pi \eta \mu n \omega M_0 R_1 \delta .$$

The pickup coil is resonated at the frequency ω, so that the voltage at the input to the preamplifier is

$$v = 0.7 \pi \eta \mu n \omega M_0 Q R_1 \delta .$$

If T_n is the noise temperature of the sharply tuned pickup coil, then the r.m.s. noise voltage $\overline{v_n}$ is (12)

---

[1] Sauereisen Adhesive Cement No.1 Paste, Saureisen Cement Co., Pittsburgh 15, Penn., U.S.A.

$$\overline{V_n} = \sqrt{\frac{kT_n}{C}} \quad ,$$

where C is the capacitance resonating the pickup coil.

The parameters of the coil circuit and the preamplifier are chosen so that thermal noise from the resonant circuit is the dominant noise source. This is easily done. The bandwidths of the preamplifier and amplifier are greater than that of the tuned pickup coil, so that the S/N ratio at the amplifier output is

$$\frac{V}{\overline{V_n}} = \pi \eta n \mu \omega M_0 Q R_1 \delta \sqrt{\frac{C}{kT_n}}$$

This expression includes the improvement of $\sqrt{2}$ in the S/N ratio introduced by phase sensitive detection (12).

The boxcar integrator enhances the S/N by $\sqrt{\frac{R_b C_b}{\tau_c}}$ for repetition rates greater than about $(50 \text{ ms.})^{-1}$, so that the final S/N ratio S is

$$S = \pi n \mu \eta \omega R_1 M_0 Q \delta \sqrt{\frac{C R_b C_b}{kT_n \tau_c}} \, .$$

The parameters in this equation which are listed below have a temperature dependence.

(i) The nuclear magnetic moment/unit volume $M_0 \propto T^{-1}$ (1), where T is the sample temperature.

(ii) $\delta \propto \sigma^{-\frac{1}{2}}$ and σ has a complicated temperature dependence. For simplicity the high temperature approximation $\sigma \propto T^{-1}$ will be used (9), even though the Debye temperature for most metals falls within the temperature range of interest. Thus $\delta \propto T^{\frac{1}{2}}$.

(iii) $Q = \frac{\omega L}{R_n}$ where R_n, the total series damping resistance varies with temperature. If the damping is only due to

eddy currents in the metal then $Q \propto \sigma^{\frac{1}{2}} \propto T^{-\frac{1}{2}}$. However, in practice the resistance of the coaxial cable forms a large part of the damping resistance. This varies in temperature between room temperature at one end and the temperature of the sample at the other end, so that the noise temperature T_n of the tuned circuit is usually different from T, lying between T and room temperature. The dependence of T_n on R_n is not known, but $T_n \propto R_n$ seems a reasonable assumption. Thus $Q \propto T_n^{-\frac{1}{2}}$.

(iv) $\tau_c \propto (\Delta\omega)^{-1}$ and $Q = \frac{\omega}{\Delta\omega}$ so $\tau_c \propto Q \propto T_n^{-\frac{1}{2}}$.

(v) In a metal sample the Korringa relation $T_1 T$=constant holds (1). The repetition time for the boxcar is $T_r = KT$, where K is a constant.

$$\therefore T_r \propto T^{-1}.$$

The effective time constant $\tau' = \frac{T_r}{\tau_s} R_b C_b$ of the boxcar is a temperature independent constant determined only by the sweep time.

$$\therefore R_b C_b \propto T_r^{-1} \propto T.$$

Combining all these temperature dependences gives

$$S \propto T_n^{-\frac{3}{4}} .$$

The important feature of this simple analysis is that there is little improvement in S/N on going to low temperatures; the increase in M_o being compensated for by a decrease in δ and the decreasing effectiveness of the boxcar integrator. Experimentally it was found that S improved by about 50% on going from room to liquid nitrogen temperature. This gives $T_n \propto T^{\frac{1}{4}}$ as the approximate temperature dependence in this

region, so $S \propto T^{-\frac{3}{8}}$. If this temperature dependence is extrapolated to lower temperatures and allowance made for the onset of anomalous conduction, then cooling from nitrogen temperature to $4.2^{\circ}K$ would increase S tenfold. Actually the temperature dependence of T_n on T is even less below nitrogen temperature because even at this temperature most of the noise is coming from the parts of the tuned circuit near room temperature. Thus cooling the sample to a lower temperature does not reduce the noise temperature very much. These facts, plus the experimental difficulties with acoustic oscillations, are the reasons why no measurements at liquid helium temperatures have been attempted.

The other parameter which can affect S is the resonant frequency. If it is assumed that the tuning capacitance C is the same for all frequencies, the frequency dependent parameters vary as follows.

(i) The inductance $L \propto n^2$, but $\omega \propto L^{\frac{1}{2}}$, so $n \propto \omega^{-1}$.

(ii) $\delta \propto \omega^{\frac{1}{2}}$.

(iii) $M_o = \chi H_o$ and $\gamma H = \omega$, so $M_o \propto \omega$.

(iv) Q is usually frequency dependent. However, bandwidth restrictions require Q to be kept reasonably constant so that over a moderate frequency range Q is frequency independent. This is a good approximation since even if Q does vary with frequency it is almost cancelled by the opposing variation of τ_c.

Thus $S \propto \omega^{\frac{1}{2}}$

This is in reasonably good agreement with the experiments. Changing frequencies from 6 to 9Mc/s. increased S by about 30%. In addition recovery from the rf pulses is better at the higher frequency since a higher low frequency cutoff can be used. Measurements were thus usually made at the highest convenient frequency.

These conclusions are not valid above about 20Mc/s since in this region the grid noise of the preamplifier input stage increases and also its decreasing input impedance becomes important.

3.13 The Measurement of Spin-Lattice Relaxation Times

The most common method of measuring T_1 is to use a 180° pulse followed by a 90° pulse at a variable time t later. The amplitude of the induction tail following the second pulse varies as $1-\exp(-\frac{t}{T_1})$, so that T_1 can easily be obtained. When a boxcar integrator is used the spacing between the pulses is linearly increased with time so that the exponential increase of amplitude is recorded directly on the chart.

Unfortunately this method cannot be used for metal single crystals for several reasons. One of these is that there are no 90° or 180° pulses of the conventional type because of skin effects (Appendix III). There are pulse lengths which give maximum amplitudes and even pulse lengths which give no amplitude which could be used for the equivalent of a 180° - 90° pulse train. However, the signal is well below the noise level. Therefore tuning the apparatus so that it is first

exactly on resonance, and then finding the right pulse length, is an impossible job when a boxcar integrator must be used. The other big difficulty is that the signal is typically about one tenth of the noise level, so that any baseline distortion must be less than about one hundredth of the noise level for even a moderately accurate measurement of T_1. This is a far more stringent requirement than is usually required in pulsed NMR apparatus and is very difficult to attain.

For these reasons, an alternative method of measurement was devised which eliminates these difficulties at the expense of being very laborious.

Let a spin system have a large static magnetic field H_o applied along the z axis with a linear magnetic field $2H_1 \cos\omega t$ normal to it. In the rotating reference frame there is an effective magnetic field

$$\underset{\sim}{H}_e = H_1\hat{i} + (H_o + \frac{\omega}{\gamma})\hat{k}$$

making an angle $\theta = \tan^{-1}\left[\frac{H_1}{H_o + \frac{\omega}{\gamma}}\right]$ with the z axis. If the nuclear magnetism M_o is initially aligned along H_o, then on application of the rf pulse the components of M_o perpendicular to H_e relax towards it with a time constant somewhat longer than T_2 (13), so that eventually the magnetism is completely aligned along H_e with magnitude $M_o \cos\theta$. When the rf pulse is switched off the components of the magnetism perpendicular to H_o decay in a time of the order of T_2. The magnetism along the z axis thus has an amplitude

$M_z = M_o \cos\theta |\cos\theta|$.

It has so far been assumed that no spin-lattice relaxation occurs. This requires the rf pulse length to be much less than T_1 while still being many times T_2. If a short second rf pulse is applied at a time t later the height of its induction tail is proportional to

$$M_z = M_0\{1-\exp(-\tfrac{t}{T_1})\} + M_0\cos\theta\,|\cos\theta|\exp(-\tfrac{t}{T_1}).$$

From this T_1 is easily obtained.

This is the basis of the method used in the metal single crystals. A rf pulse of 200μs, or longer, is applied to bring the spin system to equilibrium in the rotating reference frame in the manner just described. T_2 is less than 50μs in nearly all the metals, while T_1 is usually several milliseconds even at room temperature, so the inequalities concerning the pulse length are easily satisfied. The rapid decrease of H_1 with depth means that some nuclei will not relax in the rotating reference frame since H_1 will be much smaller than the local fields. However this, along with phase effects, has little practical effect on the state the spin system is left in when the pulse is switched off.

M_z is measured with a rf pulse about 15μs long applied at a variable time later on. The time lag is measured with a double beam oscilloscope, as described previously.

The height of the induction tail is measured by the boxcar integrator used with a gate about T_2 wide (6). The magnetic field is linearly swept through the resonant value so

that M can be got from the recorder trace. The reference phase is usually adjusted so that the recorder trace bears some resemblance to an absorption curve. This is not necessary, but makes measurements from the recorder chart easier.

A series of measurements is made, firstly with t increasing and then with t decreasing. The measurements for each value of t are then averaged. This approximately averages out any steady drift in gain of the system and also decreases the statistical error of each point. Typically measurements are made for about 30 different values of t.

There are several advantages of this method. The first one is that the apparatus does not have to be tuned for exact resonance, nor does it have to stay exactly on resonance for the duration of the measurement. A phase sensitive system is very sensitive to frequency, or magnetic field drifts of one tenth of the linewidth or more, so the latter condition is quite a stringent one to fulfil. The second advantage is that sweeping through the line eliminates any errors from baseline droop, or distortion, as any distortion is common to both the signal and the off resonance baseline its amplitude is measured from.

The main disadvantage of the method is that it takes about three hours to measure T_1, as compared to about half an hour by more conventional methods. This means that the drift in gain of the apparatus must be small, or at least a constant drift in the same direction. This was usually the case, but sometimes there would be sudden jumps in gain causing some

error in the final value of T_1.

The results were either analysed by means of a conventional log plot, or by a least squares fit using the U.B.C. Computing Centre I.B.M. 7040 computer. The errors quoted for each result are standard deviations estimated from the scatter, plus the 2% error in timing. Much of the noise in these experiments is from non-random sources such as machinery switching on and hence the errors do not obey a normal distribution. The errors should thus only be regarded as an indication of how reliable each result is.

3.14 Measurement of Spin-Spin Relaxation Times

In aluminium powders T_2 was measured by applying a short rf pulse and linearly sweeping in time a narrow boxcar gate about 5μs. wide through the induction tail (6). The measurements were made with H_0 well off resonance, so that the chart recording is similar to a damped sine wave. Doing this avoids the difficulty of keeping the apparatus on exact resonance and also makes it easier to reduce the effects of baseline distortion.

This method could not be used on single crystals because of their poor S/N ratio and also because close to the rf pulse the baseline was badly distorted. Instead, a similar method to that used for measuring T_1 was used. A short rf pulse was applied and at a time t later, a narrow boxcar gate was swept through resonance by linearly varying the magnetic field. The gate was then manually shifted to a different value of t and

the measurement repeated. This gives the signals shown in Fig. 4.1. If $t \gg T_2$, the peak to peak amplitude (AB or AC on Fig.4.1b) is proportional to $2M_0$ to a high degree of accuracy. However if $t \ll T_2$, the peak to peak amplitude is less than $2M_0$ because of the finite value of H_1. This can be corrected for by making sweeps through resonance at several slightly different times and superimposing them to get an accurate measurement of the envelope of the oscillations. This can then be used to correct the peak to peak amplitude of the sweeps.

3.15 Measurement of Absorption and Dispersion Modes

A pulsed NMR apparatus with phase sensitive detection and a boxcar integrator can give recorder traces equivalent to the unsaturated absorption and dispersion modes, $\chi''(\omega)$ and $\chi'(\omega)$ measured by steady state apparatus. The basis of the method, as developed by Clark (2), will be given here, while the mathematical description and instrumental distortions that occur are given in Appendix IV.

A short rf pulse is applied to the sample. A very wide boxcar gate which completely covers the whole of the free induction decay is used. The output of the boxcar can be shown to be a linear combination of χ' and χ''. By appropriate choice of the reference phase either χ' or χ'' can be obtained. If the magnetic field is now swept linearly through the resonance value recordings are obtained which are equivalent to those obtained by steady state apparatus. This type of measurement is easily done on the present apparatus, but

suffers from the disadvantage that T_2 in metals is so short that there is considerable instrumental distortion (Appendix IV). It does have the advantage that χ' and χ'' can be unambiguously separated. This has not been possible in any of the steady state measurements on single crystals which have all used marginal oscillators. To obtain the full benefits of this advantage over the steady state method it is also necessary to simultaneously accurately measure the magnetic field. A simultaneous measurement of the magnetic field using a simple marginal oscillator was tried, but failed because there was mutual pickup between the marginal oscillator and the pulsed NMR apparatus. Possibly completely shielding both coil systems would eliminate this problem.

3.16 Possible Improvements to the Apparatus

As it stands at present the apparatus is not as good as it should be for measuring T_1 at room and liquid nitrogen temperatures for the following reasons.

(i) The original idea was to measure the anisotropy in T_1 at very low magnetic fields near the superconducting threshold. Thus the apparatus was originally designed to work at 750 Kc/s. However, after quite a few months this idea was abandoned, at least temporarily, as the experimental difficulties were too great. The apparatus was then converted to work in the region of 5 to 10Mc/s. There are however still some remnants of this initial stage of development in some parts of the apparatus, notably the overly elaborate gated power amplifier circuit.

This does not detract very much from the apparatus's performance but does decrease its reliability.

(ii) The dewars and sample holders were built for the 6" magnet so they are smaller than is necessary for the 12" magnet and also have no electromagnetic shielding.

(iii) The samples available are of assorted sizes and also many of the factors involved had to be found out by experiment. Thus the coils are usually not the optimum design.

From these considerations, and also some other points, it is clear that there are two major ways in which the apparatus can be improved.

The most important improvement is to rebuild the transmitter so that it is simpler and can give more power into a lower impedance load. This would enable a lower Q transmitter coil to be used, while also getting a larger H_1. At present a 90° pulse is about $15\mu s$ long. A more powerful transmitter could reduce this to about $5\mu s$ and a lower Q coil could reduce the recovery time by about $5\mu s$. With the very short values of T_2 occurring in metals these improvements could easily increase the S/N ratio by 50%.

The second improvement would be to build a metal dewar system and a sample holder specifically for use with the 12" magnet at liquid nitrogen, or room temperatures. This would enable larger diameter samples to be used. More mechanical rigidity could be built into the electrical leads to the sample holder and also to the sample holder

itself. All these features would reduce the effect of acoustic oscillations, and incidently noise caused by bubbling of the liquid nitrogen. There would also be room to completely surround the coil system by a metal shield to reduce rf pickup from external sources without causing significant deterioration in its electrical performance. It would also be desirable to standardize the sample sizes, but unfortunately there is often no choice in the size that samples are grown in.

There are no significant improvements which can be made to the amplifier and recording system. Measurements and calculations both show that it is already performing at the minimum possible noise level.

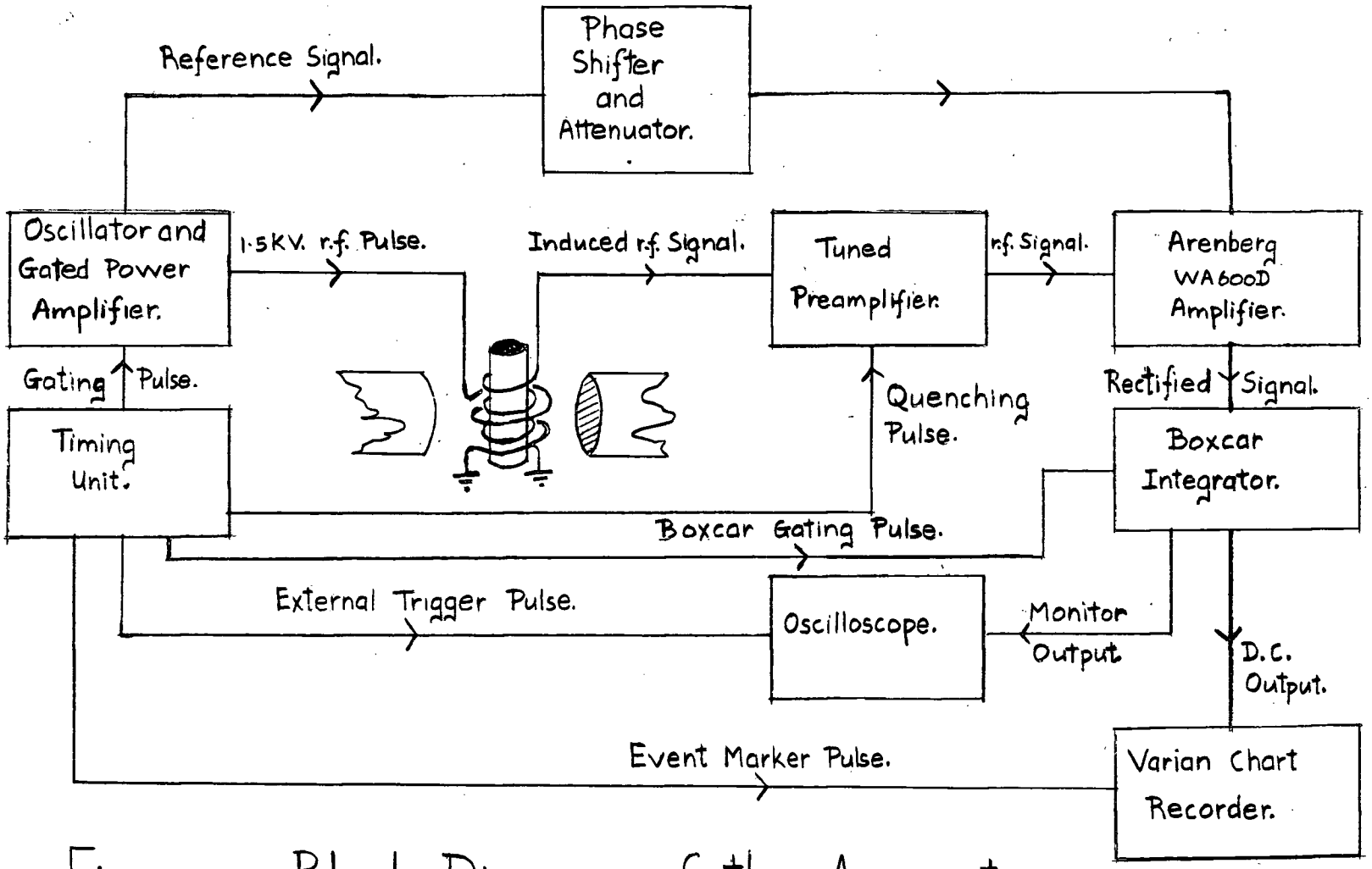

Figure 3.1. Block Diagram of the Apparatus.

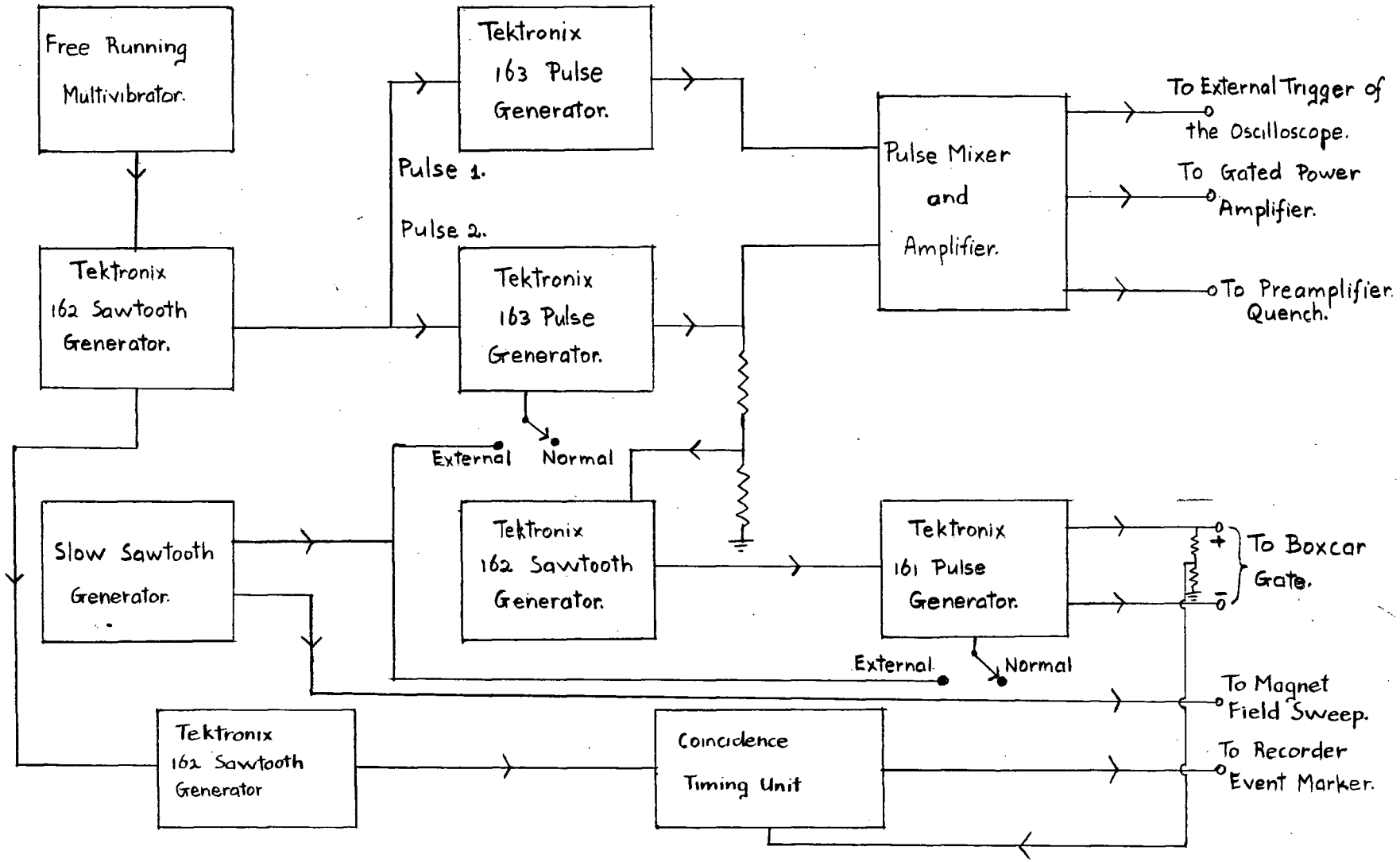

Figure 3.2. Block Diagram of the Timing Unit.

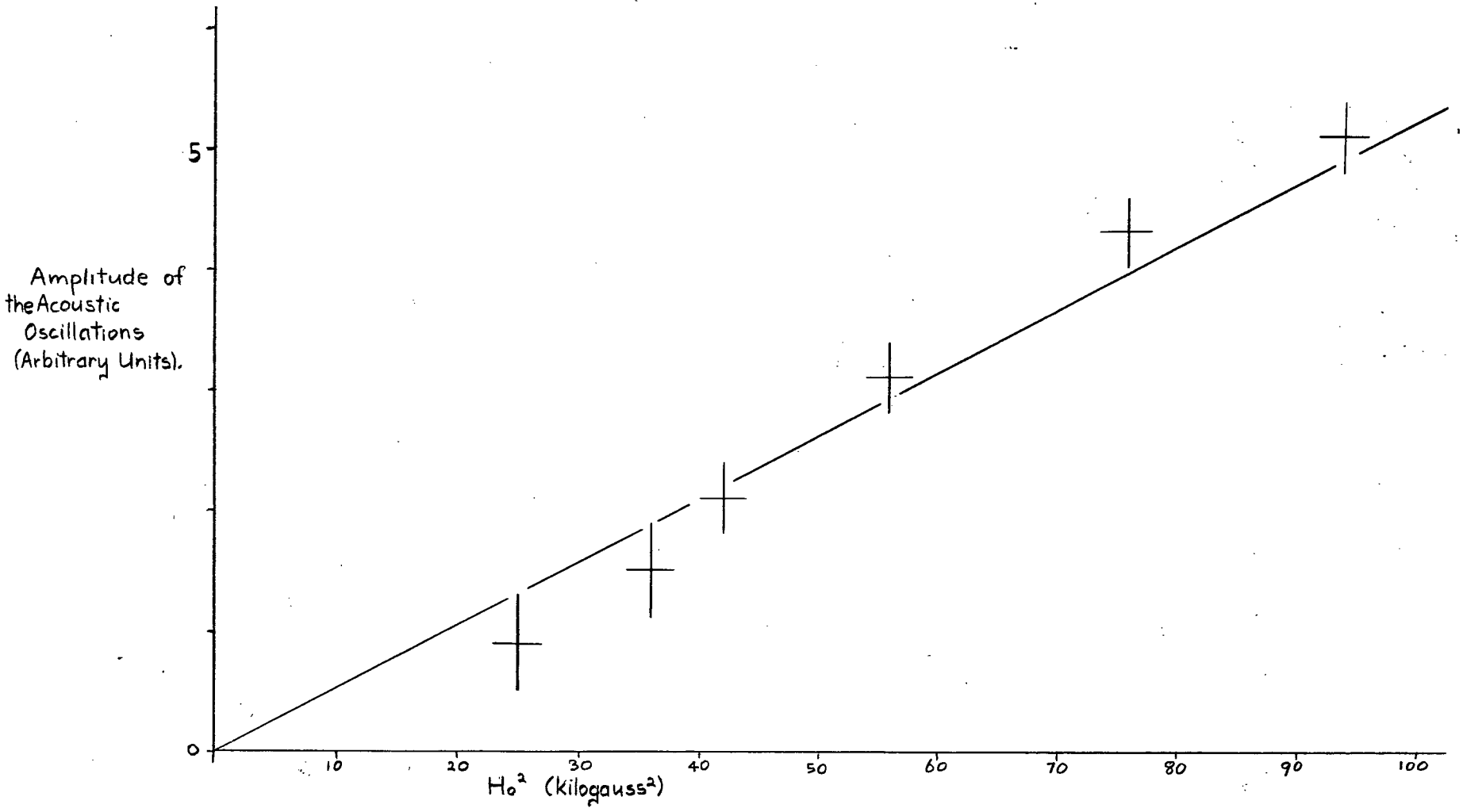

Figure 3.5 Variation of the Acoustic Oscillation Amplitude With Magnetic Field Strength.

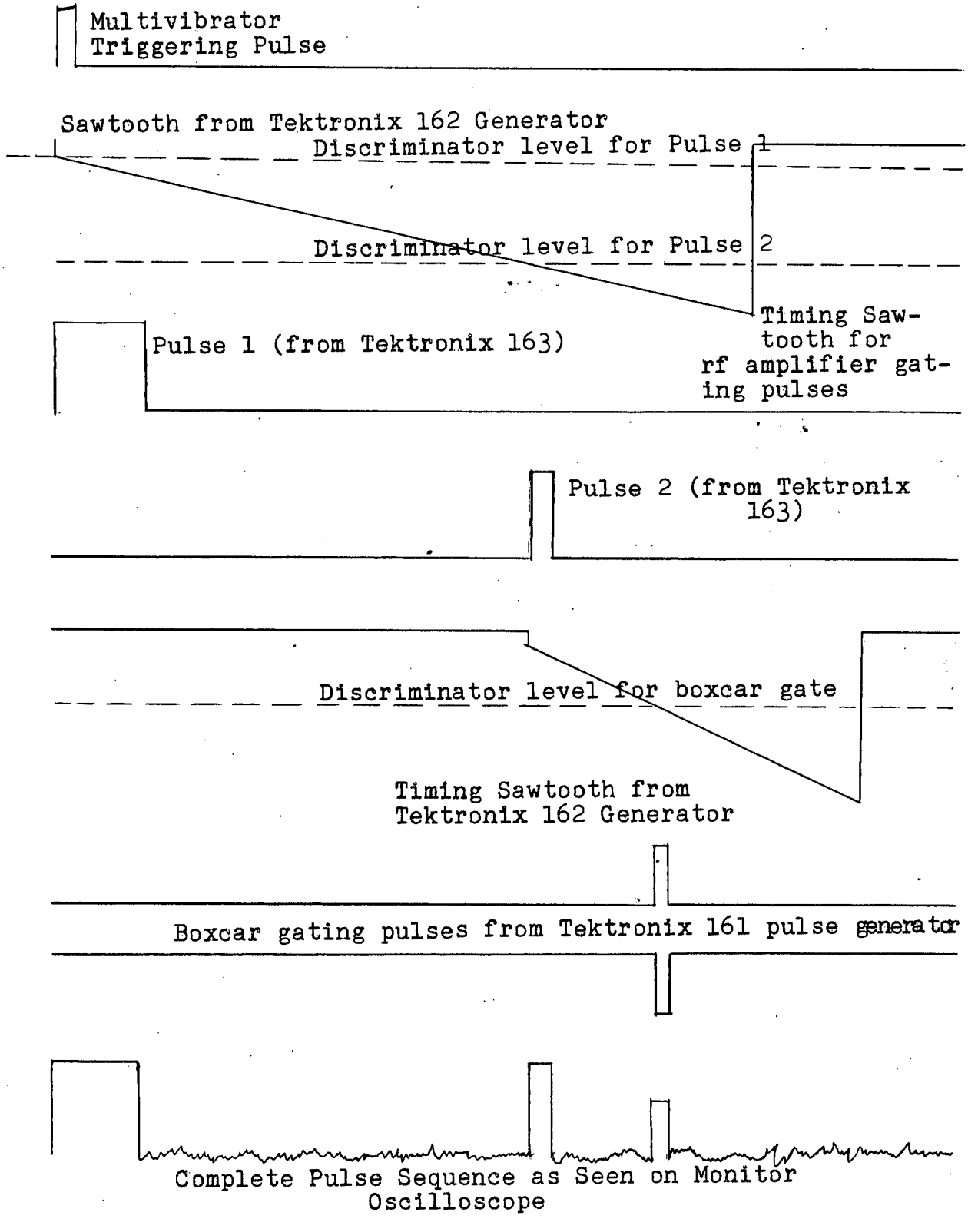

Fig. 3.6 Diagram of the Most Commonly Used Two Pulse Sequence

CHAPTER IV

THE EXPERIMENTAL RESULTS

'To observations which ourselves we make,
We grow more partial for the observer's sake.'
- Pope.

Although the main aim of this work was to search for anisotropic spin-lattice relaxation times, a secondary aim was to determine the possible uses and limitations of pulsed NMR in metal single crystals. This part of the work verified the theory of the apparatus developed in the preceeding chapter. Spin echoes were also observed and their properties studied.

Spin-lattice relaxation measurements were attempted in a number of metals. Some of these were selected for definite reasons, but most were only tried because they were available. This random approach to the selection of samples was mainly because many metals cannot be grown in conveniently sized crystals, except at a prohibitive cost, so that one had to use whatever samples were readily available. None of the metals with large quadrupole interactions had detectable signals, but four other metals gave good enough signals for T_1 measurements to be made. These were aluminium, vanadium, niobium and white tin. An upper limit was placed on the T_1 anisotropies in vanadium and tin. Spin-spin relaxation measurements were also made in tin and these gave the strengths of the pseudo-dipolar and pseudo-exchange interactions.

Throughout this work the intention was to use a scandium crystal for the main search for T_1 anisotropy. This is because it is a transition metal with a non-cubic lattice, has a large orbital contribution to T_1, and a small quadrupole interaction. These features made it an excellent candidate for this search. Unfortunately, the firm which agreed to supply the crystal were unable to grow one after eight attempts so that this idea had to be abandoned.

4.1 Aluminium Single Crystal

Signals were observed at a frequency of 7Mc/s. at both room and liquid nitrogen temperatures. The S/N ratio was usually about 20 when a boxcar integrator was used. This allowed fairly accurate measurements of T_1 to be made. T_2 was too short to measure.

In the T_1 measurements the first pulse was 300μs long and the second was 20μs long. The 60μs wide boxcar gate started 40μs after the beginning of the second pulse and used a time constant of 1ms. The repetition rate was $(35\text{ms.})^{-1}$ for the room temperature, and $(90\text{ms.})^{-1}$ for the 78°K. measurements. On the trace of the sweep through resonance the amplitudes between the points A,B and B,C (Fig. 4.1) were measured and then averaged. Choosing these points, rather than the signal amplitude from the baseline EF, increases the S/N ratio and eliminates the need to sweep from a long way off resonance. T_1 was then got from a log plot of this amplitude.

At 295°K., $T_1T=(1.8\pm0.3)$sec.deg. while at 78°K. $T_1T=(1.7\pm0.1)$ sec.deg. Combining these results gives $T_1T=(1.7\pm0.1)$sec.deg. over the temperature range 78°K. to 295°K. This agrees well with $T_1T=(1.80\pm0.05)$sec.deg. obtained for a powder from 1.2°K. to 930°K. (15).

The experimental value of T_1T is about 20% longer than the value predicted from the experimental Knight shift and the Korringa relation, but agrees well with the value calculated using the Korringa relation modified to take electron correlations into account (1).

The length of the first pulse was varied from 150μs. to 400μs. without any noticeable effect on the amplitude of the induction decay after the second pulse. A T_1 measurement taken with a second pulse 15μs. long gave the same value as the earlier measurements with a 20μs. pulse. On the basis of the theory given in the last chapter, this lack of sensitivity of the results to the pulse lengths was expected.

Aluminium has a cubic lattice, a nearly spherical Fermi surface, and a dominant contact interaction. Anisotropy in T_1T is thus very unlikely and was not looked for.

4.2 Vanadium Single Crystal

A series of measurements were made on V^{51} at both 295°K. and at 78°K. These gave values of (0.79 ± 0.03)sec.deg. at 295°K. and (0.78 ± 0.02)sec.deg. at 78°K. which are in excellent agreement with the value of (0.788 ± 0.007) sec.deg. obtained for powders over the temperature range 20°K. to 295°K. (20).

Because of the cubic lattice $T_1 T$ was not expected to be anisotropic (21). However the measurements at 78°K. were taken with several different magnetic field orientations. No anisotropy was detected in measurements made with errors of ±3%.

T_2 could not be measured, but seemed to be shorter than that of aluminium.

If the experimental value of $T_1 T$ is used in the Korringa relation, it gives a Knight shift of 0.21% instead of the experimental value of 0.56%. This discrepancy is too large to be explained by many-body effects. The reason for it becomes clear when the electronic structure of vanadium is studied in detail.

The following description of the electronic structure of transition metals is based on an article by Mott (23). The conduction band is believed to consist of a narrow d band with a high density of states overlapping an s band with a low density of states. The Fermi energy lies in the region where the bands overlap. The s band is usually described in terms of nearly free electron Bloch functions, while the d band is much more localised and so is described by the tight binding approximation. However, it is impossible in principle to separate the density of states into independent bands derived wholly from s, p, or d functions, even in the tight binding approximation. The mixing of states (hybridization) which occurs can drastically alter some properties of the transition metals. The most important effect of hybridization of the d

wave functions is to introduce a deep minimum in the middle of the density of states curve for b.c.c. lattices, but not for f.c.c. lattices. Hybridization of the s and d bands does not greatly alter the density of states curve, but affects other properties in a manner which is not clearly understood at present. In most metals the situation is complicated by the s band containing a certain amount of p, or higher, wave functions as well. Due to their coulomb repulsion there are large correlation effects between electrons in the s and d bands whose role is unknown. The spin-orbit interaction causes small energy shifts which are usually ignored.

Because of the difficulty of treating hybridization and correlation effects, they are usually neglected and the assumption made that the s and d bands can be treated independently. This is called the rigid band model.

Vanadium lies in the first long transition period and has five electrons outside the filled core. Its density of states curve has been experimentally determined and shows the basic features of a 4s band containing about 0.5 electrons/atom and a much narrower 3d band containing 4.5 electrons/atom (25). This high density of d electrons is the reason that the Korringa relation does not hold.

Using the rigid band model, the Knight shift and spin-lattice relaxation times in vanadium powders have been thoroughly examined, both experimentally (25) and theoretically (27). Of necessity there are a number of unknown factors and

gross assumptions in the analysis of the results so that the conclusions are only qualitative. Because of the low density of states in the 4s band, the contact term plays a minor role. The dominant contribution to the Knight shift is from orbital paramagnetism, with a secondary contribution from core polarisation. The contact term provides about 10% of the spin-lattice relaxation. The rest of the relaxation is by means of orbital and core polarisation. At the moment it is impossible to decide which of these terms is the larger, but it is probably the orbital term (25,27). This is supported by measurements on superconducting vanadium which show that the Knight shift is due to a spin independent term (28,25). However some caution should be used in the interpretation of this type of experiment since the behavior of the Knight shift in some non-transition metals differs from that predicted on the basis of the BCS theory. The most likely explanation for this deviation involves spin-orbit coupling and scattering of electrons from the sample surface (61). It is not known to what extent these effects occur in superconducting transition metals.

The experimental value of T_1T is twice the calculated value (27). Butterworth (29) showed that this difference was unlikely to be caused by errors in choosing the band structure parameters. The most probable reason is that the calculated relaxation time uses a density of states derived from the electronic specific heat (27,29). This includes a contribution from electron-electron and electron-phonon interactions which

do not contribute to relaxation (46). Thus the calculated relaxation time would be too short. Even in comparatively simple metals the electron-phonon interaction can double the electronic specific heat (57) and so is large enough to explain the difference between the experimental and the theoretical values. s-d hybridization effects might also contribute to the difference.

4.3 Niobium Single Crystal

Niobium is a transition metal with a cubic lattice and electronic and mechanical properties similar to those of vanadium. It also has five electrons outside a filled core, but lies in the second long transition period.

At room temperature $T_1 T$ was found to be (0.34 ± 0.01) sec. deg. and at 78°K. was (0.31 ± 0.01) sec. deg. These values are the average of two measurements at each temperature. The S/N ratio was about 15 at both temperatures. Acoustic oscillations caused some trouble at liquid nitrogen temperatures.

These values disagree with the 0.19 sec.deg. measured by Asayama and Itoh in the region 2°K. to 77°K. (58), but agree moderately well with the value of (0.36 ± 0.01) sec.deg. obtained by Butterworth for the temperature range 20°K. to 290°K. (29). He found that impurities did not have a strong effect. A powder sample contaminated by 1% oxygen, 0.2% hydrogen, and 0.08% nitrogen had a $T_1 T$ only 10% below that of a very pure foil sample. The sample used by Aszyama contained 0.5% of metallic impurities, as well as the gaseous

impurities, which were probably responsible for the large increase in the relaxation rate. Quadrupole effects might also be important, although Butterworth found that annealing a powder sample made no difference to either the signal intensity, or to T_1T. The difference between the present measurement and that of Butterworth is not due to a systematic error since the values measured for vanadium agreed to within experimental error. It is also unlikely to be only a statistical variation. The niobium sample used in the present measurement contains about 0.1% of metallic impurities and negligible gaseous impurities (Appendix II). The difference between the results could thus be due to impurities. The small temperature dependence of T_1T supports this, although this might be due to statistical fluctuations.

4.4 Metals With Large Quadrupole Interactions

Measurements were also attempted on a number of metals with large quadrupole interactions. In these metals the lines are well separated so that cross relaxation should be by non-secular terms only and hence of about the same magnitude as spin-lattice relaxation, or weaker. The only experimental value is about 2ms. in technetium (60). This is much longer than T_2, but is considerably shorter than T_1. However it seems safe to assume that the system has a fictitious spin of $\frac{1}{2}$ for at least the initial part of the decay. This means that the signals should be quite weak.

If either pseudo-dipolar, or pseudo-exchange effects occur, T_2 will be very short. This decrease in T_2 becomes very important for metals with atomic weights of about 100 or more. Most of the metals studied were in this region.

The large quadrupolar interaction makes this class of metals very hard to study using steady state NMR apparatus and powdered samples so that there have been very few measurements made on this class of metals. It was thus considered worthwhile spending some time searching for signals in them, even though the short T_2 and fictitious spin of $\frac{1}{2}$ would make them very hard to find.

(i) Indium.

At a frequency of 6Mc/s. a search for a signal was made from 3.0 KG. to 6.5 KG. at both 295°K. and 78°K. Searches were made with the magnetic field both parallel and perpendicular to the crystal axis of symmetry. At 9Mc/s. sweeps were made from 4.0 KG. to 11.2 KG. at both 78°K. and 295°K. In this case the magnetic field was parallel to the axis of symmetry. The repetition rate was such that signals with $T_1 T \lesssim 10$ sec.deg. should have been seen. The room temperature signal has been seen with steady state apparatus in a powder (32), so that it was known that the right region was being searched. Acoustic oscillations gave only minor trouble and vanished when the sample was immersed in glycerine.

Signals were not seen, even though calculations showed that there was a reasonably good chance of seeing them (Chp.4.7).

There are three possible explanations for the failure to see a signal. The first of these is that $T_1 T$ is longer than about 10sec.deg. This is not very likely since lithium is the only metal known to have $T_1 T$ longer than 5sec.deg. and all nuclear-conduction electron interactions become stronger with increasing atomic number because of the increase in electron density near the nucleus.

Indium is very soft and even light pressure can cause the surface to become polycrystalline. Anisotropic thermal expansion, or some inadvertantly rough handling, could thus cause the surface to become polycrystalline. This would render the satellite lines unobservable and reduce the intensity of the central line by over 50%, thus possibly making it unobservable. However X-rays taken before and during the measurements showed no sign of a polycrystalline surface layer.

Because of the amplifier recovery time of about 15μs., a weak signal with T_2 less than about 20μs. is unobservable. Indium has an atomic number of 115 and so probably has pseudo-exchange and pseudo-dipolar interactions so that T_2 is probably quite short. This is the most likely reason that no signal was seen.

(ii) Rhenium.

A search was made from 5.0 KG. to 11.2 KG. at a frequency of 9Mc/s. at both room and liquid nitrogen temperatures. No signals were seen. This was not unexpected since the computed S/N ratio was considerably less than one. There were

also very large acoustic oscillations, even after immersion in glycerine. The atomic number is 185 so that T_2 should be much less than that due to dipolar interactions alone.

(iii) Bismuth.

Bismuth is an unusual metal with some non-metallic properties. These arise because it has a very small number of free electrons, which gives it a high electrical resistance and an extremely large magneto-resistance (9,33).

A room temperature search was made from 8.2KG. to 11.2KG. at a frequency of 7Mc/s. The repetition rate was $(0.2\text{sec.})^{-1}$ and the boxcar gate started 20μs. after the beginning of the rf pulse. A similar search at 78°K. used a repetition rate of $(0.63\text{sec.})^{-1}$. At both temperatures several different magnetic field orientations were tried. Acoustic oscillations were seen at 78°K., but were not large enough to cause trouble. Powder measurements had been made at 4.2°K.(34), so that the approximate position of the lines was known. Under these conditions any signal of reasonable intensity with $T_2 \gtrsim 15\mu$s. and $T_1 T \lesssim 50$ sec.deg. should have been seen. However, there was no sign of a signal.

A calculation of the signal amplitude showed that it should have been seen. This calculation ignored the effects of the magneto-resistance. The change in tuning capacitance required by application of a 10KG. magnetic field showed that at 78°K. the magneto-resistance approximately doubled the skin depth. This is in rough agreement with the measured

magnetoresistance of bismuth (33). It was originally hoped that the S/N ratio might be improved by the increase in skin depth caused by the magnetoresistance. This is not necessarily so. The S/N ratio is proportional to $Q\delta$ and if Q depends only on the sample then $Q \propto \delta\sigma$, so that the $S/N \propto \delta^2\sigma$. However $\delta^2 \propto \sigma^{-1}$, so that the S/N ratio is independent of σ and hence does not depend on any magnetoresistive effects. This is probably the case in bismuth since on tuning the apparatus it was noticed that the Q was lower than for any other sample and that the Q increased on going to 78°K. This tuning was done without the magnetic field on, only the final tuning being done with the magnetic field applied. In all the other metals the Q depended on the circuit resistance and was approximately temperature independent. If the Q had been limited by the circuit resistance in the case of bismuth as well, then an increase in δ due to magnetoresistance would have increased the S/N ratio.

From steady state measurements L.C. Hebel found that bismuth had a line about 80 gauss wide which saturated easily (quoted in reference 35). From this one can deduce that $T_2 \sim 10\mu s.$ and that $T_1 T \gg 25$sec.deg. These are both quite plausible values; the long $T_1 T$ resulting from the small number of free electrons/atom and the short T_2 from pseudo-exchange and pseudo-dipolar interactions. It is most likely that these unsuitable values of $T_1 T$ and T_2 are the reason that no signals were seen.

(iv) Antimony.

Antimony is a metal with similar characteristics to those of bismuth, so that it was not expected to see a signal. A brief search was made at 78°K. at a frequency of 9Mc/s. from 6.5KG. to 11.2KG. No lines were seen.

(v) Gallium.

This metal has the very low melting point of 303°K. To try to avoid melting the crystal all measurements were made at 78°K. The sample was immersed in glycerine to dampen the large acoustic oscillations present.

A search was made at 78°K. which would detect signals with $T_2 \geq 15\mu s$. and $T_1 T \leq 10$ sec.deg. The frequency was 9Mc/s. and the field was swept from 5.1KG. to 10.3KG. One line was found at about 6.7KG. with a S/N of about 3. This line was independent of the magnetic field orientation. It was later found that eddy currents generated by the rf pulses had melted the surface of the crystal so that the observed line was probably that from molten Ga^{71}. The observed line agreed reasonably well with this identification as far as both the position and the calculated S/N ratio were concerned. It was too weak to make any measurements on.

This surprising melting of the crystal probably occurred because glycerine has a very low thermal conductivity. It is a solid at 78°K. and even when liquid it has a high viscosity, so that little convective cooling can occur. There is thus a poor thermal contact between the sample and the liquid

nitrogen bath and so the heating effect of the rf pulses is cumulative. A calculation showed that after a few hours the sample temperature would rise from 78°K. to its melting point. This is approximately the length of time that the apparatus is allowed to run for, for stabilizing purposes, before a measurement is made. The heating process is also aided by the low thermal conductivity of gallium which allows the surface temperature to rise about 10°K. above that of the interior for many milliseconds.

After discovering this sample heating effect, the use of glycerine to dampen acoustic oscillations was discontinued.

4.5 Copper Wire and Other Spurious Signal Sources

Two resonances due to the copper wire in the pickup coil were often observed. They were identified by their positions, relative intensities, and spin-lattice relaxation time. The signals were quite strong; the amplitude of the Cu^{63} resonance being 70% of that of the Al^{27} single crystal resonance. This is because the surface area of the wire in the coil is nearly the same as the surface area of a single crystal sample. The efficiency factor is nearly unity, while copper has a large magnetic moment and so a strong signal is got.

Very strong signals could also be picked up from fluorine and hydrogen nuclei in the teflon and insulation near the pickup coil. These signals limited low magnetic field sweeps because they obliterated signals over a region of many

hundred of gauss in the region of 2KG.

4.6 Isotopically Pure Tin Single Crystal

This is a thin crystal of isotopically pure Sn^{119} wrapped around a copper core (59). The S/N ratio was quite good at 78° K., while T_1 was about 200μs. These features made it a good sample to use for studying some of the experimental details.

(i) Variation of the Induction Tail Height With the rf Pulse Lengths.

The first experiment was to study the validity of the expression derived for the induced voltage occurring after application of a rf pulse (Appendix III). To do this the induction tail height was measured as close to the rf pulse as possible with a narrow boxcar gate. The measurements were then repeated for various rf pulse widths. The induction tail height was corrected for spin-spin relaxation. This correction used T_2 measured at the same magnetic field orientation. Spin-Spin relaxation occurring during the rf pulse was corrected for by taking the time origin as the centre of the rf pulse (13). This correction is exact for a uniform H_1 much larger than the local field, but is only an approximate correction in the present case. However, the correction is always less than 30%, so that the error will not be large. The corrected induction tail heights were then plotted against the rf pulse length (Fig. 4.4). The theoretical expression was fitted to the experimental results on the assumption that a $\frac{1}{2}\pi$ pulse at the surface of the metal was

10μs. long. This value is in reasonable agreement with $H_1 = (13 \pm 2)$ gauss obtained from a fluorine resonance in the coil mounting if the increase of H_1 at the surface of the sample is considered (Chap. 3.10).

The pulse widths fit the data quite well for pulse lengths up to about 50μs. long. The small deviation for short pulse lengths is because the rf pulses are not quite rectangular. It is not clear whether the discrepancy beyond 50μs. is due to experimental causes such as heating of the sample, or represents a breakdown of the theory. The most likely cause of this would be effects from the region in which H_1 is comparable to the local field. It was found that in the theoretical expression the ratio of the maximum positive going and negative going amplitudes were very sensitive to the form of the phase factors. If the phase term is $\cos^2 x$ the ratio is 0.45, but if it is $\cos x \cos(\frac{x}{\sqrt{2}})$ the ratio is 1.2. However apart from the amplitudes, the shape of the curve is relatively insensitive to the phases. The experiment thus verifies the basic features of the theory, but indicates that it might be too simple. A discussion of the quantitative agreement of the equation with the experimental S/N ratios is given at the end of this chapter.

(ii) The Spin-Lattice Relaxation Time.

The symmetry axis ([001] axis) makes an angle of 28° with the cylindrical axis of the copper core. This is far from the optimum angle of 90°, so that tilting the crystal

through 23° was tried. This suffered from the disadvantages of reducing the induced voltage and of drastically increasing the acoustic oscillations. The latter were the important difficulty as they saturated the amplifier for about 100μs. Mounting the sample in porcelain cement reduced the oscillations to a more manageable size. T_1 measurements were made at 78°K., but the experimental scatter caused by acoustic oscillations was over 20%. There was thus little chance of measuring any anisotropy in T_1. The most accurate measurement gave $T_1 T=(45\pm15)$ms.deg., while the scatter of results showed that there was no anisotropy greater than 50% at the magnetic field orientations used.

Measurements were then made at 78°K with the crystal mounted vertically. This reduced the acoustic oscillations to only several times the thermal noise level. T_1 was approximately 500μs. while T_2 was about 200μs. It was thus necessary to spoil the magnetic field until $T_2^* \simeq 30\mu s$. The first pulse was 90μs. long and the second one 20μs. long. When H_o was approximately along the [100] axis $T_1 T=(35\pm2)$ms.deg., while when H_o was in the (010) plane and making an angle of 62° with the [001] axis $T_1 T=(33\pm3)$ms.deg. These results are given on Figure 4.3 and show no anisotropy within the experimental error.

The average value of $T_1 T=(34\pm2)$ms.deg. agrees with the value of $T_1 T=(34\pm1)$ms. deg. found by Asayama and Itoh (58) over the temperature range 4.2°K. to 120°K. for powders. It

disagrees with the measurement of Spokas and Slichter (15) at 78°K. of $T_1T=(54\pm4)$ms.deg. in powders. It is impossible to tell which of these measurements is the more reliable. Spokas and Slichter made only one measurement which was incidental to their main experiment whilst Asayama and Itoh's measurement of T_1T in niobium, which was made at the same time, is unreliable.

The form of the angular dependence of the orbital and dipolar relaxation is not known for a tetragonal lattice. Calculations using the free electron approximation (63), and the tight binding approximation, show that for a cubic lattice it is a sum of terms of the form $a'+b'\cos^4\phi$, where ϕ is the angle between H_o and the [001] axis. This sum is isotropic for a cubic lattice. It is plausible that for a non-cubic lattice the sum is of the form $(T_1T)^{-1}=a+b\cos^4\phi$. To this must be added the isotropic contribution c due to the contact and core polarisation terms. If the measured values of T_1T are fitted to the above expression they give

$$b=(1.5\pm3.0)\times10^{-3}\text{ms.}^{-1}\text{deg.}^{-1}$$

However, b is not expected to be negative, so that it has about 70% probability of being in the range 0 to 4.5×10^{-3}ms.$^{-1}$ deg.$^{-1}$

From the present measurements it has not been possible to detect any anisotropy. However, the requirements for a useful measurement of any anisotropy are now much clearer. In any NMR experiment it is very hard to measure T_1 with better

than 2% accuracy and in the present case 5% accuracy is the best that can be obtained. The length of time required for such accurate measurements make it impractical to measure T_1 at more than a few angles. The angles at which T_1 must be measured are for H_o along the [001] axis and along the [100] axis. Since the assumed angular variation of T_1 may be wrong, measurements should also be made with H_o along the [110] and the [101] axes as a check. With the assumed error of 5% in T_1 an anisotropy of 4ms.deg. would be detectable.

An upper limit can be placed on a by using the free electron Korringa relation. A recent calculation on the Knight shift in superconducting tin (61) indicates that about 15% of the isotropic value of 0.713% (64) is due to spin-orbit and Van Vleck paramagnetism. Thus the relaxation due to the contract term is about 2×10^{-2} ms.$^{-1}$ deg.$^{-1}$ This gives a $\lesssim 8\times10^{-3}$ ms.$^{-1}$ deg.$^{-1}$

If the anisotropic relaxation is due to only one mechanism, the ratio b/a depends only on the symmetry of the electron wave functions at the Fermi surface. It is thus a parameter of considerable theoretical importance.

(iii) Spin-Spin Relaxation Times.

T_2 was measured from the free induction decay by the method described in Chapter 3.14. Considerable care was taken that the resonance was not swept through so quickly that the oscillations were distorted by more than a few percent. Timing was done by means of marker pips with 100μs. separation taken from the timing unit and displayed on the oscilloscope,

along with the rf pulse and boxcar gate. The rf pulse was 15μs. long, whilst the boxcar gate was 10μs. wide.

Measurements were made at 78°K. in both the 12" and the 6" Varian magnets. The sample was mounted vertically so that the [001] axis made an angle of 62° to the plane of rotation of H_0, while the [010] axis lay within 15° of this plane. Measurements were made at five different orientations of H_0 with respect to the (010) plane.

The most important feature of these measurements is that the free induction decay is exponential for times up to at least $2.5T_2$ (Fig. 4.8). The other decays do not have such good statistics, but still showed that the decay was exponential out to at least $2T_2$. The line shape in natural tin is squarer than Gaussian (65), so that these results are clear evidence that extreme exchange narrowing occurs in isotopically pure tin.

The line shape is broadened by the finite time that spin-lattice relaxation allows a nucleus to remain in a given state. This is known as lifetime broadening. The calculation of this effect for the general case is very complex, but for a spin $\frac{1}{2}$ system with a Lorentzian line it can rigorously by shown that the induction tail is still exponential with a decay constant T_2' given by (1)

$$(T_2')^{-1} = (T_2)^{-1} + (2T_1)^{-1}.$$

In applying this correction to the experimental results it was assumed that T_1 was 430μs. at 78°K. The error in T_1 is neglected since it contributes at most a systematic error of

5% to T_2. It should be noted that the lifetime broadening effect is not large enough to be the cause of the exponential decay.

Table 4.1. Spin-Spin Relaxation Times by Free Induction Decay

Angle of H_0 from (010) plane.	T_2' (μs.)	T_2 (μs.)
-30°	200±7	260±10
-30°	190±7	245±10
+10°	150±10	180±15
+10°	175±20	220±25
+30°	200±10	260±15
+55°	170±10	210±15
+100°	150±7	180±10

It takes about a day to make each measurement so that a detailed study of the anisotropy would take a long time. It was thus decided to use Clark's method of measuring the line shape (Chapter 3.15) to obtain the relative anisotropy and then use the free induction values of T_2 to get the absolute anisotropy. It only took a day to make a study of the line shape as a function of orientation so that several weeks were saved.

For the line shape measurements a boxcar gate 1ms. wide was used. This started about 20μs. from the true time origin and covered all of the free induction decay. Care was

taken that the line was swept through slowly enough to avoid distortion. Distortion still occurred due to the signal not being exactly in phase with the reference signal. The line shape is very sensitive to any errors in this phase setting. After considerable experimentation, this phase distortion was reduced to about the noise level and the measurements then were made. To analyse the line shape the midpoint was chosen and then the two amplitudes with the same frequency deviation from this midpoint were averaged. This approximately averaged out the residual phase distortion and also increased the S/N ratio by $\sqrt{2}$.

The resulting curves are Lorentzian for at least several line widths from the central frequency (Fig. 4.9), again strong evidence for exchange narrowing. The half widths and maximum amplitudes were both measured. As expected for exchange narrowing, when the half widths increased the amplitudes decreased by approximately the same fraction.

Two corrections to the line widths had to be considered. The first of these was the distortion introduced by the deadtime (Appendix IV). This reduced all the half widths by about 10%, but caused a much smaller error in their relative values. Apart from the narrowing, it caused little distortion in the line shape. For these reasons, it was ignored. A correction also had to be made for lifetime broadening. The half width is the reciprocal of T_2 so that the lifetime broadening corrections already obtained for T_2 were used to

give the half width corrections.

Further analysis of the line widths requires a closer study of the exchange narrowing process. In a reference frame rotating at the resonant frequency a spin only feels the local field, which it precesses about at a frequency of the order of the line width. If only a dipolar interaction is present, the magnetic field fluctuations occur at about the instantaneous Larmor frequency so that the spins can follow them reasonably well. This gives the dipolar line width. If an exchange interaction $\mathcal{H}_{ex} = \sum_{i<j} J_{ij} \underline{I}_i \cdot \underline{I}_j$ is also present the rate of change of the dipolar Hamiltonian $\mathcal{H}_1$ is

$$\hbar \dot{\mathcal{H}}_1 = -i [\mathcal{H}_0 + \mathcal{H}_{ex}, \mathcal{H}_1]$$
$$\simeq -i [\mathcal{H}_{ex}, \mathcal{H}_1]$$

If $\mathcal{H}_{ex} \gg \mathcal{H}_1$ the local field fluctuates at a rate about equal to the exchange interaction constant J. This is much faster than the Larmor frequency so that the averaged field which the spins feel is much less than the local field. The line is thus much narrower than the dipolar line.

The random function model of Anderson and Weiss casts this physical picture into a quantitative form (1,66). In this model it is assumed that the random fluctuations of the local field $\Delta\omega(t)$ from the resonant frequency ω_0 are Guassian in amplitude with a mean square value ω_p^2 equal to the second moment. Their time variations are described by the correlation function

$$\langle \Delta\omega(t) \Delta\omega(t+\tau) \rangle = \omega_p^2 g(\tau).$$

A form for $g(\tau)$ must be chosen on the basis of physical plausibility and mathematical tractibility. The physical restrictions on $g(\tau)$ are that the second moment is unaffected by the exchange interaction and that the fourth moment must remain finite. The simplest expression which satisfies these requirements in the Gaussian

$$g(\tau)= \exp(-\tfrac{1}{4}\pi\omega_e^2\tau^2).$$

$\omega_e \sim J$ is an average exchange frequency. With this assumption the free induction decay for the exchange narrowed region becomes

$$G(t)=\exp(-\frac{\omega_e^2}{\omega_p^2}\, t\ ) .$$

This expression holds except when $t \ll \omega_e^{-1}$, where the decay tends towards a Gaussian. The line shape corresponding to G(t) is a Lorentzian out to a frequency $\sim\omega_e$ where it falls off quite rapidly, keeping the second and fourth moments finite.

From G(t), the fourth moment is $\langle\omega^4\rangle=3\omega_p^4+\frac{1}{2}\pi\omega_e^2\omega_p^2$. The fourth moment can also be calculated in terms of the lattice structure by means of Van Vleck's method of traces. The two expressions have a similar form so that, by comparison, ω_e can be written in terms of the lattice structure and exchange and dipolar interactions. The resulting expression is so complicated that ω_e is customarily assumed to be isotropic.

The line width is ω_p^2/ω_e . The second moment for white tin has been calculated by computer so that the form of ω_p^2 is known. If ω_e is isotropic, the anisotropy of the

measured line widths should be proportional to ω_p^2. The fit is reasonably good (Fig. 4.11) and, considering the experimental errors involved, shows that ω_e is isotropic, or very nearly so. The largest error is due to slight misalignment of the crystal. The magnetic field orientation traces out a complicated trajectory (Fig. 4.10) and slight changes in this cause large changes in the hill to valley ratio of the second moment. The inverses of T_2 for five different orientations of H_o are also plotted on the same graph and agree well with the line width variations. They also give the absolute line widths.

ω_p^2 is the sum of the second moments due to dipolar and pseudo-dipolar interactions. These both have the same angular dependence, so that $\omega_p^2 = \langle\omega_d^2\rangle(1+B)$, where $\langle\omega_d\rangle^2$ is the dipolar second moment and B is the fraction of pseudo-dipolar exchange present.

$$T_2 = \frac{\omega_e}{\langle\omega_d^2\rangle(1+B)}$$

Using all of the measured T_2 s, along with their corresponding calculated dipolar second moments gives

$$\omega_e = (1+B)(7\pm1.5)10^3 \text{ rad}^2. \quad \text{----------(1)}$$

The absolute value of these parameters cannot be obtained without making an independent measurement involving them. In this case a measurement of T_2 in a natural tin crystal was made at 78°K. The S/N ratio was poor, being about three, so that nothing could be said about the free induction decay other than it decayed faster than an exponential decay. Steady state

measurements show that the line is nearly Gaussian (65) so that the line was analysed by assuming it was Gaussian. This gives $T_2 = (120 \pm 20)\mu s.$, after applying a correction for T_2 broadening. This corresponds to a second moment of (1.3 ± 0.2)Kc/s . This is in excellent agreement with the steady state value (68).

Natural tin contains two isotopes, Sn^{117} and Sn^{119} , of approximately equal abundances. The width of the Sn^{119} line thus contains a number of contributions (1,52).

(a) Dipolar broadening between like and unlike spins.

$$M_2^d = \tfrac{3}{4}\gamma^4\hbar^2 I(I+1)\sum_{ij} b_{ij}^2 + \tfrac{1}{3}\gamma_1^2\gamma_3^2\, S(S+1)\hbar^2\sum_{ij} b_{ij}^2 ,$$

where the summations are only taken over the lattice sites occupied by the appropriate isotope. $b_{ij} = r_{ij}^{-3}(3\cos^2\theta_{ij} - 1)$. Tin has approximately equal gyromagnetic ratios and abundances F and so the expression simplifies to

$$M_2^d = \tfrac{13}{16}\gamma^4\hbar^2 F\sum_{ij} b_{ij}^2 ,$$

where the summation is now taken over all the lattice sites.

(b) Pseudo-dipolar broadening.

This adds a term BM_2^d to the second moment.

(c) Pseudo-exchange broadening between unlike nuclei.

The exchange coupling $\sum_{ij} J_{ij}(\underline{I}_i \cdot \underline{S}_j)$ does not commute with $\mathcal{H}'$ if the spins are unlike and so contributes a term to the second moment. For tin this is

$$M_2^{ex} = \tfrac{1}{4}F\sum_i J_{ij}^2(r),$$

with the summation over all lattice sites.

(d) Exchange narrowing between like spins.

In natural tin the exchange frequency is $F\omega_e$. F is about 0.08 and so the exchange frequency is much less than the dipolar frequency and can thus be neglected.

$\sum_j b_{ij}^2$ has already been computed so that the total second moment in natural tin can be calculated. It is

$$\langle \Delta\omega^2 \rangle = 7.5 \times 10^6 (1+B) + 2.5 \times 10^{-1} J^2.$$

In evaluating J the lattice structure has been roughly taken into account. White tin consists of two interpenetrating body-centred tetragonal lattices with a c/a ratio of 0.55 (67). Each atom has six nearest neighbours about $3.1A^\circ$ away and 12 next nearest neighbours about $4A^\circ$ away. Atoms further away than this were not considered. J is the value of the exchange constant at the nearest neighbours and was assumed to vary as r^{-3} in summing over the other sites.

Assuming a Gaussian line and using the measured value of T_2 to determine $\langle \Delta\omega^2 \rangle$ gives

$$(7 \pm 1) \times 10^7 = 7.5 \times 10^6 (1+B) + 2.5 \times 10^{-1} J^2. \qquad \text{----------(2)}$$

The next step relates J and ω_e and involves the most drastic step of the whole analysis, justifiable only by expediency. The relation between J and ω_e should be obtained by equating the fourth moment $3\omega_p^4 + \frac{1}{2}\omega_p^2\omega_e^2$ to the fourth moment calculated from the lattice structure by the method of the traces. The latter involves a triple summation over

all the lattice sites and even for just the 12 atoms out to next nearest neighbours is a prohibitively complicated calculation, while summing over fewer atoms is not physically justifiable. The relation

$$\frac{\langle \Delta\omega^4 \rangle}{3\langle \omega_p^2 \rangle} \simeq \frac{0.12 J^2 d^2}{\gamma^4 \hbar^2 (l^2+m^2+n^2-0.2)}$$
$$= 1.7\times10^{-8} J^2$$

obtained for a simple cubic lattice (1) thus had to be used. The lattice spacing d is assumed to be $3A^\circ$, the nearest neighbour spacing. For $\langle\langle \omega_p^2 \rangle\rangle$ an average of the computed values for the white tin lattice is used. This must also include the pseudo-dipolar contribution. This was obtained by iteration. The calculation was first carried through without the pseudo-dipolar contribution to obtain an approximate value of B and this was then used in obtaining a more accurate value of $\langle \omega_p^2 \rangle$. Because of the large experimental errors and the dominance of the exchange term, it was not necessary to repeat the cycle. The value finally adopted was $\langle \omega_p^2 \rangle = (8.1\pm0.8)\times10^7 \text{ rad}^2$.

This gives

$$\langle \Delta\omega^4 \rangle \simeq 3.4 J \langle \omega_p^2 \rangle^2$$
$$\simeq \tfrac{1}{2}\pi \langle \omega_p^2 \rangle \omega_e^2$$
$$\omega_e^2 = (2.2\pm0.2) J^2. \qquad \text{----------(3)}$$

This neglects the dipolar contribution to the fourth moment, a good approximation for extreme exchange narrowing.

Substituting this expression in the equation for the second moment in natural tin and then eliminating 1+B gives a

quadratic equation in ω_e. The solution of this equation is

$$\omega_e = (2.0 \pm 0.3) \times 10^4 \text{radians}.$$

This corresponds to an exchange constant of

$$J = (2.2 \pm 0.3) \text{Kc/s}.$$

Using the above value of ω_e gives

$$B = 1.9 \pm 0.5.$$

By comparing the line width they measured in white tin powder by steady state methods with the calculated dipolar moment, Karimov and Schegolev (68) obtained $J = (2.5 \pm 0.1)$Kc/s. However, they neglected the pseudo-dipolar contribution. If their results are re-analysed with the pseudo-dipolar contribution from the present experiment included, they give $J = (2.1 \pm 0.2)$Kc/s. There is thus excellent agreement between the two experiments. Jones (65) also attempted to measure J. There are numerical errors in his determination of the second moment and an incorrect lattice structure was used in his second moment computation so that his results are wrong. A determination of B has not been made before.

The whole analysis has rested on the twin assumptions that the dipolar field fluctuations have a Gaussian correlation function and that the dipolar line shape is Gaussian. Little can be said about the reliability of the correlation function other than that it is plausible. The effect of deviations from the Gaussian form is unknown. More definite statements can be made about the assumption of a Gaussian line shape. The line shape parameters of interest are the second moment

of the dipolar line and the fourth moment of the exchange narrowed line. The dipolar second moment can be rigorously calculated in terms of the known lattice structure. The total second moment has to be measured in natural tin but, provided the S/N ratio is good enough, this can accurately be done for non-Gaussian lines by an appropriate analysis of the free induction decay. In the case of extreme exchange narrowing, the contribution to the fourth moment from the exchange interaction usually dominates the dipolar fourth moment. If this is so, the total fourth moment is insensitive to the dipolar line shape and so the values of B and J obtained should be unaffected by moderate deviations from a Gaussian dipolar line shape. More explicitly, Anderson and Weiss found that the two most extreme dipolar line shapes likely, a square spectrum and an exponential one with equal second moments, had exchange narrowed line widths which differed by about 50%. It thus seems that the measured values of B and J do not contain large errors due to the assumption of a Gaussian line shape, but could possibly contain large errors due to defects in the random fluctuation model.

The last stage should be to compare the experimental values of J and B with values calculated from the tin band structure. However neither the accuracy of the measurements, nor that of the calculated values, warrants such a step at the present time. The main feature to note is the large value of B. This implies that a large number of the Fermi surface

electrons are of p, or higher character. The relatively large anisotropic Knight shift substantiates this.

(iii) Spin Echoes.

At liquid nitrogen temperature tin has $T_1 \sim 0.5$ms. and $T_2 \sim 200\mu$s. If T_2 is reduced by destroying the homogeneity of the magnetic field, it is possible to get spin echoes.

In the first measurement two rf pulses 15μs. and 30μs. long and separated by 200μs were used. The homogeneity was such that $T_2^* \sim 30\mu$s., while the repetition rate was $(10\text{ms.})^{-1}$. By varying the magnetic field the boxcar was swept through resonance at 10μs. intervals from 60μs. to 250μs. after the second pulse. A narrow boxcar gate of 10μs. was used and all the times were measured between the centres of the pulses and boxcar gate. The magnetic moment measured by a sweep was then plotted against the time after the second pulse (Fig. 4.3). The graph shows a spin echo which is 180° out of phase with the induction tail and with a symmetrical envelope whose time constant is the same as that of the induction tail. Its maximum occurs at 200μs. after the centre of the second pulse. On removal of the first pulse the spin echo vanished. The measurements were repeated with several different separations between the rf pulses. The amplitude of the echo increased as the pulse separation decreased.

The next experiment was to apply two pulses 200μs. apart with a 30μs. wide boxcar gate set on the echo maximum. The magnetic field was then swept through resonance with

varying values of the reference phase. As the phase was varied by 90°, the plot of magnetic moment versus magnetic field changed from an absorptive to a dispersive shape.

So far the spin echo had behaved in exactly the same fashion as a spin echo in a non-metallic substance with a homogeneous H_1. In the next series of measurements, the differences became apparent. T_2^* was reduced to 20μs. for these experiments. Two rf pulses separated by 150μs. were used along with a boxcar gate 40μs. wide set on the echo maximum. The widths of the two pulses were then varied while keeping the ratio of their widths fixed at 1:2. The graph of echo height against the first pulse width showed that the maximum amplitude occurred when the first pulse was about 10μs. wide (Fig. 4.4). The first pulse width was then kept fixed at 10μs. and the second pulse width varied from 5μs. to 90μs. The maximum amplitude occurred when the second pulse was about 20μs. wide (Fig. 4.5).

These results can be explained by a simple extension of the classical spin echo theory of Hahn (62) to the case of a metal in the normal skin effect region. For simplicity, only the case of a phase coherent system set to detect the absorption mode and operating at the resonant frequency is considered. The sample is approximated by an infinite plane so that the rf magnetic field at a depth z from the surface is $H_1 = H_{1_0} \exp(-\frac{z}{\sqrt{2}\delta}) \cos(\frac{z}{\sqrt{2}\delta})$. Replacing ω_1 by $\omega_1(z) = \omega_1 \exp(-\frac{z}{\sqrt{2}\delta})$ in Hahn's theory and taking account of the phase coherence allows the magnetic moment $M_{se}(z,t)$ producing the spin echo at a depth z to be

simply calculated. The spin echo induced voltage is then (Appendix III)

$$v_{se}(t) = \int_0^\infty \exp(-\tfrac{z}{\sqrt{2}\delta})\cos(\tfrac{z}{\sqrt{2}\delta})M_{se}(z,t)dz$$

$$= M_0 \exp\left[\tfrac{1}{2}\left(\tfrac{2T-t}{T_2^*}\right)^2 - \tfrac{t}{T_2}\right]\int_0^\infty \exp(-\tfrac{z}{\sqrt{2}\delta})\sin[\omega_1(z)\tau_1]$$

$$\sin^2\left[\tfrac{1}{2}\omega_1(z)\tau_2\right]\cos^2(\tfrac{z}{\sqrt{2}\delta})dz.$$

T_2 is the spin-spin relaxation time due to dipolar and exchange effects, while T_2^* is the transverse relaxation time due to the inhomogeneous magnetic field. T is the time interval between the two rf pulses of duration τ_1 and τ_2 seconds respectively. By writing $\sin(\omega_1\tau_1)\sin^2(\frac{1}{2}\omega_2\tau_2)$ as $\sin(\omega_1\tau_1)+\frac{1}{2}\left[\sin\{\omega_1(\tau_2-\tau_1)\} - \sin\{\omega_1(\tau_2+\tau_1)\}\right]$, v_{se} becomes a sum of integrals of the form $\int_0^\infty \exp(-x)\cos^2(x)\sin(\omega_1\tau_1 e^{-x})dx$. These have already been evaluated (Appendix III), so that a quantitive test of v_{se} can be made. The calculated variation of spin echo amplitude with rf pulse length has been plotted in Figs. 4.4 and 4.5 for both the metallic and non-metallic cases. It was assumed that a $\frac{1}{2}\pi$ pulse at the surface of the sample was 9μs. The theoretical expression is in good qualitative agreement with the experimental points and would be in quantitative agreement if it was assumed that the $\frac{1}{2}\pi$ pulse was about 8μs. long. This is possible since these measurements were not made under exactly the same experimental conditions as those of Fig. 4.2.

For the spin echo measurements of T_2, the first pulse was 10μs. long and the second one was 20μs. long. A 30μs. wide boxcar gate was used. If the pulse separation (taken

between centres) was T, the gate centre was located at a time T after the centre of the second pulse. After each sweep through resonance T was altered manually. Timing was by means of the double beam oscilloscope and marker pips from the timing unit. All the measurements were made at 78°K. The spin echo decays were all exponential (Fig. 4.13) with a decay constant T_2' which was corrected for lifetime broadening in the same fashion as the free induction decays to give T_2.

Table 4.2. Spin-Spin Relaxation Times by Spin Echoes

Angle of H_0 from (010) plane.	T_2' (μs.)	T_2 (μs.)
+10°	120±10	140±12
+30°	170±15	210±20
+55°	105±5	120±7
+100°	105±5	120±7

When the values of T_2 obtained by free induction decay and by spin echoes were plotted against magnetic field orientation (Fig. 4.13) it was surprisingly found that T_2 obtained by spin echoes was always shorter than T_2 measured by free induction decay. The difference ranged from 20% to 55% of the value of the free induction T_2.

There are three possible reasons for this large difference in values. The first of these is spin diffusion in the spin gradient caused by the large inhomogeneity in H_1. For a spin ½ system the surplus of spins in one orientation

p(x,t) obeys the diffusion equation (1).

$$\frac{\partial p}{\partial t} = Wa^2 \nabla^2 p.$$

W is the probability/second that two nuclei undergo a mutual spin flip and a is the separation between the nuclei. $W \sim J$, the exchange constant, so that $Wa^2 \sim 10^{-12}$ cm^2/sec. Spin diffusion alters T_2 because the phase and attenuation of the induced signal depend on the depth of the spins from the surface and so if the spin concentration changes with time, T_2 is altered. For spin diffusion to reduce the free induction T_2 by 10% the spins must travel a distance of about 0.05δ in the time T_2. The distance travelled in the time T_2 is $(2Wa^2T_2)^{\frac{1}{2}}$. This is about one lattice spacing, so that spin diffusion effects are negligible. Because of this very slow velocity spin diffusion should not have any effect on the spin echoes either.

The second possibility is that two of the approximations made in deriving the spin echo equation are not valid and that obscure phase effects associated with this cause the error in T_2. In the derivation it is assumed that the pulse lengths are negligible compared to T_2 and T_2^*. If this is so, then relaxation in the rotating reference frame occurs during the rf pulse and it is easily shown that the only effect of this is to reduce the echo amplitude without affecting the measured value of T_2. However in the present case the pulse lengths are about 10μs. while T_2 is about 150μs., so that relaxation in the rotating reference frame only occurs within about δ of the surface. Spin-spin relaxation for the case when

$\gamma H_1 \sim T_2^{-1}$ has only been calculated for a two spin system (13). In this, non-secular terms in the rotating reference frame drastically modify relaxation during the rf pulse, but have no effect on the free induction decay after the rf pulse is over, apart from altering the initial time origin and amplitude. This suggests that there should be no error in T_2 obtained from the free induction decay in the case of an n spin system. Although they intuitively seem independent of the pulse separation, it is possible that these non-secular terms cause the reduction in T_2 in spin echoes.

Hahn's theory also contains the more drastic assumption that $\gamma H_1 \gg (T_2^*)^{-1}$. This means that the magnetic moments precess about the constant magnetic field H_1, dipolar fluctuations having negligible effect on the precession. In these experiments, this requirement does not even hold at the surface of the metal. It is quite possible that this is the reason for the smaller T_2. The restriction on H_1 could be removed from the theory if it were not for the ensuing avalanche of algebraic manipulations.

The breakdown of these two approximations suggests that dividing v_{se} into the product of a time dependent and a phase dependent factor is only approximately correct. There are two experimental checks of this which can be made. The first one would be to measure T_2 as a function of H_1 using approximately $\frac{1}{2}\pi$ and π pulses at the surface of the metal for each value of H_1. Unfortunately the apparatus could not do this. However

the second check of measuring T_2 as a function of pulse length was attempted. The first pulse length was kept fixed at 10μs. while the second pulse length was varied.

Table 4.3 Variation of Spin Echo T_2 With Pulse Length

Angle of H_0 from (010) plane.	Length of Second pulse (μs.).	T_2' (μs.) Spin echo.	T_2' (μs.) Free induction
+30°	10	180±20	---
+30°	20	170±15	200±10
+55°	10	115±5	---
+55°	20	105±5	170±10
+55°	30	105±5	---

Although the experimental errors prevent a definite conclusion, it seems that there is a small dependence of T_2 on pulse length. There could also be a dependence on the first pulse length, but the poor S/N prevented any experimental examination of this. The experiment has failed to show the cause of the bulk of the descrepancy though.

The final possibility is that the difference is due to the effect of the exchange term. In the laboratory frame the Hamiltonian of the system is

$$\mathcal{H} = \gamma\hbar\sum_i I_{iz} + \gamma^2\hbar^2 \tfrac{1}{2}\sum_{i\neq j}\left[\underset{\sim}{I}_i\cdot\underset{\sim}{I}_j - 3r_{ij}^{-3}(\underset{\sim}{I}_i\cdot\underset{\sim}{r}_{ij})(\underset{\sim}{I}_j\cdot\underset{\sim}{r}_{ij})\right] r_{ij}^{-3} + \sum_{ij} J_{ij}(r_{ij})\underset{\sim}{I}_i\cdot\underset{\sim}{I}_j .$$

The Hamiltonian in a reference frame rotating at a frequency ω becomes

$$\mathcal{H}_r = \gamma\hbar\sum_i (H_0 - \tfrac{\omega}{\gamma}) I_{iz} + \mathcal{H}'' ,$$

where $\mathcal{H}'' = \gamma^2\hbar^2 \frac{1}{4}\sum_{(i\neq j)} r_{ij}^{-3}(1-3\cos^2\theta_{ij})(3I_{iz}I_{jz}-\underset{\sim}{I}_i\cdot\underset{\sim}{I}_j)+\frac{1}{2}\sum_{ij} J_{ij}\,\underset{\sim}{I}_i\cdot\underset{\sim}{I}_j$.
Before the first pulse, the density matrix describing the spin system is

$$\rho(0) = \frac{\exp(-\frac{\hbar\mathcal{H}}{kT})}{Tr[\exp(-\frac{\hbar\mathcal{H}}{kT})]} \quad .$$

The Zeeman term is much larger than the dipolar and exchange terms and $kT \gg h\mathcal{H}$, so that one can assume that $\rho(0) \propto I_z$. The amplitude of a signal is proportional to $Tr\left[\rho(t)I_x\right]$, where $\rho(t)$ is the density matrix describing the spin system in the frame rotating at the frequency ω of the applied rf pulses. Following Abragam (p. 498), the maximum amplitude of the spin echo at resonance becomes

$$E(2T) = Tr\big[\exp(-i\mathcal{H}'T)\exp(-i\gamma H_1\tau_2)\exp(-i\mathcal{H}'T)\exp(-i\gamma H_1\tau_1)$$

$$I_z \exp(i\gamma H_1\tau_1)\exp(i\mathcal{H}'T)\exp(i\gamma H_1\tau_2)\exp(i\mathcal{H}'T)I_x\big],$$

where τ_1 and τ_2 are the first and second pulse lengths respectively and T is the pulse separation. The problem is now formally solved; the remaining steps consisting of expanding the exponential operators in a power series and then evaluating the resulting traces. The attenuation and phase factors due to the spin echo being in a metal could then be taken care of in the same fashion as for the free induction decay.

In practice, the mathematical complexity involved has prevented E(2T) from being evaluated for even a two spin system. The rigorous quantum mechanical theory thus at present says nothing about the effect of the exchange interaction on spin echoes. Statistical theories, such as that of Anderson

and Weiss, are not suitable for describing the spin echoes since they contain ad hoc assumptions and, by their nature, average out many of the detailed interactions which might be expected to modify the exchange effects.

Because of the dipolar coupling, the nuclei are not an equivalent sites, so there is no theoretical prohibition on exchange effects being observed by spin echoes (1).

In the density matrix formalism the free induction decay is proportional to $Tr[\exp(-i\mathcal{H}t)I_x\exp(i\mathcal{H}t)I_x]$. The first two terms of this have been evaluated in the presence of both exchange and dipolar interactions (1). The first term (second moment) is unaffected by exchange, but the second term (fourth moment) is increased by it. In the case of exchange narrowing the series must approximate an exponential series, so that obviously the exchange must also affect many higher terms in the expansion.

The theoretical situation is that the exchange interaction affects the free induction decay in a way consistent with the experimental results in both the density matrix and statistical theories. The density matrix theory says nothing about the spin echo case while the Anderson-Weiss theory gives the same T_2 for both free induction and spin echo decays. However this is not conclusive because of the type of assumptions involved in their theory. These considerations suggest that the exchange interaction affects the spin echoes, but it is impossible to say whether or not the spin echo T_2 should be

the same as that of the free induction decay.

All of the obvious reasons for the difference between the spin echo and free induction relaxation times have now been examined. The only definite conclusion is that spin diffusion effects are negligible. All of the obvious experimental possibilities, such as a systematic error in positioning the box-car gate on the echo, were eliminated by the preliminary experimental investigation, or by the method used in taking the data. Pulse width effects were experimentally shown to be small. There still remains the possibility of experimental effects caused by H_1 being too small. It is also possible that the difference in T_2 is an intrinsic feature of systems with approximately equal dipolar and pseudo-exchange interactions. The oscillatory variation of the pseudo-exchange interaction with distance might be of some importance in causing this.

4.8 The Experimental S/N Ratios

An expression for the S/N ratio has been derived (Chap. 3.12) which can now be compared with the experimental S/N ratios determined for six different metals under varying conditions. The S/N ratio at the amplifier output is

$$S' = \pi\eta\mathfrak{G}\, n\mu\omega M_0 R_1 Q \left(\frac{C}{kT_n}\right)^{\frac{1}{2}}.$$

In calculating this Q is arbitrarily assumed to be 20 and temperature independent, T_n is assumed to be the sample temperature and C is taken as 80pf. The other parameters depend on the individual sample and coil and are known, except for

δ. For some metals δ can be accurately calculated at the temperatures of interest, but for other metals the electrical conductivity had to be estimated. The boxcar enhancement factor is $\left(\frac{R_b C_b}{\tau_c}\right)^{\frac{1}{2}}$. τ_c was estimated from the bandwidth of the tuned circuit to be $2\mu s$. Using these values, a table comparing the theoretical and experimental S/N ratios can be constructed.

Table 4.4 Experimental and Theoretical S/N Ratios

Metal	S/N at Amplifier Output, S′.	Boxcar Enhancement factor	Final S/N	Experimental S/N ratio	Temperature °K.
Al^{27}	0.08	130	10	15	295
"	0.2	30	6	10	78
V^{51}	0.4	22	8	30	295
"	1	7	7	45	78
Nb^{93}	1	30	30	80	295
"	3	30	90	50	78
Ga^{71}	0.006	4	0.02	--	295
"	0.04	7	0.3	--	78
"	0.09	12	1	3	303
Sn^{119}	0.1	90	9	15	78
Natural tin	0.01	150	1.5	3	78
In^{111}	0.05	12	0.5	--	295
"	0.1	12	1	--	78
Bi^{209}	0.02	7	0.1	--	295
"	0.2	7	1.5	--	78
Sb^{121}	0.02	7	0.15	--	295
"	0.06	7	0.04	--	78
Re^{187}	0.01	7	0.07	--	295
"	0.02	7	0.15	--	78

The agreement between the calculated and experimental values is very good considering the number of ill defined quantities involved. The experimental S/N ratio was only crudely measured and was not corrected for spin-spin relaxation. If this were done, it would double most of the experimental S/N ratios. The reduction in S/N caused by acoustic oscillations was not allowed for either. In niobium this is the main noise source at 78°K.

If spin-spin relaxation is allowed for, the experimental S/N is usually about four times the experimental value. Part of this difference is undoubtedly due to incorrect values of some parameters and to the simplifications in the theory. The remainder of the descrepancy is probably because the sample surface is not perfectly smooth, but contains irregularities with dimensions much larger than the skin depth. These increase the effective surface area and hence increase the induced signal. Provided that the Q is limited by the external circuit resistance, this will increase the S/N by some factor in the region of two. In any case, the difference between the theoretical and experimental S/N ratios is now known, so that the theory can confidently be used to predict the expected S/N ratio of a sample to within a factor of two in the temperature range in which the skin effect is normal.

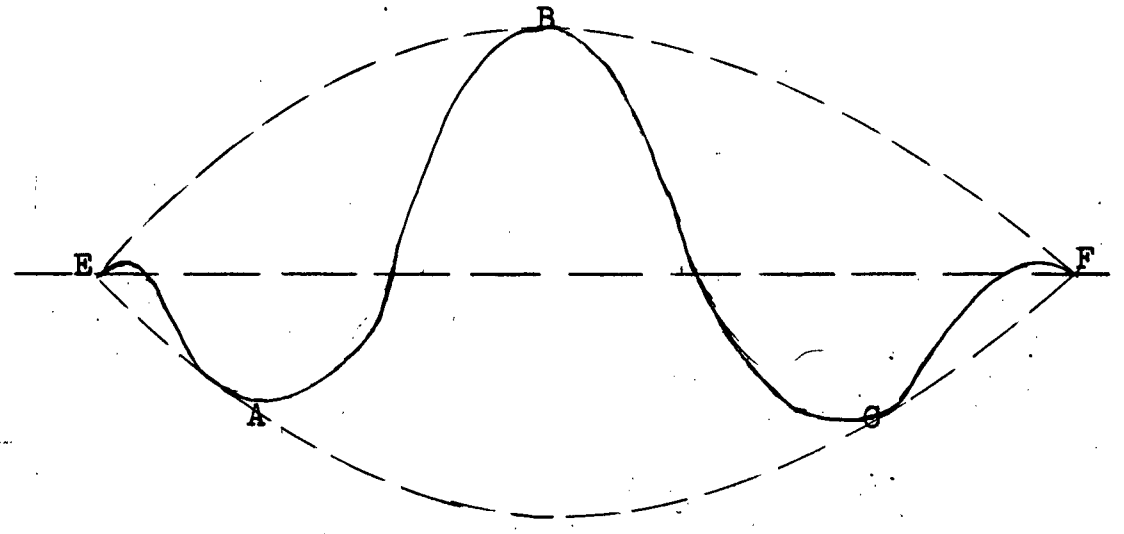

Figure 4.1a Sweep Close to the rf Pulse

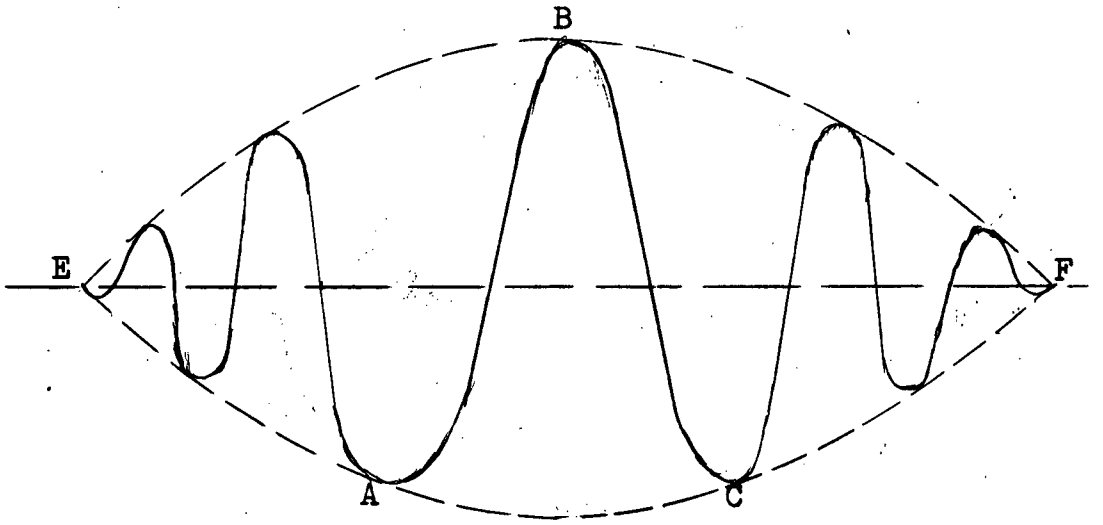

Figure 4.1b Sweep at a Time About T_2 after the rf Pulse

Typical Chart Records of a Sweep with a Narrow Boxcar Gate Through the Free Induction Tail.

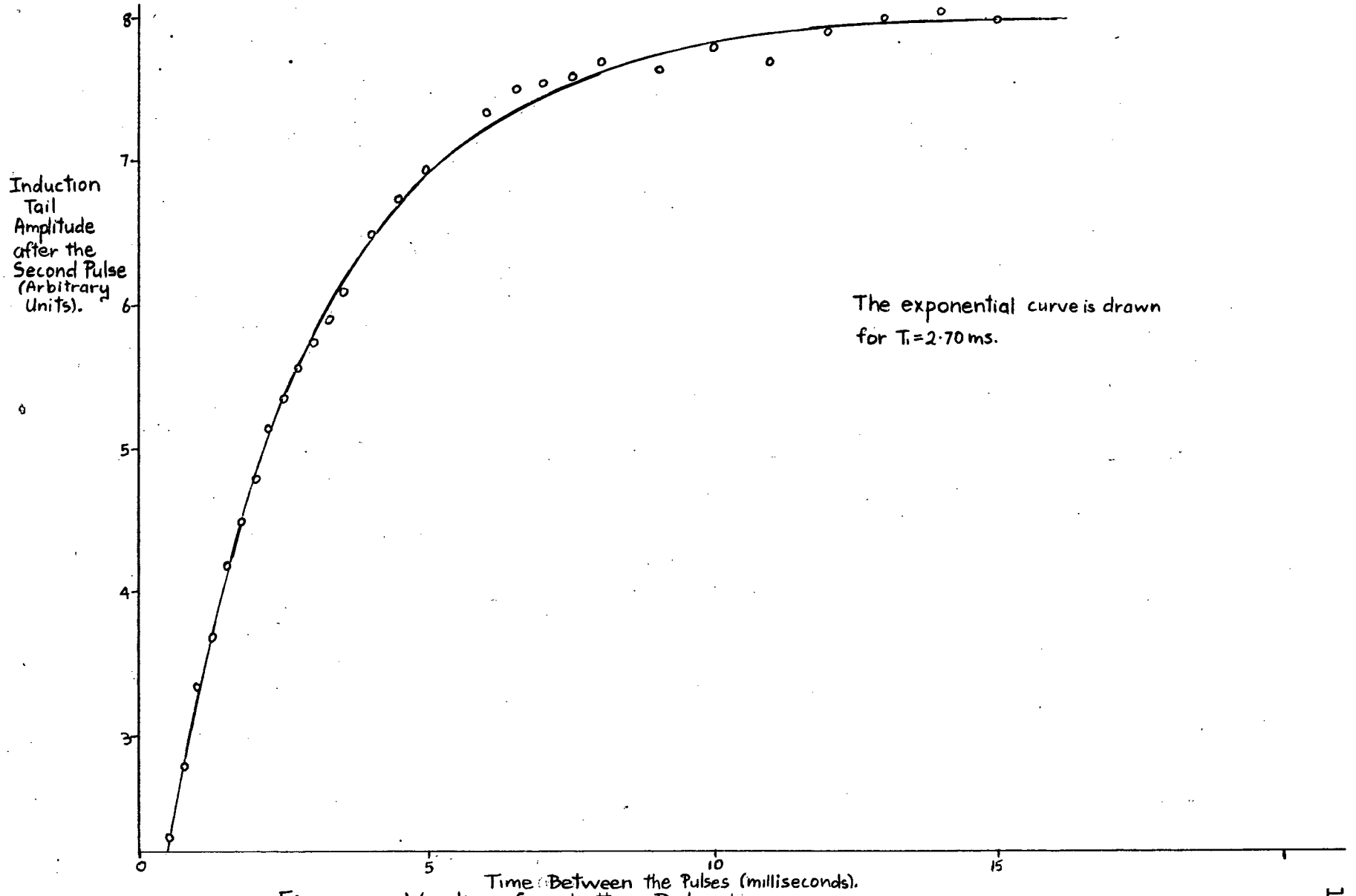

Figure 4.2. Vandium Spin-Lattice Relaxation.

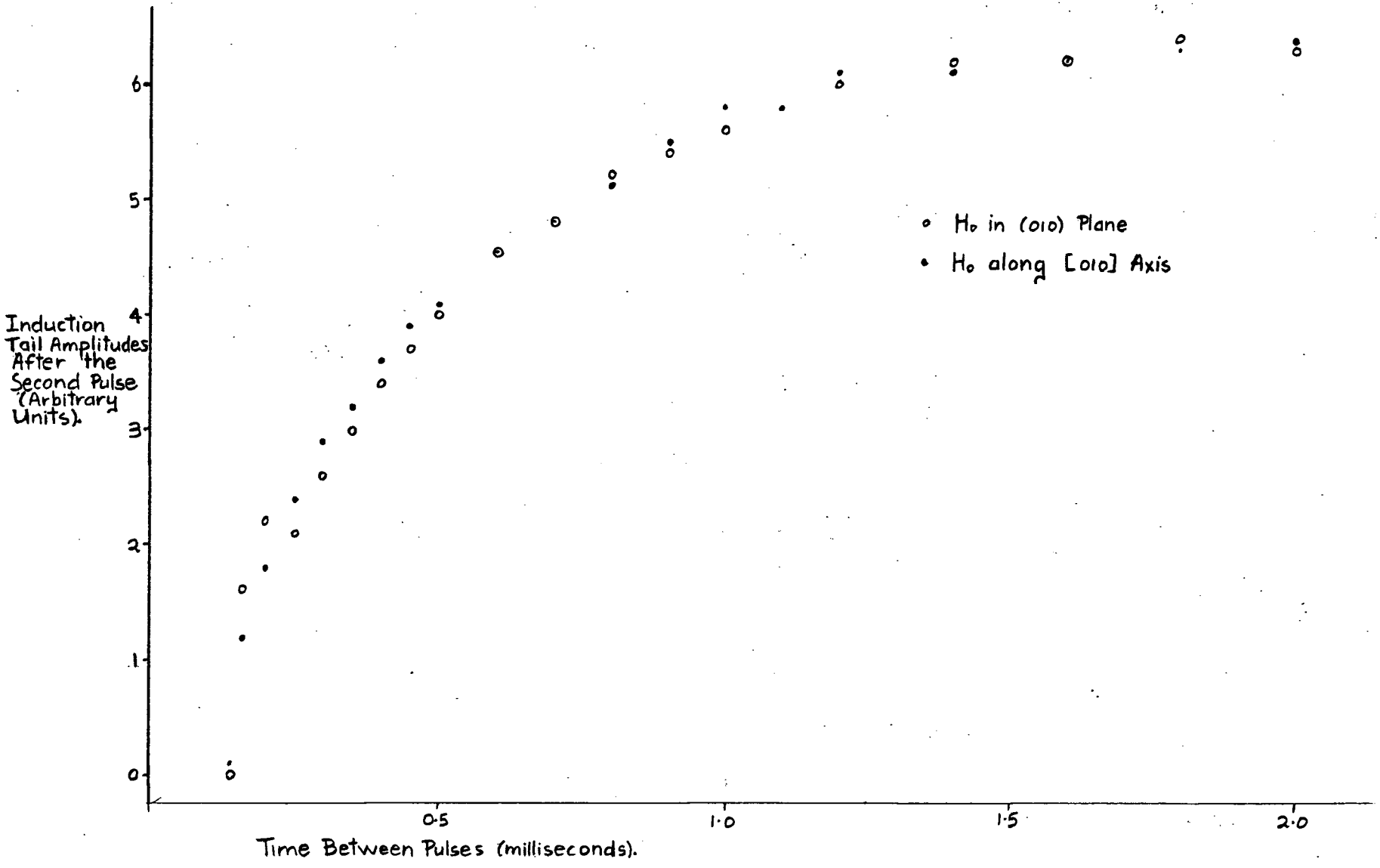

Figure 4.3 Spin-Lattice Relaxation Time Anisotropy in Isotopically Pure Tin.

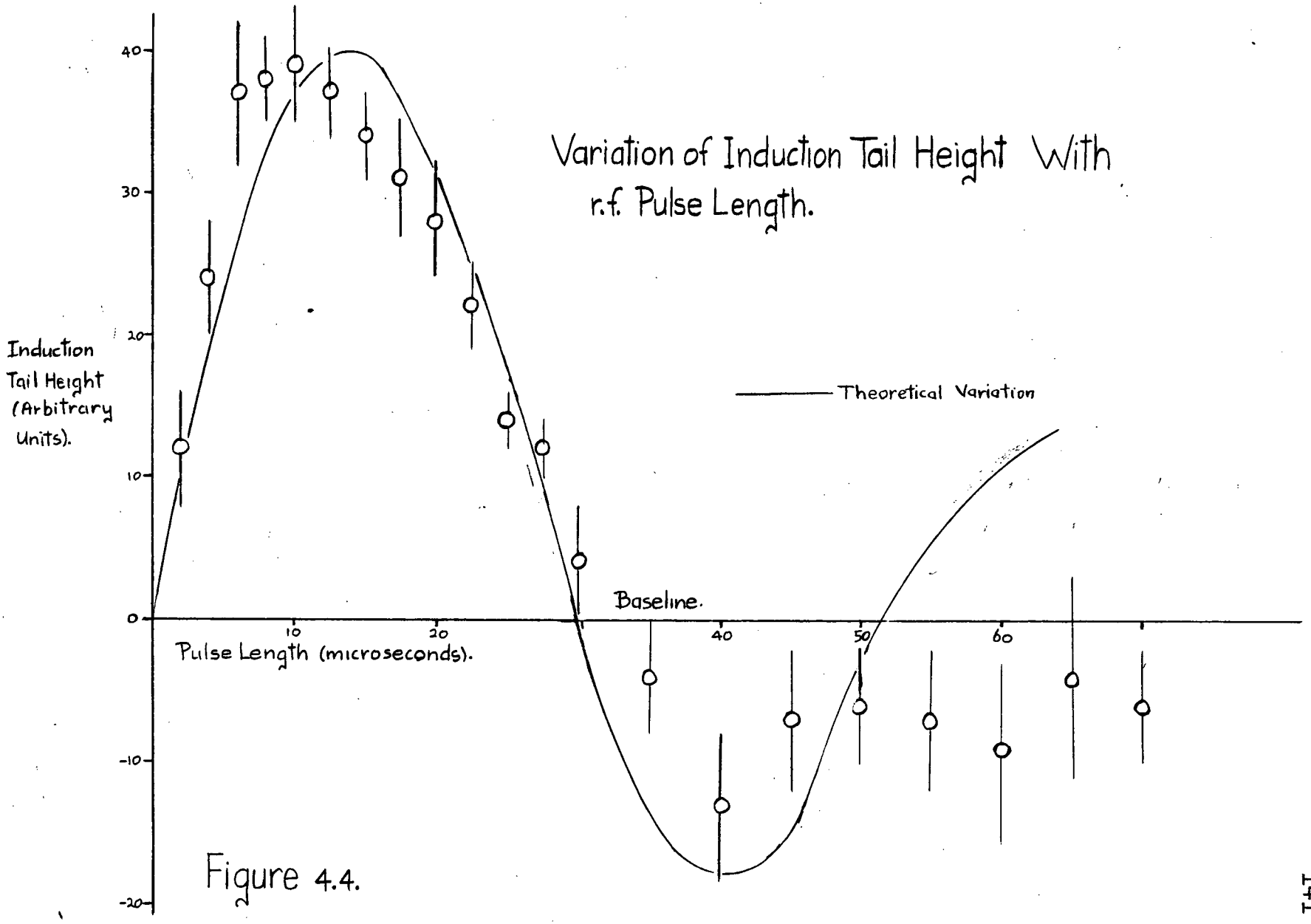
Variation of Induction Tail Height With r.f. Pulse Length.
Induction Tail Height (Arbitrary Units).
40
30
20
10
0
-10
-20
10
20
40
50
60
Pulse Length (microseconds).
Baseline.
Theoretical Variation

Figure 4.4.

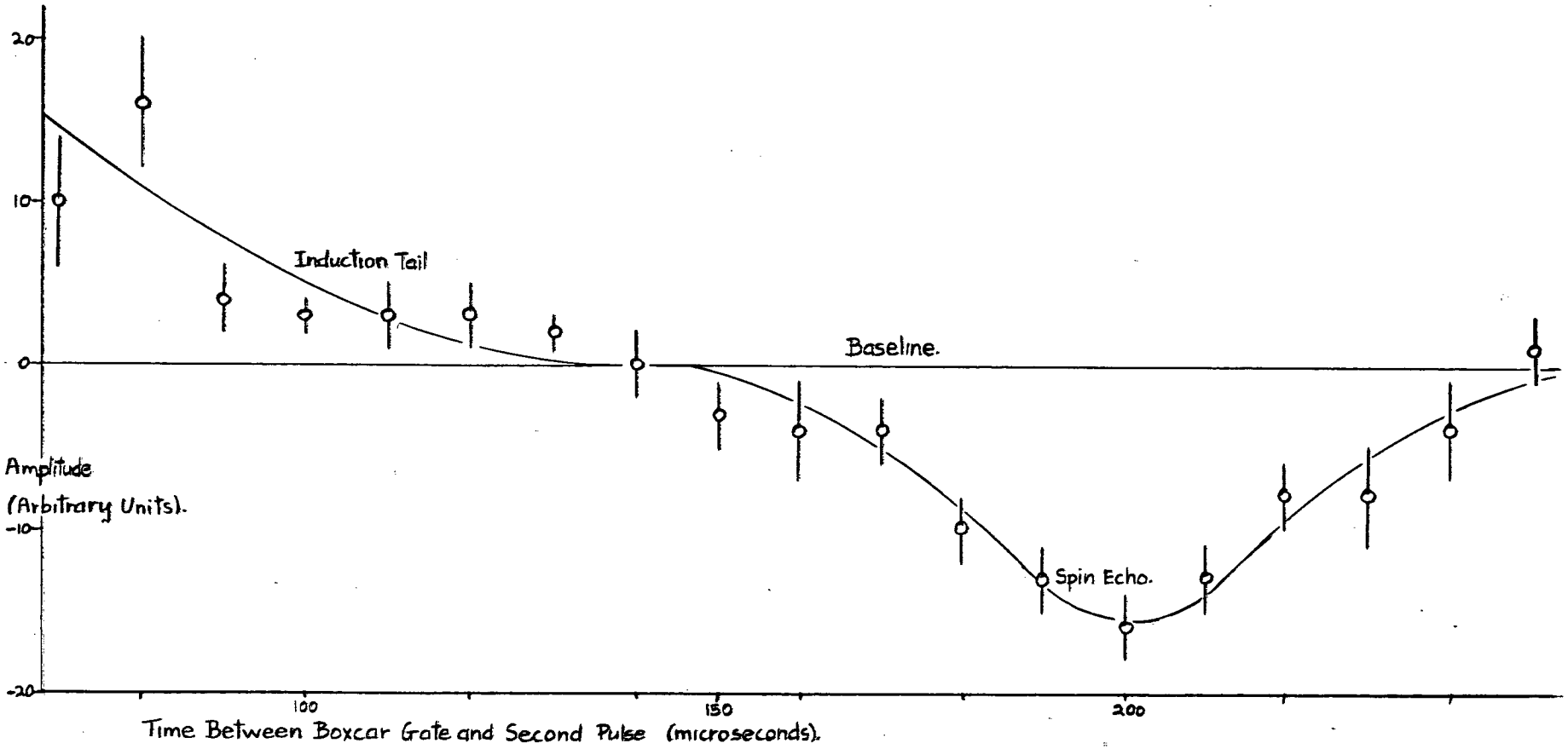

Figure 4.5 A Spin Echo.

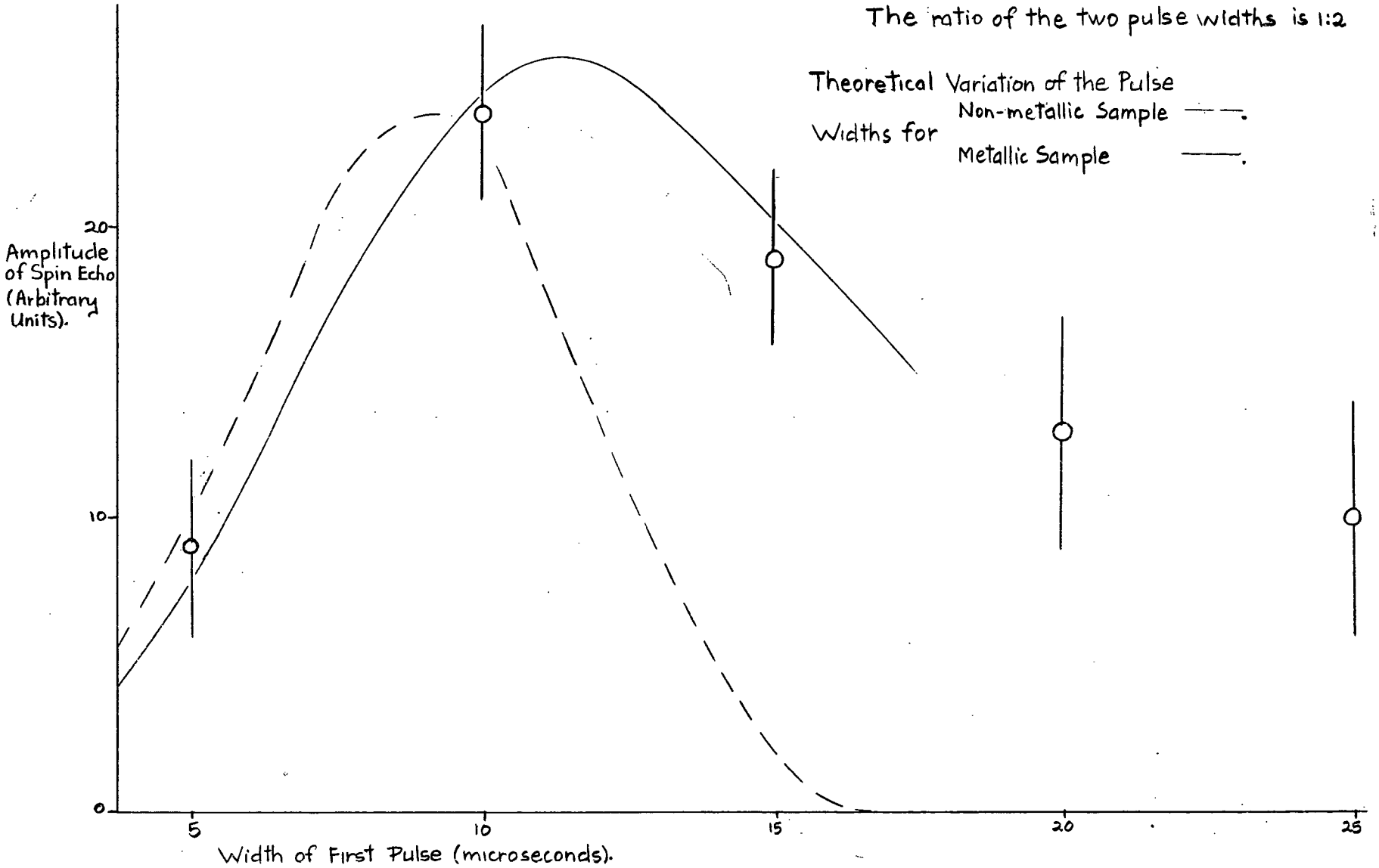

Figure 4.6 Variation of Spin Echo Amplitude With the r.f. Pulse Widths.

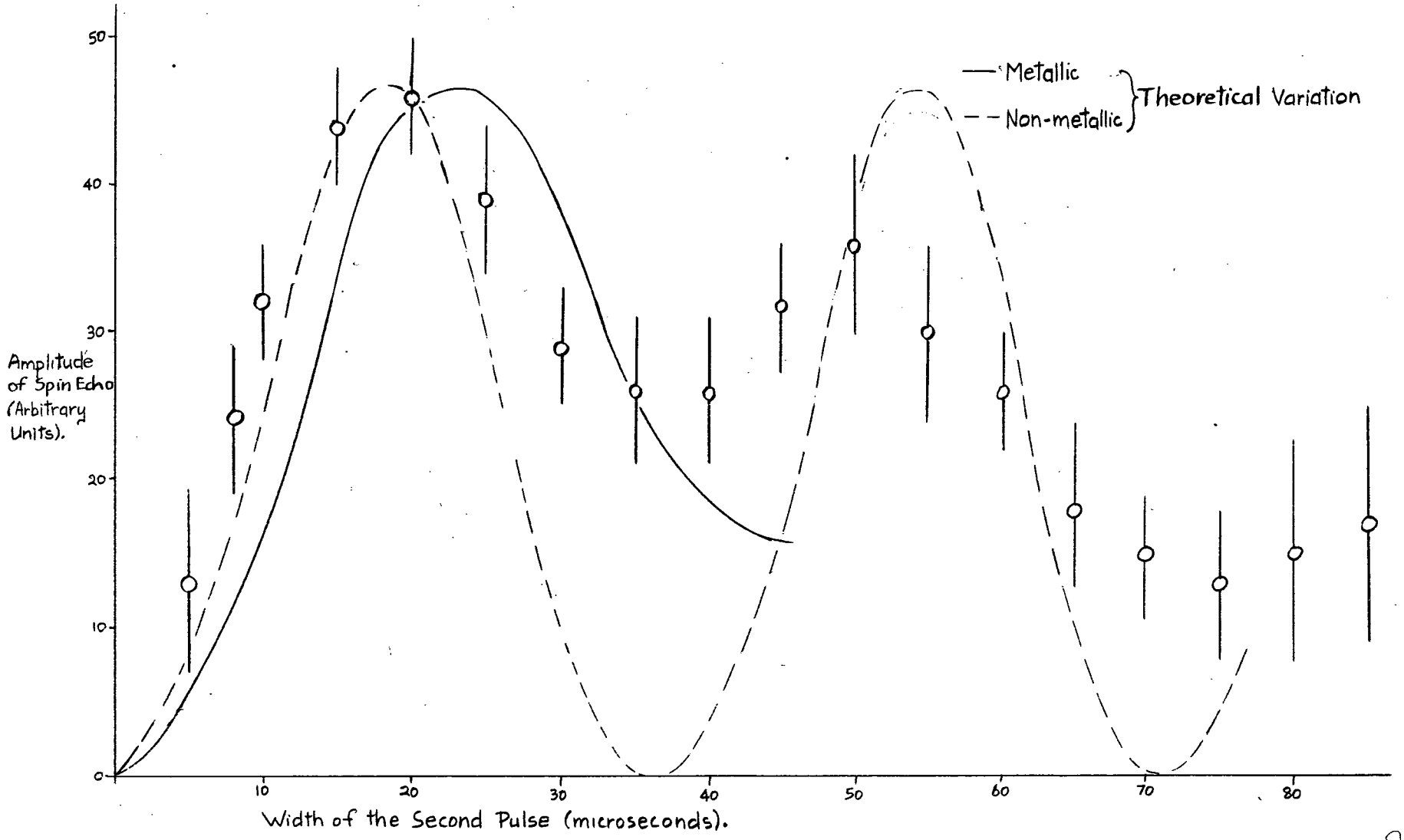

Figure 4.7 Variation of the Spin Echo Amplitude With Second Pulse Width.

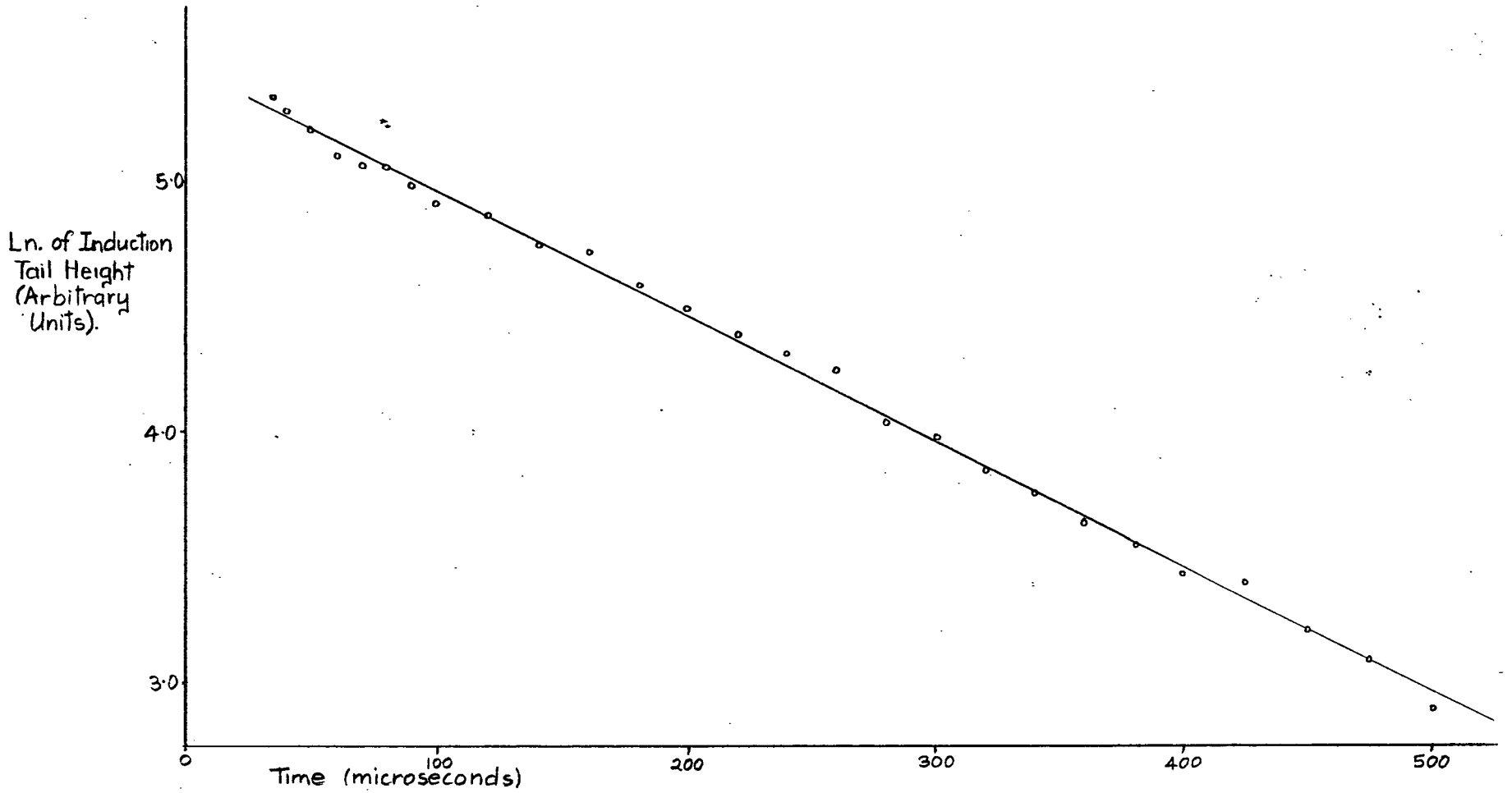

Figure 4.8 Spin-Spin Relaxation Time by Free Induction Decay.

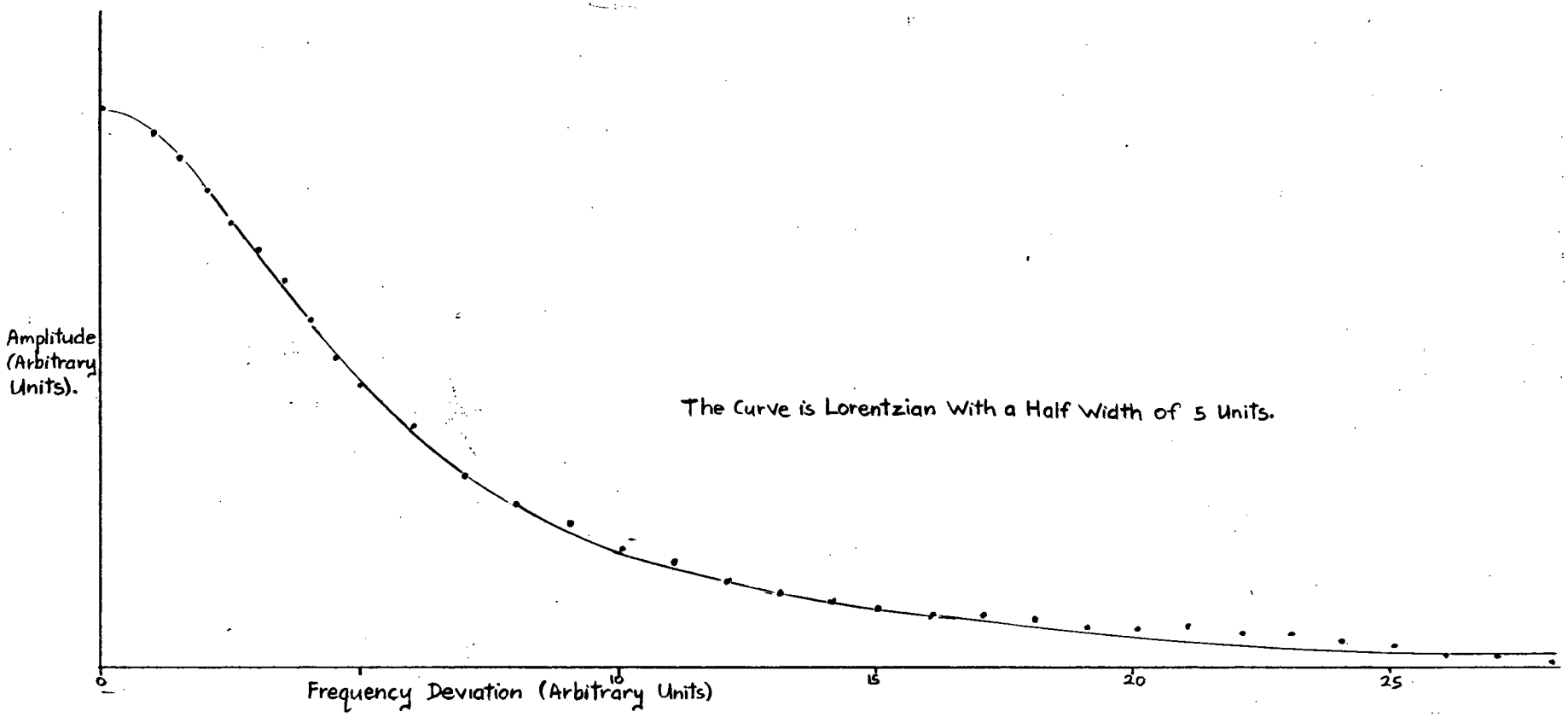

Figure 4.9 Lorentzian Line Shape in Isotopically Pure Tin.

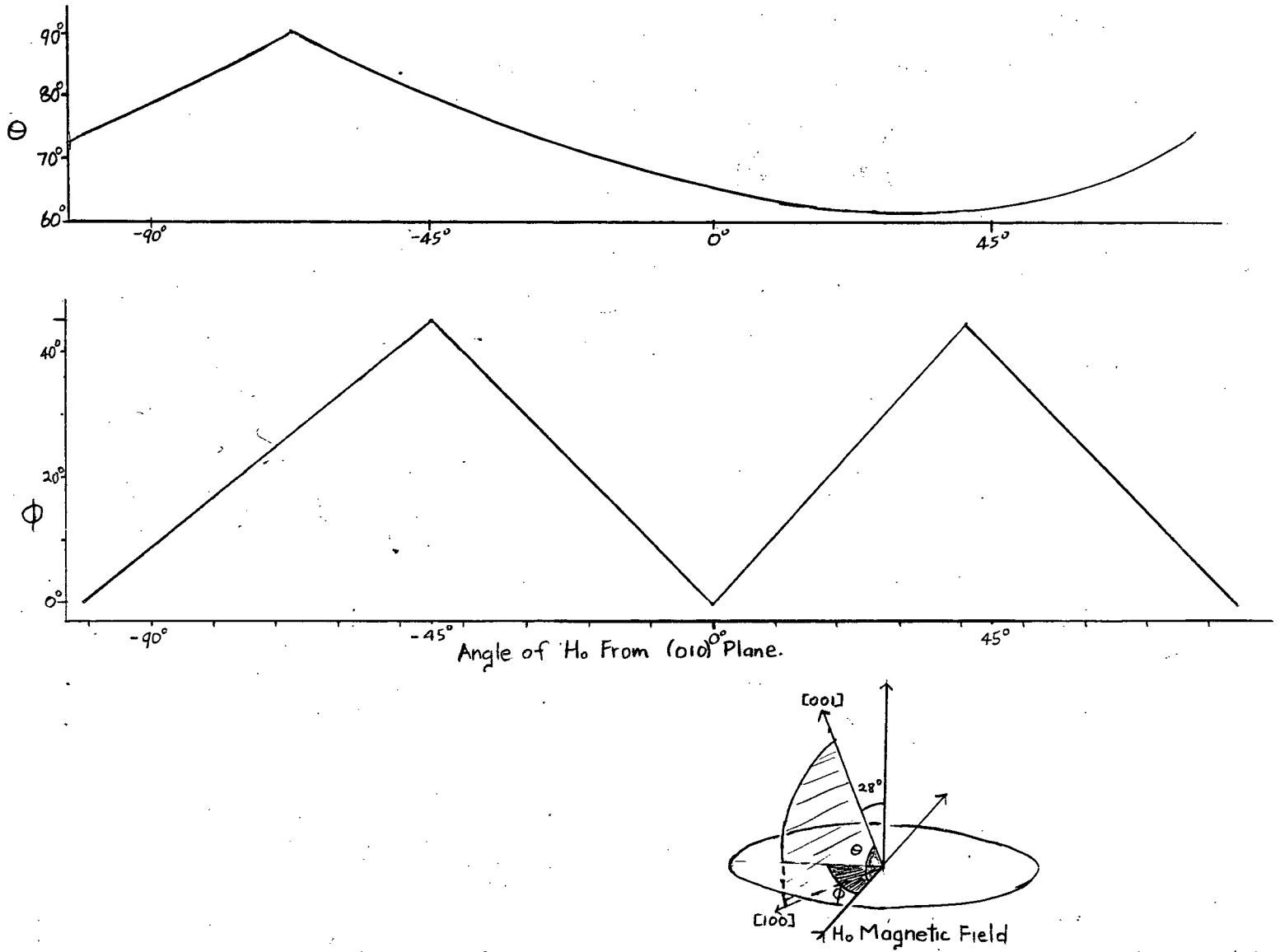

Figure 4.10 Relative Orientation of the Crystal and Magnetic Field.

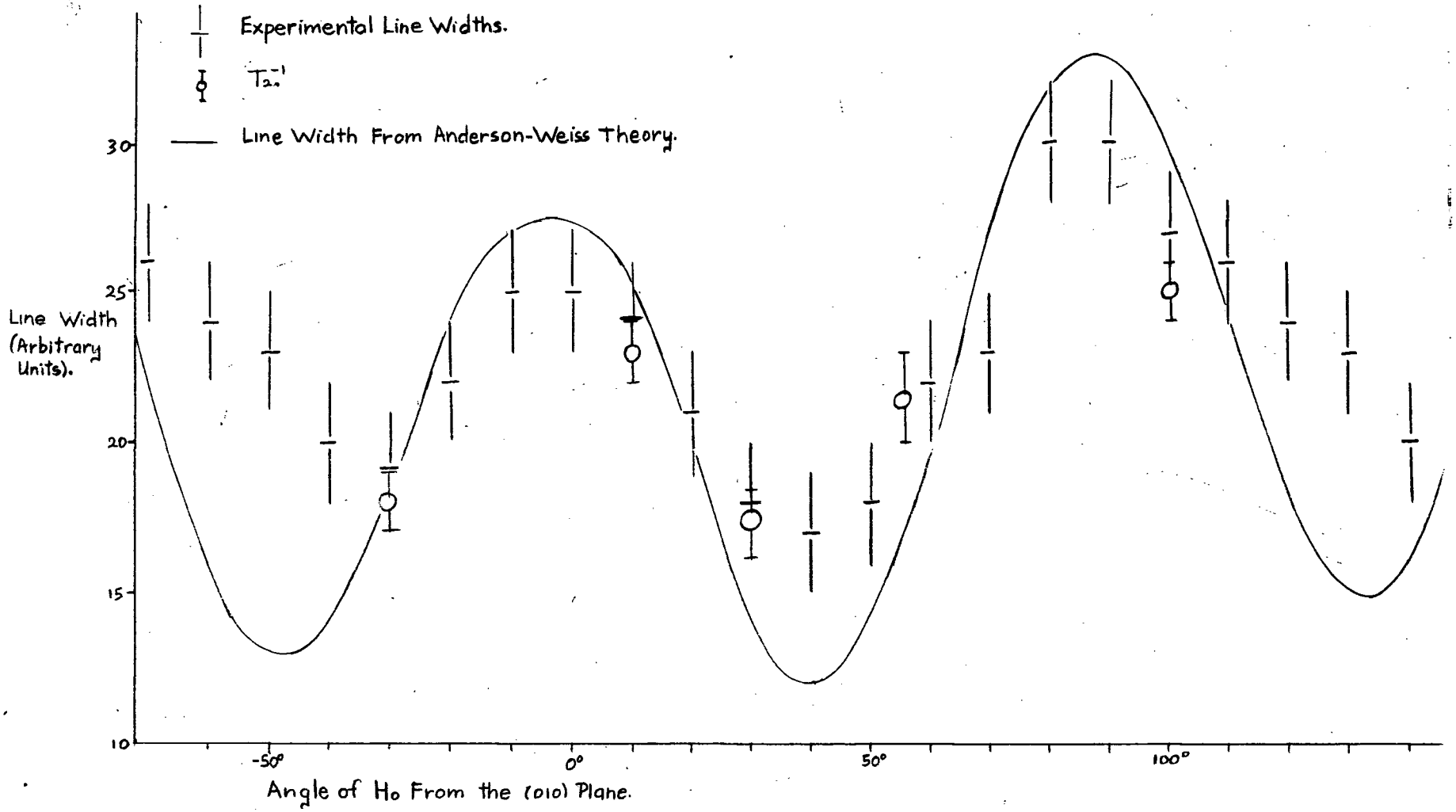

Figure 4.11 Anisotropy of the Line Width in Isotopically Pure Sn^{119}.

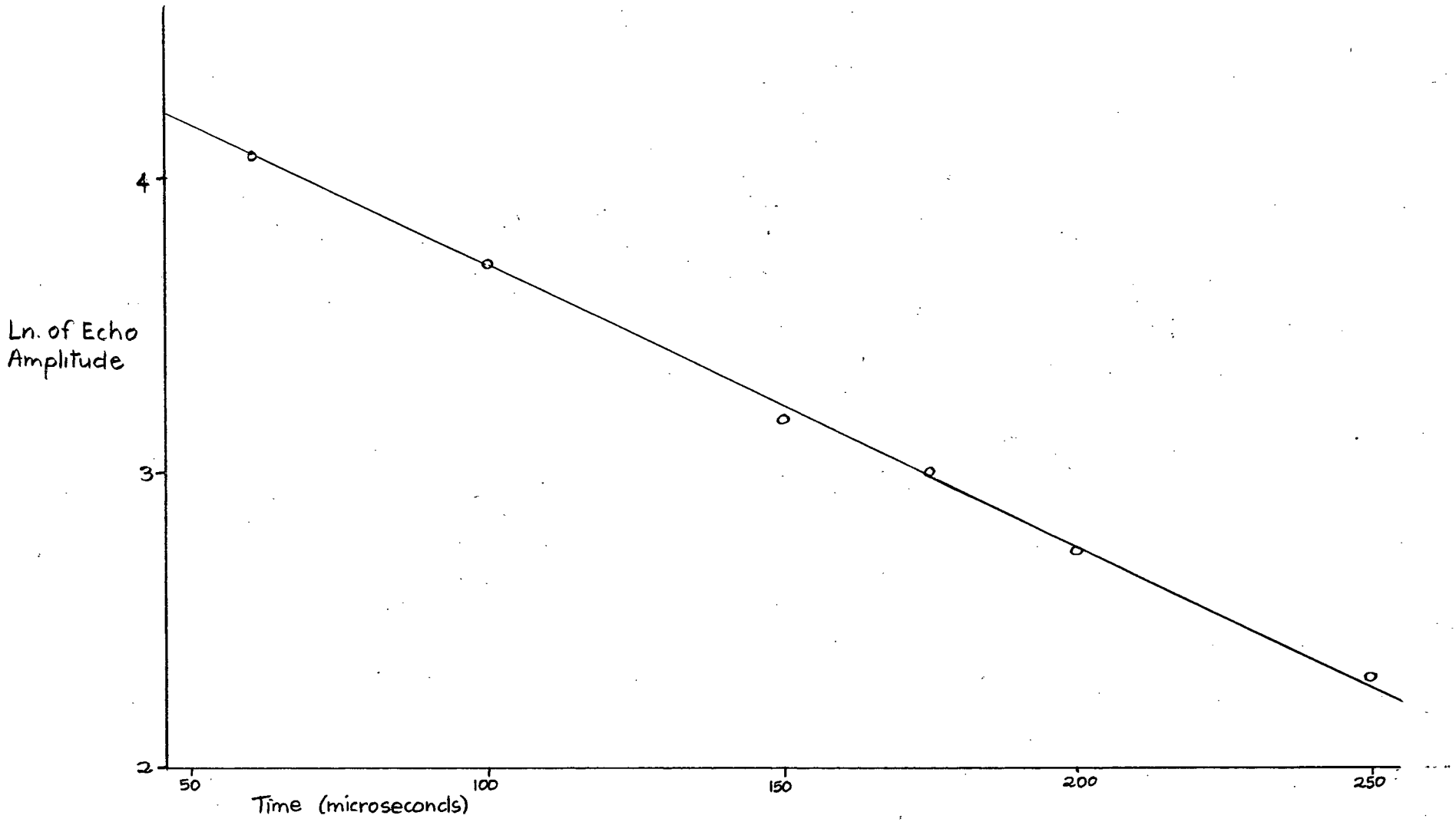

Figure 4.12 Spin-Spin Relaxation Time by Spin Echoes.

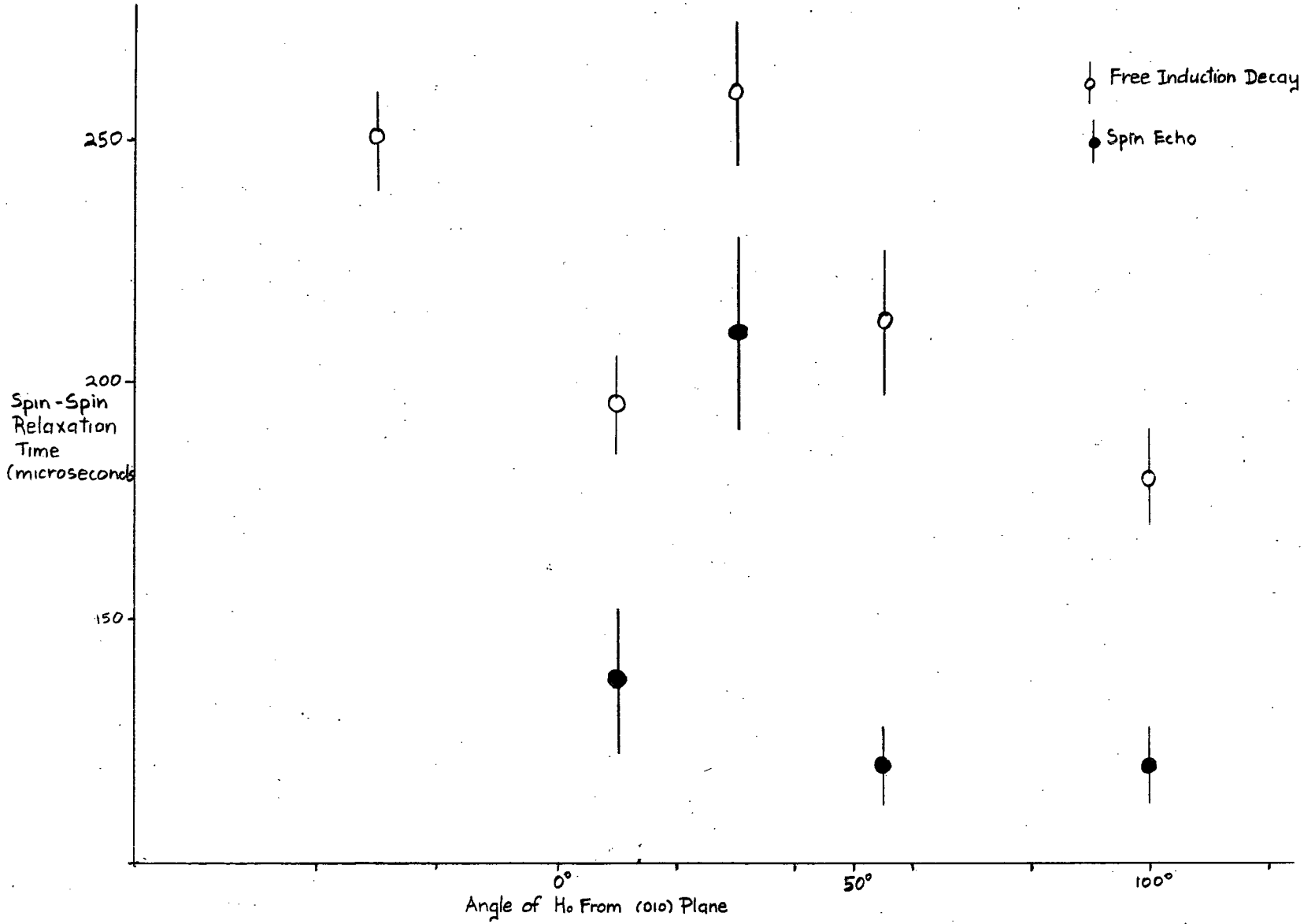

Figure 4.13 Spin Echo Anisotropy in Isotopically Pure Tin.

CONCLUSION

'Begin at the beginning, and go on till
you come to the end: then stop.'

- Alice in Wonderland.

In this thesis the feasibility of measuring T_1 and T_2 in metal single crystals at liquid nitrogen temperature has been established. It has been shown that reasonably accurate measurements can be made provided $T_2 \gtrsim 30\mu s.$ and $T_1 \lesssim 2 sec.deg.$ A reasonably complete theory of the apparatus has also been developed and experimentally confirmed.

The big failure in this work has been the inability to eliminate acoustic oscillations. Until a way is found of drastically reducing them, measurements cannot be made at liquid helium temperatures. The apparatus has restricted usefulness until such measurements can be made. The gain in S/N would probably be moderate, but would certainly be enough to allow the successful completion of several experiments which are at present either indecisive, or impractical. The more important reason for going to helium temperature is that the pulsed apparatus could then be used in conjunction with steady state apparatus on the same sample, so that more varied and accurate data could be obtained. In particular, the pulsed apparatus can give a more accurate idea of the line shape than the marginal oscillators used in the steady state work. Lifetime broadening is also unimportant at helium temperature. Alternative experimental procedures involving

digital devices for improving the S/N ratio, such as the Enhancetron, might be more satisfactory than the boxcar integrator at low temperatures.

There are several experiments which could be done on the present apparatus at 78°K. The most obvious ones are to attempt to measure the anisotropy of T_1 in scandium and in isotopically pure tin. The latter experiment would involve regrowing the crystal at a more suitable orientation. The series of measurements done on isotopically pure, and natural tin to obtain the exchange constants could readily be done on cadmium. Experiments of this type on a series of alloys with systematically varying compositions might give quite detailed information on the pseudo-exchange interaction.

Spin echoes were also observed and their basic features studied. The fact that they have a shorter T_2 than the free induction decay clearly requires a more intensive study. Measurements in tin oxide would obviously be very helpful. Once the cause of this has been found, spin echoes could be useful for measuring T_2 in those paramagnetic alloys which have a short T_2^* because of spatially varying static magnetic fields in the sample.

The attenuation and phase shifts of an rf field penetrating a metal in the normal skin effect region are well understood. The theory for the rf penetration in the case where the electron mean free path approaches the skin depth is not quite so clearcut (the anomalous skin effect). Fairly

rigorous theories have been developed, but they involve assumptions concerning the internal reflection of electrons from the surface of the metal. An experimental investigation of the anomalous skin effect region would thus be desirable. Pulsed NMR is capable of doing this because the induction tail height as a function of rf pulse length is very sensitive to the phase shifts. If a study of phase shifts alone was contemplated, there may be other ways of using the apparatus which would give more, or better, information on the phases. Measurements on particles of varying sizes would also give considerable information. The results of steady state measurements also depend on the skin effects, but they are less sensitive to them and extracting information on the phase shifts is even harder than in the pulsed case.

It is logical to try to extend experiments of this type to the superconducting region. However, in superconductors the static magnetic field only penetrates about 500A°, while the rf field penetrates somewhat further. Experiments using single crystal are thus not possible, except by using field cycling techniques in which they are at a disadvantage compared to powders. However a study of the phase shifts as the metal goes from the anomalous to the superconducting region is quite possible in metals like vanadium. Calculations show that there should be a satisfactory S/N ratio and temperatures can easily be held to within 0.01°K. at helium temperatures. Powders might give a better S/N ratio, but they do not have the

well defined and easily studied surface structure of a single crystal. NMR measurements on particles of varying sizes, and also on films of varying thicknesses, have revealed a Knight shift dependence on sample dimensions which is imperfectly understood. Pulsed NMR with a coherent system on this type of sample might give additional information. However, it would require a long period of careful and ingenious experimentation to even see a signal.

After the speculative nature of the preceeding paragraphs, it is fitting to conclude with some words of caution. Pulsed NMR experiments are difficult, involving many compromises, and have a S/N ratio which is rarely good enough to give an answer of the required accuracy. A critical examination of any prospective experiment is thus desirable. In particular, most experiments can be done far more accurately on powders. It is usually only where anisotropic properties are involved that a single crystal experiment may be worthwhile.

POSTSCRIPT

When the writing of this thesis was nearing completion the author became aware of the work of Gara (69). He has recently measured the spin-lattice and spin-spin relaxation times in metal single crystals by a pulsed method, but his experimental procedure was so different that there has been little overlap with this work.

He used an incoherent pulse system and a combined transmitter-receiver coil. This lacks the versatility of a coherent system and is susceptible to amplifier non-linearity. It suffers from the major disadvantage that in a T_1 measurement the amplitude of the free induction decay following the second pulse is not a simple exponential function of the pulse separation, unless the two pulse lengths are in a certain ratio which is determined by a mixture of theory and experiment. The second pulse was about $\frac{3}{4}\pi$ long and gave the maximum free induction decay amplitude while the first pulse was about $\frac{\pi}{4}$ long. A complicated method of analysing the results was necessary. The rest of the pulse circuitry, amplifiers, and boxcar integrator were similar to those used in this work.

Most of his measurements were made at liquid helium temperatures. Acoustic oscillations were a major problem, but he almost eliminated them by several ingenious techniques. One of these was to coat the sample with a layer of epoxy resin with nylon filings embedded in it. This quite effectively damped the acoustic oscillations, but had the defect

that the epoxy resin was paramagnetic enough to significantly shorten the free induction decay. The other method was to etch narrow grooves about a millimetre deep in the crystal. These considerably reduced the acoustic oscillations. It should be noted that in several respects his acoustic oscillations behaved differently to those observed in this work. This is probably because he mounts his sample by cementing one end of it to a holder, whilst in the present experiments the centre of the rod is clamped and the ends are free.

He measured T_1 in Al^{27} and Cu^{63} single crystals at $4.2^{\circ}K$. with several different magnetic field orientations. Within his experimental error of $\pm 2\%$ he detected no anisotropy in T_1. His values were $T_1T = (1.81 \pm 0.02)$sec.deg. for aluminium and (1.275 ± 0.015)sec.deg. for copper. Both of these are in excellent agreement with the powder values. The S/N was about 20 when observed on the oscilloscope. Free induction measurements were also made on the crystals and gave second moments which were in good agreement with values measured by steady state methods. Experiments made with varying sample and coil radii showed that the optimum S/N ratio occurred when the ratio of the radii was about 0.8. This is in good agreement with the theory developed in this thesis.

Gara's work has covered different experimental aspects of the subject than those done in this work. However, some aspects of the theory of the apparatus in this thesis could be reviewed and extended in the light of his work. In particular

some of the conclusions and comments regarding working at liquid helium temperatures need modifying.

BIBLIOGRAPHY

'And out of olde bokes, in good feith, cometh
all this newe science that men lere.'

- Chaucer.

(1) Abragam, A., "The Principles of Nuclear Magnetism," Oxford University Press, London (1961).

(2) Clark, W.G., Rev. Sci. Instr. 35, 316 (1964).

(3) Sommerfeld, A., "Electrodynamics," Academic Press, New York (1964).

(4) Blume, R.J., Rev. Sci. Instr. 32, 1016 (1961).

(5) Blume, R.J., Rev. Sci. Instr. 32, 554 (1961).

(6) Hardy, W.N., Ph.D. Thesis, University of British Columbia (1964).

(7) Military Standardization Handbook Selected Semiconductor Circuits, U.S. Department of Defence, 1960.

(8) Lowe, I.J. and Barnaal, D.E., Rev. Sci. Instr. 34, 143 (1963).

(9) Mott, N.F. and Jones, H., "The Theory of the Properties of Metals and Alloys," Dover Publications Inc., New York (1958).

(10) "Handbook of Chemistry and Physics," 44th Ed., Chemical Rubber Publishing Co., Cleveland (1963).

(11) Hunter, J.L, "Acoustics," Prentice-Hall Inc., New York (1957).

(12) Van der Ziel, A., "Noise," Prentice-Hall Inc., New York (1956).

(13) Barnaal, D. E. and Lowe, I.J. Phys. Rev. Letters 11, 258 (1963).

(14) Margenau, H. and Murphy, G.M., "The Mathematics of Physics and Chemistry," 2nd Ed., D. Van Nostrand Co., Inc., Princeton (1955).

(15) Spocas, J.J. and Slichter, C.P., Phys. Rev. 113, 1463(1959).

(16) Rowland, T.J., "Nuclear Magnetic Resonance in Metals," Pergamon Press, Oxford (1961).

(17) Masuda, Y., J. Phys. Soc. Japan 12, 523 (1957).

(18) Anderson, A.G. and Redfield, A.G., Phys. Rev. 116, 583 (1959).

(19) O'Reilly, D.E. and Tsang, T., Phys. Rev. 128, 2639 (1962).

(20) Butterworth, J., Phys. Rev. Letters 5, 305 (1960).

(21) Obata, Y., J. Phys. Soc. Japan 18, 1020 (1963).

(22) Kittel, C., "Quantum Theory of Solids," John Wiley and Sons Inc., New York (1963).

(23) Mott, N.F., Advances in Physics 13, 325 (1964).

(25) Butterworth, J., Proc. Phys. Soc. 83, 71 (1964).

(26) Mattheiss, L.F., Phys. Rev. 134A, 971 (1964).

(27) Yafet, Y. and Jaccarino, V., Phys. Rev. 133A, 1630 (1964).

(28) Clogston, A.M., Gossard, A.C., Jaccarino, V. and Yaget, Y., Phys. Rev. Letters 9, 262 (1962).

(29) Butterworth, J., Proc. Phys. Soc. 85, 735 (1965).

(32) Torgeson, D.R., and Barnes, R.G., Phys. Rev. Letters 9, 255 (1962).

(33) Fawcett, E., Advances in Physics 13, 139 (1964).

(34) Hewitt, R.R. and Williams, B.F., Phys. Rev. Letters 12, 216 (1964).

(35) Yafet, Y., J. Phys. Chem. Solids 21, 99 (1961).

(36) Kittel, C., "Introduction to Solid State Physics," 2nd Ed., John Wiley and Sons, Inc., New York (1956).

(37) Ziman, J.M.,"Electrons in Metals," Taylor and Francis Ltd., London (1963).

(38) Landau, L.D. and Lifshitz, E.M., "Statistical Physics," Pergamon Press, Oxford (1959).

(39) Kubo, R. and Obata, Y., J. Phys. Soc. Japan 11, 547 (1956).

(40) Slichter, C.P., "Principles of Magnetic Resonance," Harper and Row, New York (1963).

(41) Boon, M.H., Physica 30, 1326 (1964).

(42) Gaspari, G.D., Shyu, W. and Das, T.P., Phys. Rev. 134A, 852 (1964).

(43) Clogston, A.M., Jaccarino, V. and Yafet, Y., Phys. Rev. 134A, 650 (1964).

(44) Pake, G.E., "Paramagnetic Resonance," W.A. Benjamin, Inc., New York (1962).

(45) Wolff, P.A., Phys. Rev. 129, 84 (1963).

(46) Kadnoff, L.P., Phys. Rev. 132, 2073 (1963).

(47) Obata, Y., J. Phys. Soc. Japan 18, 1020 (1963).

(48) Hebel, L.C., Phys. Rev. 128, 21 (1962).

(49) Borsa, F. and Barnes, R.G., Phys. Rev. Letters 12, 281 (1964).

(50) Bloembergen, N. and Rowland, T.J., Phys. Rev. 97, 1679 (1955).

(51) Tables of Eigenvalues and Eigenvectors of the Hamiltonian Describing the Combined Static Magnetic Dipole and Electric Quadrupole Interactions of a Nuclear Level., Steffan, R.M., Matthias, E. and Schneider, W., A.EC. (U.S.A.), Division of Technical Information TID-15749.

(52) Kambe, K. and Ollom, J.F., J. Phys. Soc. Japan 11, 50 (1956).

(53) Schumacher, R.T., Phys. Rev. 112, 837 (1958).

(54) Goldberg, W.I., Phys. Rev. 115, 48 (1959).

(55) Jeener, J., Eisendrath, H. and Van Steenwinkel, R., Phys. Rev. 133A, 478 (1964).

(56) Simmons, W.W. and Slichter, C.P., Phys. Rev. 121, 1580 (1961).

(57) Ashcroft, N.W., and Wilkins, J.W., Phys. Letters 14, 285 (1965).

(58) Asayama, K. and Itoh, J., J. Phys. Soc. Japan 17, 1065 (1962).

(59) Schone, H.E. and Olson, P.W., Rev. Sci. Instr. 36, 843 (1965).

(60) Van Ostenburg, D.O., Spokas, J.J. and Lam, D.J., Phys. Rev. 139A, 713 (1965).

(61) Appel, J., Phys. Rev. 139A, 1536 (1965).

(62) Hahn, E.L., Phys. Rev. 80, 580 (1950).

(63) Masuda, Y., J. Phys. Soc. Japan 13, 597 (1958).

(64) Jones, E.P. and Williams, D.Ll., Phys. Letters 1, 109 (1962).

(65) Jones, E.P., Ph.D. Thesis, University of British Columbia (1962).

(66) Anderson, P.W. and Weiss, P.R., Rev. Mod. Phys. 25, 269 (1953).

(67) Miasek, M., Phys. Rev. 130, 11 (1963).

(68) Karimov, Y.S. and Schlegolev, J.F., JETP 13, 908 (1961).

(69) Gara, A.D., Ph.D. Thesis, Washington University (1965).

APPENDIX I

DISTORTION IN THE PHASE SENSITIVE DETECTION SYSTEM

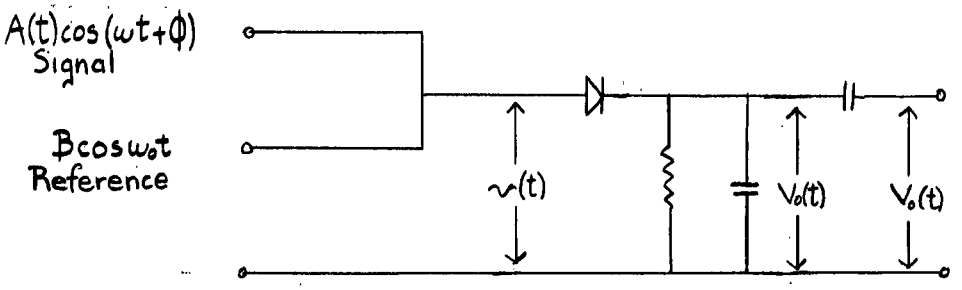

Figure I.1 Equivalent Circuit of the Phase Sensitive Detector

In the phase sensitive detection system to be analysed a small time varying signal of frequency ω and phase angle ϕ is linearly added to a much larger reference signal to give a total voltage $v(t)$ of

$$v(t) = A(t)\cos(\omega t + \phi) + B\cos\omega_0 t$$
$$= \left[A^2 + B^2 + 2AB\cos(\Omega t + \phi)\right]^{\frac{1}{2}} \cos\left[\omega_0 t - \tan^{-1}\{\delta(t)\}\right],$$

where $\Omega = \omega - \omega_0$

$$\delta(t) = \frac{A\sin(\Omega t + \phi)}{A\sin(\Omega t + \phi) + B} .$$

Provided $\omega_0 \gg \Omega$, the time dependent phase angle $\delta(t)$ will cause negligible frequency or phase modulation of the signal, so that the voltage after the signal has been rectified and the high frequency carrier filtered out is

$$V(t) = \left[A^2 + B^2 + 2AB\cos(\Omega t + \phi)\right]^{\frac{1}{2}}$$
$$= \left[A(t)\cos(\Omega t + \phi) + B\right]\left[1 + \frac{\sin^2(\Omega t + \phi)}{\{\cos(\Omega t + \phi) + \frac{B}{A}\}^2}\right].$$

If it is assumed that $\frac{B}{A} \gg 1$, the square root can be expanded to first order to give

$$V(t) = \left[A(t)\cos(\Omega t + \phi) + B\right]\left[1 + \frac{\sin^2(\Omega t + \phi)}{2\{\cos(\Omega t + \phi) + \frac{B}{A}\}^2}\right].$$

The system is A.C. coupled so the D.C. component is removed,

giving the output signal as

$$V_0(t) = A(t)\cos(\Omega t+\phi)+\frac{\sin^2(\Omega t+\phi)[A(t)\cos(\Omega t+\phi)+B]}{2[\cos(\Omega t+\phi)+\frac{B}{A(t)}]^2}\ .$$

There is thus an error except when $\sin(\Omega t+\phi)=0$. This error can become serious for $\sin(\Omega t+\phi)\simeq\pm 1$ since not only is the error near its maximum value of $\frac{A^2}{2B}$ but the signal $A\cos(\Omega t+\phi)\simeq 0$, so the fractional error is very large. If the apparatus is exactly on resonance so $\Omega = 0$ the error is reduced because there is then no time dependence in the term involving B so the A.C. coupling removes it.

APPENDIX II

DETAILS OF THE SAMPLES USED

(i) Aluminium Single Crystal.

This was supplied by Semi-elements, Inc., Pennsylvania and is a cylinder 5 cm. long by 0.7 cm. in diameter. There were actually two crystals in the sample, one being about one eighth the size of the other. The surface is rough and unetched and the purity is unknown.

Aluminium has a face centred cubic lattice and a quadrupole moment. There is one isotope with spin $\frac{5}{2}$.

(ii) Vanadium Single Crystal.

The zone refined single crystal was grown by the U.B.C. Metallurgy Department. The sample is 5 cm. long and has an average diameter of 0.6 cm. It had a smooth surface and so was not etched. A chemical analysis gave the impurities in parts per million as

Oxygen	160
Carbon	136
Nitrogen	318
Hydrogen	7.2.

V^{51} has an isotopic abundance of 99.7% and forms a body centred cubic lattice. It is a transition metal with spin $\frac{7}{2}$ and a quadrupole moment.

(iii) Indium Single Crystal.

It is a 99.999% pure cylindrical sample bought from Metals Research Co., Cambridge, England. It has the tetragonal axis perpendicular to the sample axis to within 2°. The 1.3 cm. long cylinder was etched down to 0.9 cm. diameter by an etch of

one part HCl to twenty parts of ethyl alcohol. X-raying showed that the etching removed a slightly polycrystalline surface structure.

The main isotope is In^{115} which has 96% abundance, spin $\frac{9}{2}$ and a quadrupole moment. The lattice is a face centred tetragonal structure which can also be regarded as a face centred cubic lattice elongated by 7% along one axis.

(iv) Bismuth Single Crystal.

The sample is a cylinder 3 cm. long by 0.65 cm. diameter purchased from Metals Research Co. which was not etched. The trigonal axis is within 2° of the perpendicular to the cylindrical axis.

It is 100% abundant with spin $\frac{9}{2}$, a quadrupole moment and crystallizes in a rhombohedral structure.

(v) Rhenium Single Crystal.

This was supplied by Semi-elements and is 2.8 cm. long by 0.3 cm. diameter. The symmetry axis is aligned to within 2° of the perpendicular to the cylindrical axis. The crystal is zone refined and was not etched.

There are two isotopes, Re^{185} and Re^{187} with 37% and 63% isotopic abundances respectively. They both have spin $\frac{5}{2}$ and a quadrupole moment. It has a hexagonal close packed structure and is a transition metal.

(vi) Antimony Single Crystal.

It is a cylinder 1.6 cm. long by 0.9 cm. diameter cut from a zone refined single crystal supplied by Cominco Ltd.,

Trail, B.C. The sample is 99.999% pure. The orientation of the crystal is unknown. The crystal was etched with a solution of one part concentrated nitric acid to four parts hydrochloric acid. This etch is very fast if the sample is allowed to become heated.

(vii) Gallium Single Crystal.

The crystal was grown in this laboratory by K. Nilsen from 99.9999% pure gallium. X-raying determined that it was a single crystal with its lattice symmetry axis orientated at 30 to the cylindrical axis. It is 2 cm. long by 0.9 cm. in diameter.

Both of the isotopes Ga^{69} and Ga^{71} have a quadrupole moment. They are 60% and 40% abundant respectively and crystalize in an orthorhombic structure.

(viii) Niobium Single Crystal.

The crystal is a zone refined crystal 5 cm. long and 0.6 cm. in diameter grown by the U.B.C. Metallurgy Department. No etching was done on it. The impurities, in parts per million, are

Oxygen	35
Carbon	40
Nitrogen	40
Hydrogen	2
Tantalum	500
Zirconium	500
Tungsten	300

Nb^{93} has 100% isotopic abundance, a spin of $\frac{9}{2}$, a quadrupole moment, and crystallizes in a body centred cubic lattice.

(ix) Natural Tin Single Crystal.

This sample was supplied by Metals Research Ltd. in the form of a cylinder 3 cm. long and 0.9 cm. diameter of 99.999%

purity. The symmetry axis is aligned at right angles to the cylindrical axis of the sample. An etch of one part HNO_3, one part water, and two parts acetone was used to remove the surface layer prior to the experiments.

There are two main isotopes, each with spin $\frac{1}{2}$. These are Sn^{117} with 7.7% isotopic abundance and Sn^{119} with 8.7% abundance. Neither of the nuclei has a quadrupole moment.

(x) Isotopically Pure Tin Single Crystal.

The crystal of isotopically pure tin was grown by Schone and Olsen (59). It consists of a layer about 0.25 mm. thick wrapped around a copper core about 7 mm. in diameter. The purity of the Sn^{119} is unknown, but presumably the main impurity would be Sn^{117}. The symmetry axis is at an angle of 28° to the cylindrical axis of the copper core. The X-rays taken to determine the position of this axis showed that there was negligible distortion of the single crystal and that there was no polycrystalline surface layer.

APPENDIX III

THE SIGNAL INDUCED IN THE PICKUP COIL

(a) Non-metallic Sample.

Assume that the sample is isotropic and non-ferromagnetic, so that the nuclear magnetic moment at any point in the sample is

$$M_o = \chi_o H_o$$
$$= \frac{N\gamma^2\hbar^2 I(I+1)H_o}{3kT},$$

where N is the number of atoms/m^3, γ is the gyromagnetic ratio, I the nuclear spin, T the sample temperature, H_o the applied static magnetic field, and χ_o is the static nuclear magnetic susceptibility.

In equilibrium M_o is aligned along the z axis. A linear rf magnetic field $B=2B_1\cos\omega t$, at the resonant frequency ω_0 applied perpendicular to H_o causes M_o to precess in the zy plane at a frequency γB_1, so that after a time τ it makes an angle $\alpha = \gamma B_1 \tau$ with the z axis (1). The projection of M_o in the xy plane is

$$M = M_o \sin\alpha$$

In the laboratory frame this magnetic moment rotates at a frequency ω_0 inducing a signal proportional to $M\cos\omega t$ in a pickup coil.

Now consider the sample inside a coil with n turns which is perpendicular to H_o and has an efficiency factor η. The voltage v induced in the coil is given by Faraday's equation as

$$v = \oint \underset{\sim}{E} \cdot d\underset{\sim}{l}$$
$$= -\frac{\partial}{\partial t}\int \underset{\sim}{B} \cdot d\underset{\sim}{a}.$$

The surface integral is over the cross sectional area of the coil.

The line integral is taken over a path through the sample parallel to the coil axis and then back very close to the outside surface of the coil. Along this path

$$\underset{\sim}{B} = \mu M_0 \sin\alpha \cos\omega t$$

in the sample and is zero outside it, if end effects are neglected.

$$\therefore v = \mu\omega\eta n M_0 A \sin\alpha \cos\omega t,$$

where A is the cross sectional area of the sample.

(b) Metallic Sample.

The problem is to calculate the distribution of currents and magnetic fields induced in the metal by the oscillating magnetic moment $\underset{\sim}{M}$. This induces a circulating current $\underset{\sim}{J}=\sigma\underset{\sim}{E}$ which generates a magnetic field $\underset{\sim}{H}$ opposing $\underset{\sim}{M}$.

The circulating current is given by Faraday's equation as

$$\sigma \nabla \times \underset{\sim}{E} = -\mu\sigma \frac{\partial}{\partial t}(\underset{\sim}{M}+\underset{\sim}{H}),$$

while $\underset{\sim}{H}$ is given by

$$\nabla \times \underset{\sim}{H} = \sigma \underset{\sim}{E}.$$

These equations neglect the displacement current and the magnetic moment $\chi_0\underset{\sim}{H}$ induced by the circulating current. They also assume that the metal is not in the anomalous conduction region. Standard vector manipulation now gives

$$\nabla^2 \underset{\sim}{H} = \mu\sigma \frac{\partial}{\partial t}(\underset{\sim}{M}+\underset{\sim}{H}).$$

Assume that $\underset{\sim}{M},\underset{\sim}{H} \propto \exp(i\omega t)$.

$$\nabla^2 \underset{\sim}{H} = i\delta^{-2}(\underset{\sim}{M}+\underset{\sim}{H}), \text{ where } \quad \delta^{-2} = \omega\mu\sigma.$$

Now consider an infinite plane metal sample with magnetic moments $M_x(z)$ at a depth z below the surface and with $M_y = M_z = 0$. The equation simplifies to

$$\frac{d^2 H_x(z)}{dz^2} = A^2 \left[H_x(z) + M_x(z) \right],$$

where $A = \frac{(1+i)}{\sqrt{2}\delta}$. The solution of this equation is (14)

$$H_x(z) = \exp(Az)\left[C_2 + \tfrac{1}{2}A\int M(z)\exp(-Az)dz\right] + \exp(-Az)\left[C_3 - \tfrac{1}{2}A\int M(z)\exp(Az)dz\right].$$

C_2 and C_3 are arbitrary integration constants. The boundary conditions are now fitted for the special case of an infinitely thin sheet of magnetic moments at a depth m below the surface.

i.e. $M_x(z) = \delta(m-z)$,

where $\delta(m-z)$ is a Dirac delta function.

$$\therefore H_x(z) = C_2\exp(Az)+C_3\exp(-Az) \quad \text{for } z < m,$$

$$= \left[C_2 + \tfrac{1}{2}A\exp(-Am)\right]\exp(Az)+\left[C_3 - \tfrac{1}{2}A\exp(Am)\right]\exp(-Az) \quad \text{for } z > m.$$

$$\int_0^\infty H_x(z)dz = \int_0^m \left[C_2\exp(Az)+C_3\exp(-Az)\right]dz + \int_m^\infty \left[(C_2+\tfrac{1}{2}A\exp(-Am))\exp(Az)+(C_3-\tfrac{1}{2}A\exp(Am))\exp(-Az)\right]dz$$

$$= \frac{1}{A}\left[C_2\exp(Az)-C_3\exp(-Az)\right]_0^m + \left[\left\{\frac{C_2}{A}+\tfrac{1}{2}\exp(-Am)\right\}\exp(Az) - \left\{\frac{C_3}{A}-\tfrac{1}{2}\exp(Am)\right\}\exp(-Az)\right]_m^\infty.$$

To keep the total flux finite it is necessary to put

$$C_2 = -\tfrac{1}{2}A\exp(-Am).$$

$$\therefore \int_0^\infty H_x(z)dz = \tfrac{1}{2}\exp(-Am) - 1 + \frac{C_3}{A}$$

The signal induced in the pickup coil is obtained from

$$\nabla \times \underset{\sim}{E} = -\mu\frac{\partial}{\partial t}(\underset{\sim}{M}+\underset{\sim}{H}).$$

The assumption is made that $\delta \ll R$, where R is the radius of the cylindrical sample. The voltage induced in a pickup coil wound round the sample is

$$v = -i2\pi R\eta n\mu\omega\int_0^\infty \left[M_x(z)+H_x(z)\right]dz.$$

$$\therefore v \propto \tfrac{1}{2}\exp(-Am) + \frac{C_3}{A}.$$

If the magnetic moments are at a large depth below the surface of

the metal there should be no induced voltage because the circulating currents will, by Lenze's Law, completely shield the magnetic moments.

$$\text{i.e. } 0 = \lim_{m\to\infty}\left[\frac{C_3}{A} + \tfrac{1}{2}\exp(-Am)\right].$$

$$\therefore C_3 = 0.$$

$$\therefore v_0 = -i\pi\mu n\eta\omega R\exp(-Am).$$

This is the voltage induced by a delta function magnetic moment at a depth m below the surface. The voltage induced by a distribution M(m) of magnetic moments in the metal is given by

$$v = \int_0^\infty v_0(m)M(m)\,dm$$

$$= \pi n\mu\eta\omega R\int_0^\infty M(z)\exp\left[-(1+i)\frac{z}{\sqrt{2}\delta}\right]dz.$$

It is now necessary to calculate M(z) after a rf magnetic field $2B_1\exp(i\omega t)$ has been applied parallel to the surface of the sample for a period τ. For simplicity, assume that ω is the nuclear resonant frequency. The magnetic field at a depth z in the metal is (3)

$$B(z) = 2B_1\exp\left[-(1+i)\frac{z}{\sqrt{2}\delta}\right]\exp(i\omega t).$$

In the rotating reference frame it is a static magnetic field $B_1\exp(-\frac{z}{\sqrt{2}\delta})$ lying in the plane perpendicular to H_0 at an angle $\tan^{-1}(\frac{z}{\sqrt{2}\delta})$ to the field $B_1(0)$ at the surface of the metal. The magnetic moment M(z,t) at right angles to $B_1(0)$ is

$$M_y(z,t) = M_0(t)\sin\left[\gamma B_1\tau\exp(-\tfrac{z}{\sqrt{2}\delta})\right]\cos(\tfrac{z}{\sqrt{2}\delta}).$$

$$\therefore v(t) = \pi\mu\omega n\eta R M_0(t)\int_0^\infty \exp(-\tfrac{z}{\sqrt{2}\delta})\sin(\gamma\tau B_1\exp(-\tfrac{z}{\sqrt{2}\delta}))\cos^2(\tfrac{z}{\sqrt{2}\delta})\,dz.$$

This expression can be generalised to the case when the applied rf pulse is off resonance and the phase reference axis makes an arbitrary angle with $B_1(0)$. An important feature of this equation

is that the induced voltage is of the form $M_x(t)F(z)$, where $M_x(t)$ is the nuclear magnetic moment at the surface of the sample t seconds after application of an rf pulse and $F(z)$ is the integral involving time independent phase and attenuation factors. The time evolution depends only on T_1 and T_2 so that measurements of these quantities made on single crystals should give the same values as those made on powders. In particular the free induction decay is not distorted by any phase effects.

This derivation has ignored the dipolar magnetic field. This is valid in the region in which the rf field is much greater than the dipolar field and from which the majority of the signal comes. The only measurements which might be affected by the presence of the dipolar field are those involving relaxation in the rotating reference frame where the rf field must be large.

The integral $y=\int_0^\infty \exp(-x)\sin(\gamma\tau B_1 e^{-x})\cos^2 x\,dx$ can be evaluated by expanding $\sin(\gamma\tau B_1 e^{-x})$ in a series and integrating term by term. This gives

$$y=\sum_{p=1}^{\infty}\frac{(-1)^{p+1}(1+2p^2)(\gamma B_1\tau)^{2p-1}}{4p(1+p^2)(2p-1)!}.$$

This series is quite satisfactory for numerical computation until $\gamma B_1\tau \gtrsim 10$ radians when the number of terms, and the number of significant figures in each term increases rapidly. In this derivation the sample has been treated as a cylinder with a perfectly smooth surface and a radius much greater than its skin depth. This is a good approximation to the real samples, provided that they have no surface irregularities whose dimensions are approximately equal to the skin depth.

APPENDIX IV

MEASUREMENT OF ABSORPTION AND DISPERSION MODES WITH A PULSED NMR APPARATUS

Let the free induction decay signal after a 90° rf pulse $G(t)\cos\omega_{o}t$ be fed into a phase sensitive detector using a reference frequency ω_{o} and then rectified. The output signal is proportional to $G(t)\left[\cos(\Omega t)\cos\phi+\sin(\Omega t)\sin\phi\right]$, where ϕ is the phase difference between the reference frequency and the induction signal, and $\Omega=\omega-\omega_{o}$. The time origin for the signal is the midpoint of the rf pulse (13), not the end as stated by Clark (2).

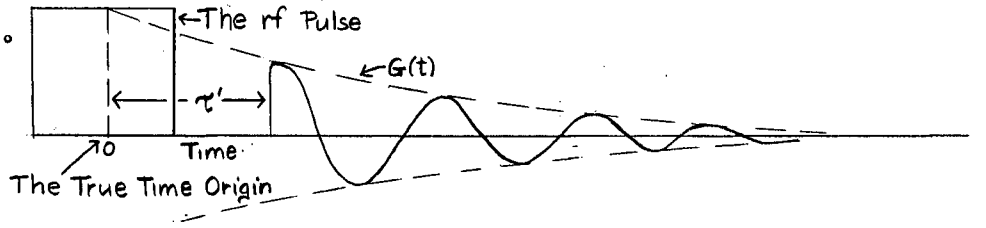

Figure IV.1 The Amplifier Output

The boxcar integrator integrates the applied signals for the duration of the gate width (6), so that if the gate covers the entire free induction decay the boxcar output is

$$V = K\int_{o}^{\infty} G(t)\left[\cos\Omega t\cos\phi+\sin\Omega t\sin\phi\right]dt,$$

where K is a constant. For most free induction decays

$$\chi''(\Omega)\propto\int_{o}^{\infty}G(t)\cos\Omega t\,dt$$

and $\chi'(\Omega)\propto\int_{o}^{\infty}G(t)\sin(\Omega t)dt$, where χ' and χ'' are the real and imaginary parts of the rf susceptibility. χ'' is proportional to the absorption mode measured by steady state apparatus.

$$\therefore V\propto\chi''(\Omega)\cos\phi+\chi'(\Omega)\sin\phi.$$

By correctly setting ϕ either χ' or χ'' can be obtained. Linearly sweeping the magnetic field through resonance then gives χ' or

χ'' on the chart recorder. Clark derived the equations for the ideal case outlined above. However, there are a considerable number of instrumental distortions which limit the usefulness of this method.

(i) Because of the finite width of the rf pulse, and the dead time of the apparatus, the boxcar gate starts at a time τ' so that the boxcar output is actually

$$V = K\int_{\tau'}^{\infty} G(t)\left[\cos(\Omega t)\cos\phi + \sin(\Omega t)\sin\phi\right] dt.$$
$$= K'\left[\chi''(\Omega)\cos\phi + \chi'(\Omega)\sin\phi\right] - K'\int_{0}^{\tau'} G(t)\left[\cos(\Omega t)\cos\phi + \sin(\Omega t)\sin\phi\right] dt.$$

Unless G(t) is known, the correction term cannot be evaluated. However, it is easy to see the effect of the instrumental distortion when $\sin\phi = 0$.

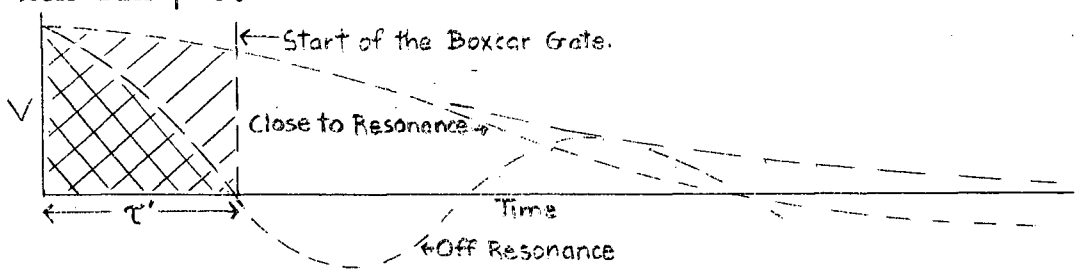

Figure IV.2 Effect of the Deadtime

Close to resonance the unmeasured area decreases quite slowly while the measured area decreases quite rapidly, since it is in the tail of the decay which is much more sensitive to slight shifts off resonance. Thus there will be little distortion of the boxcar output close to resonance. However, at a frequency $(4\tau')^{-1}$ off resonance one positive quarter cycle is unmeasured so that the output goes negative. This causes the absorption signal to be narrowed. As the frequency goes further and further from resonance it is easily seen that the output will continually

oscillate. This is the main form of instrumental distortion.

The requirement for negligible distortion is obviously to have the frequencies $f_0 \pm (\tau')^{-1}$ at which the output goes negative falling well outside the line.

i.e. $T_2 \gg \tau'$.

(ii) If $\chi''(\Omega)$ is to be the undistorted absorption mode, G(0) must be independent of Ω for all values of Ω within several linewidths of the resonance. This requires that over this region, $H_1 \doteq H_e$ in the rotating reference frame. The condition for this is that $\gamma H_1 \gg T_2^{-1}$. This is the normal condition for pulsed NMR and is actually implied by the previous condition $T_2 \gg \tau'$, since the spins must be rotated through 90° in a time less than τ'.

(iii) The method of phase sensitive detection used in this apparatus also causes some distortion. The input to the boxcar integrator is (Appendix I)

$$V(t) = G(t)\cos(\Omega t + \phi) + \frac{\sin^2(\Omega t+\phi)\left[G(t)\cos(\Omega t+\phi)+B\right]}{2\left[\cos(\Omega t+\phi)+\frac{B}{G}\right]^2}.$$

If $\Omega = \phi = 0$ (i.e. absorption mode, exactly on resonance) there is no distortion, but as soon as the frequency is off resonance ($\Omega \neq 0$) the output is distorted, giving a baseline shift. An exact calculation of this baseline shift is messy since the boxcar gate partially integrates it. It turns out that the baseline shift is fairly small and oscillates quite slowly and so causes little trouble.

If desired, the baseline shift can be eliminated by measuring two absorption signals with a phase difference of 180° between them, and then subtracting one from the other. Changing ϕ by 180° reverses the polarity of the absorption signal but, to a first approximation, does not affect the baseline shift, which is thus eliminated by the subtraction.

APPENDIX V

CIRCUIT DIAGRAMS

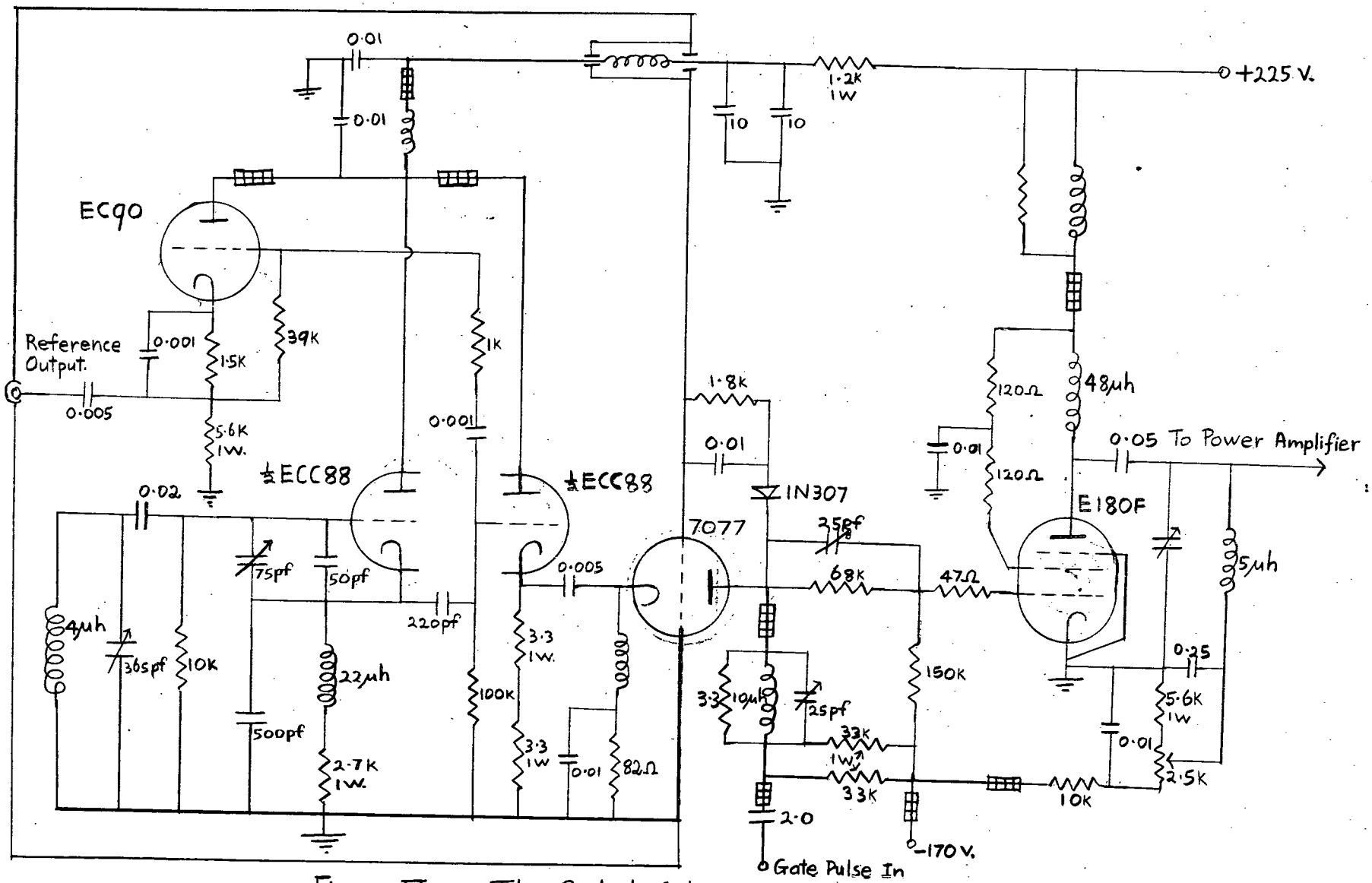

Figure V.1a. The Gated Coherent Oscillator.

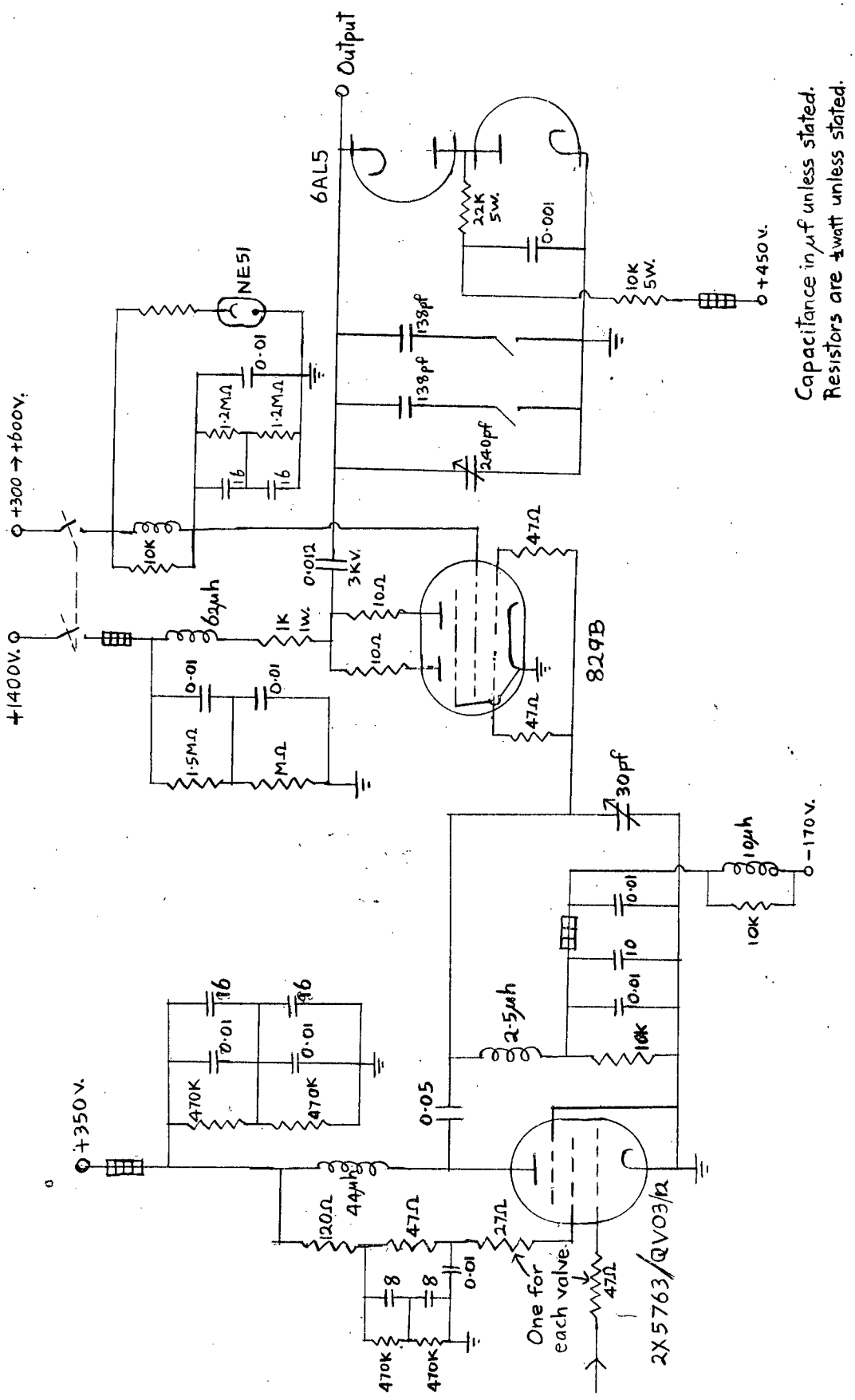

Figure V.1.b. The Power Amplifier.

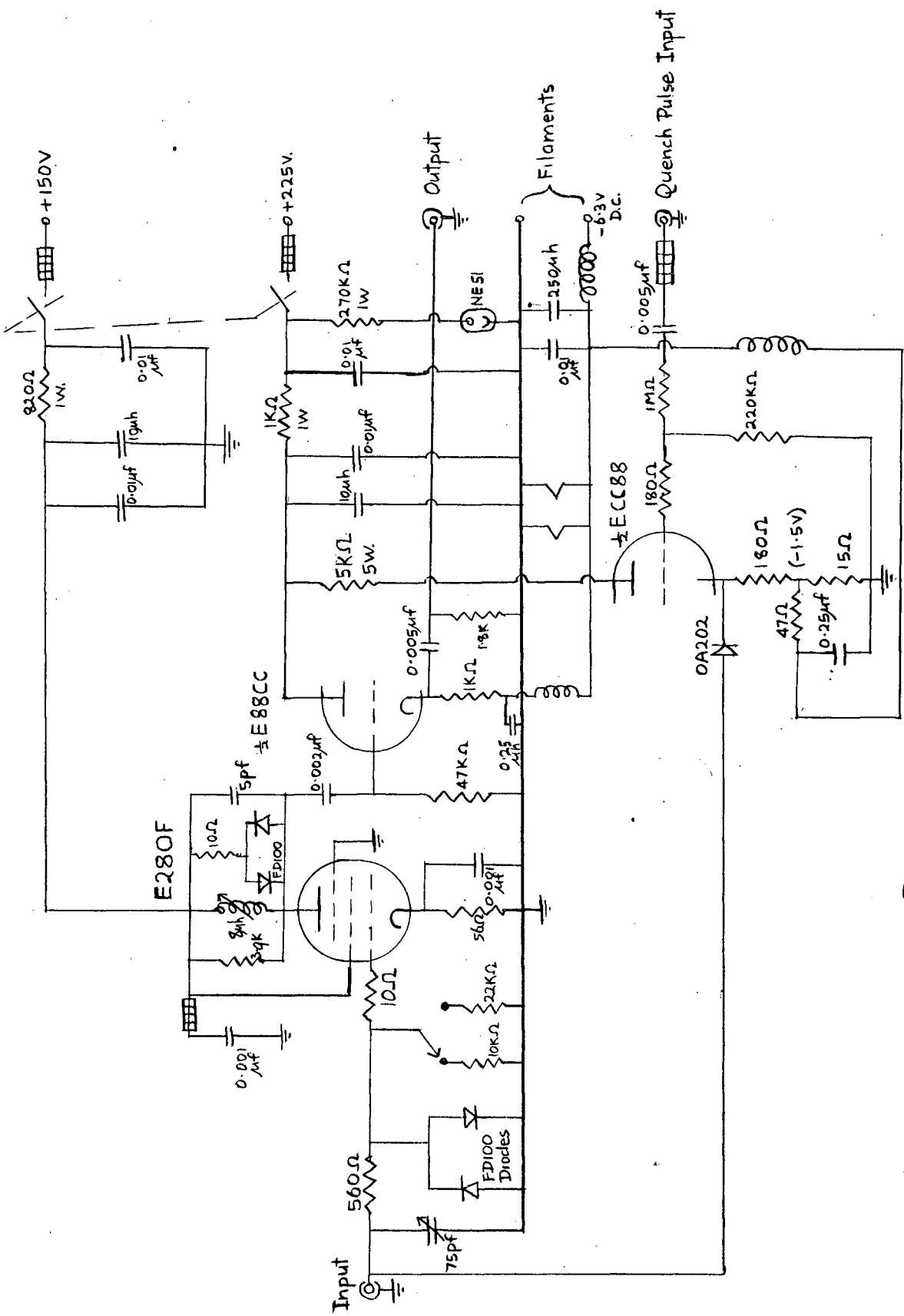

Figure V.2 The Preamplifier.

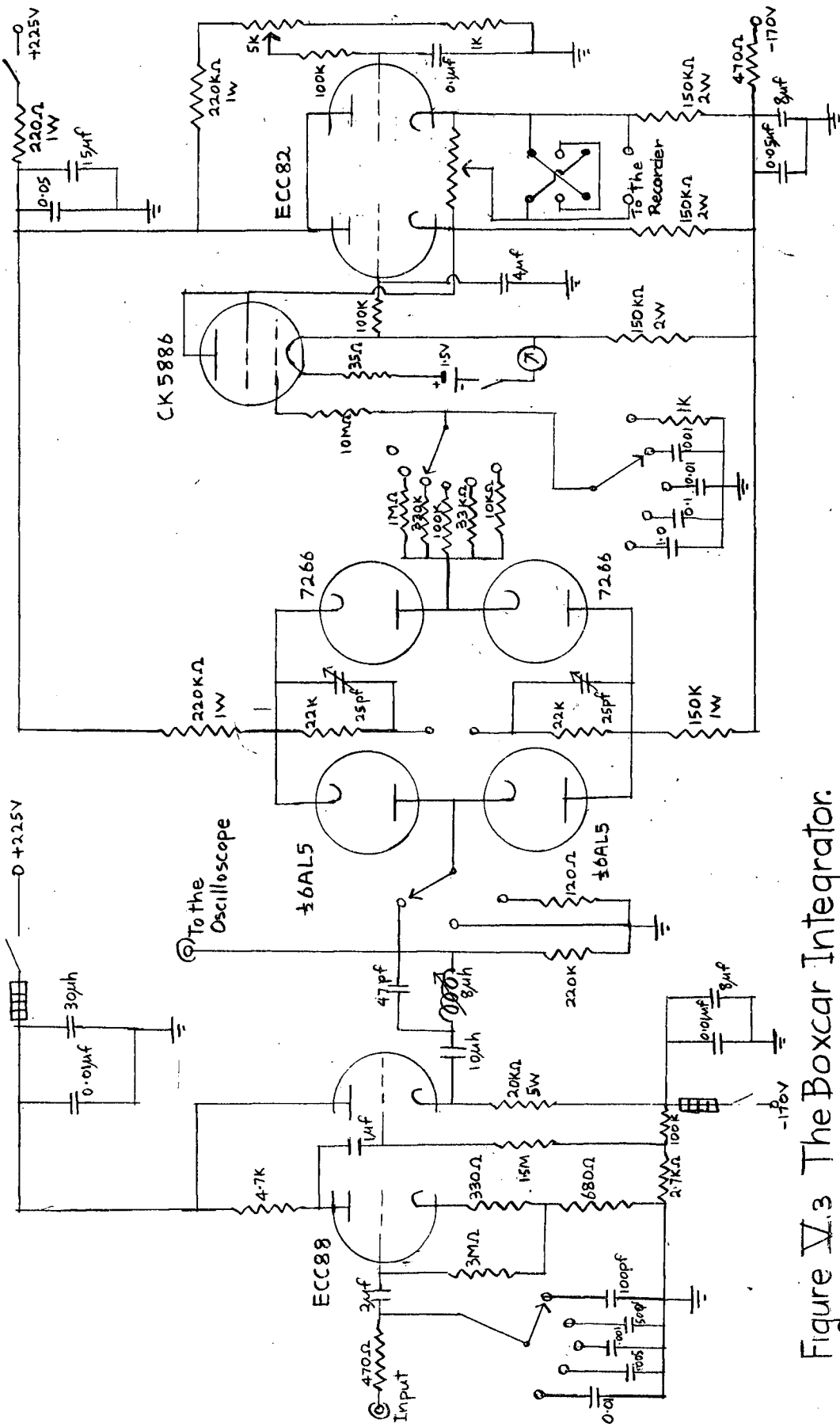

Figure V.3 The Boxcar Integrator.

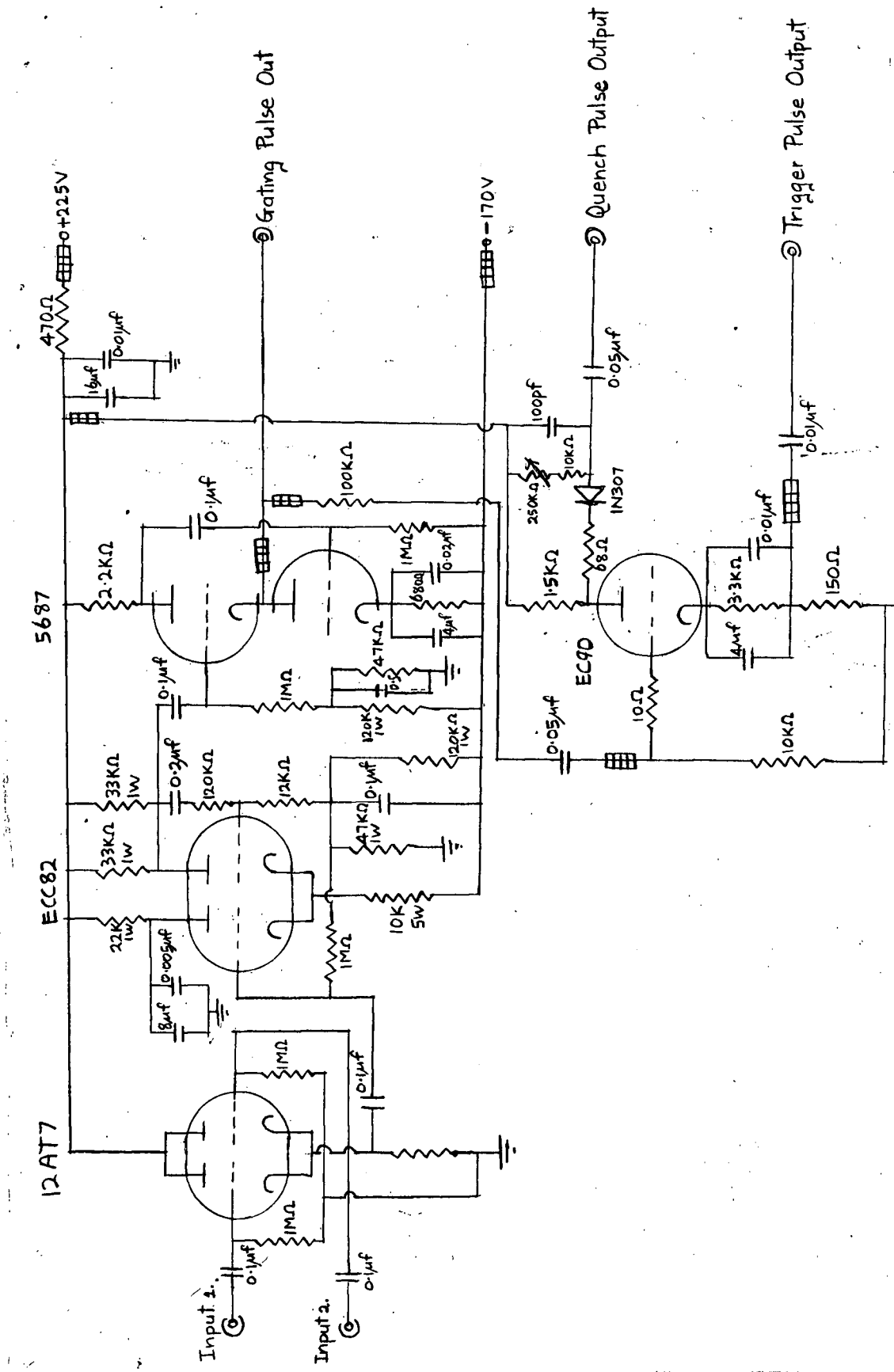

Figure V.4 Mixer, Pulse Amplifier, and Quench Pulser

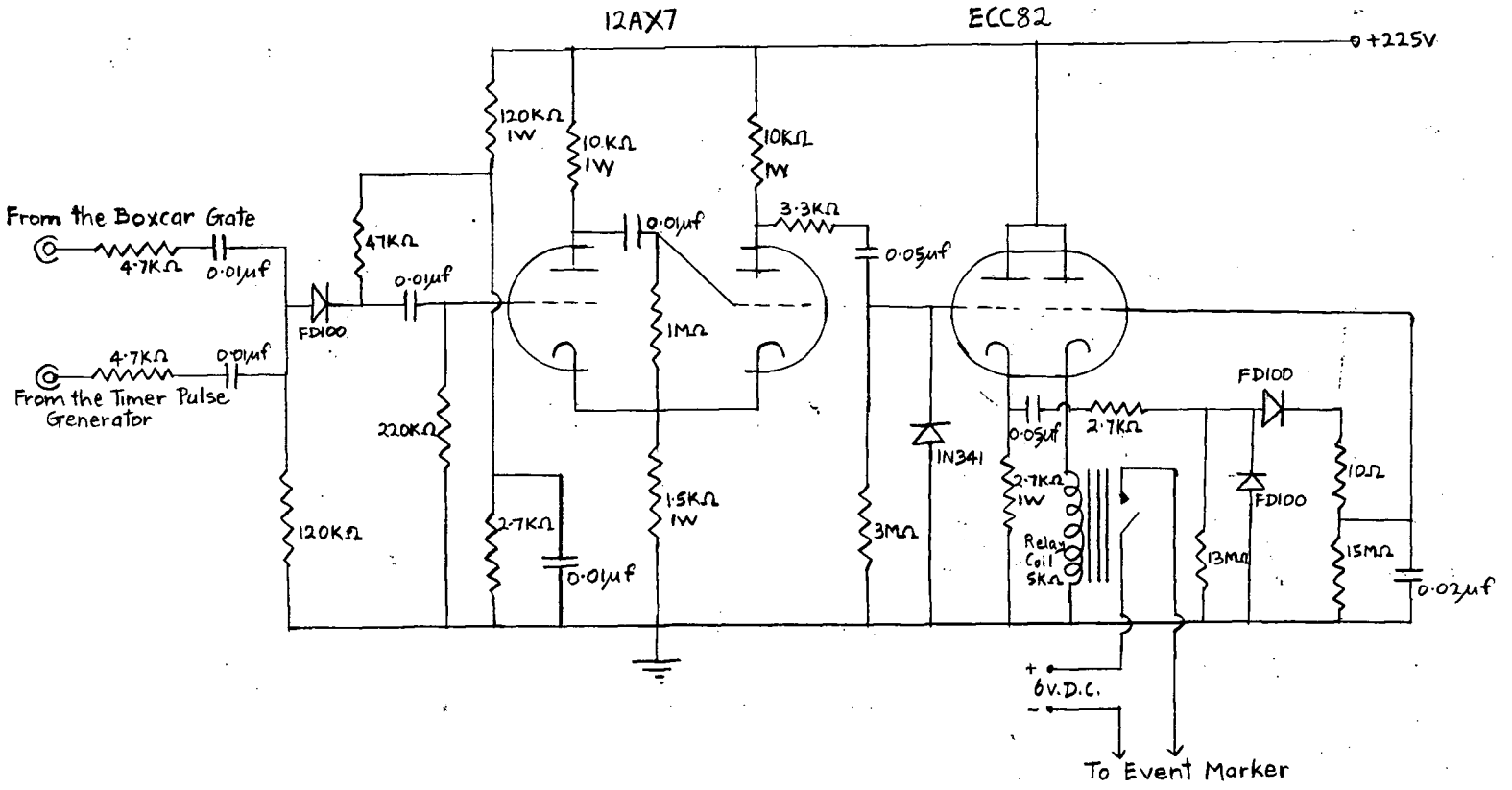

Figure V.5 The Coincidence Timing Unit.

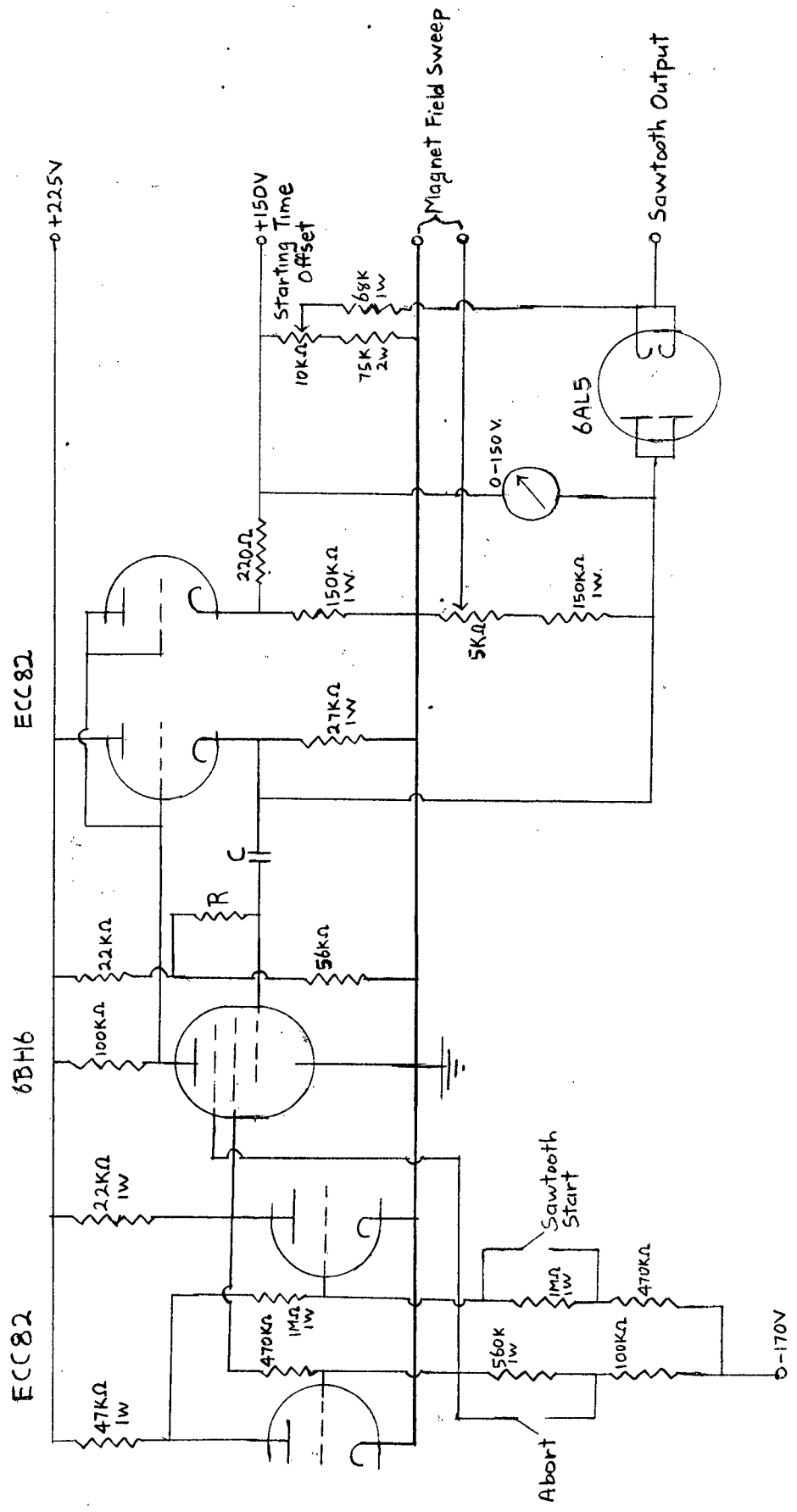

Figure V.6 Phantistron Slow Sawtooth Generator

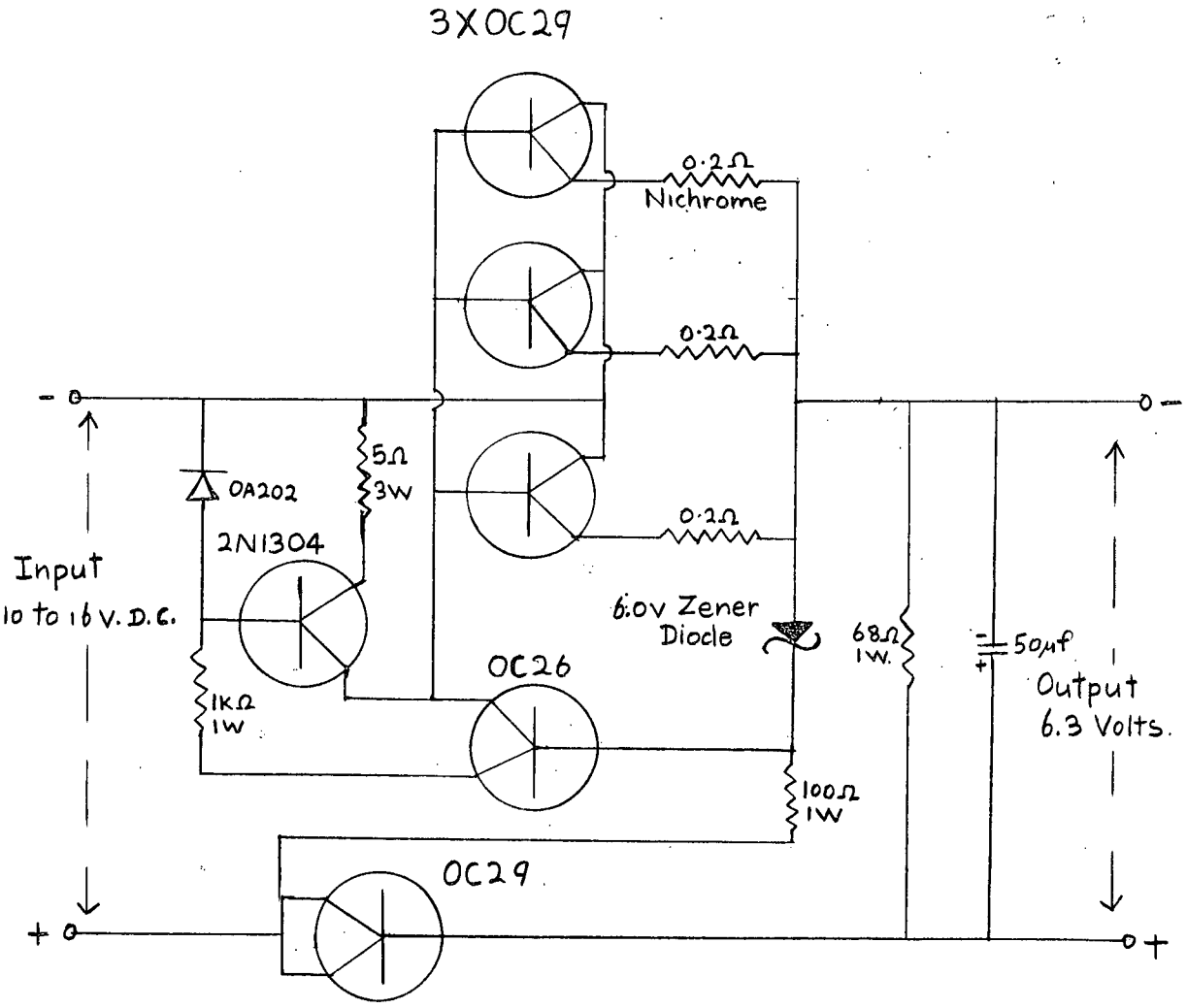

Figure V.7 Regulated Filament Power Supply